

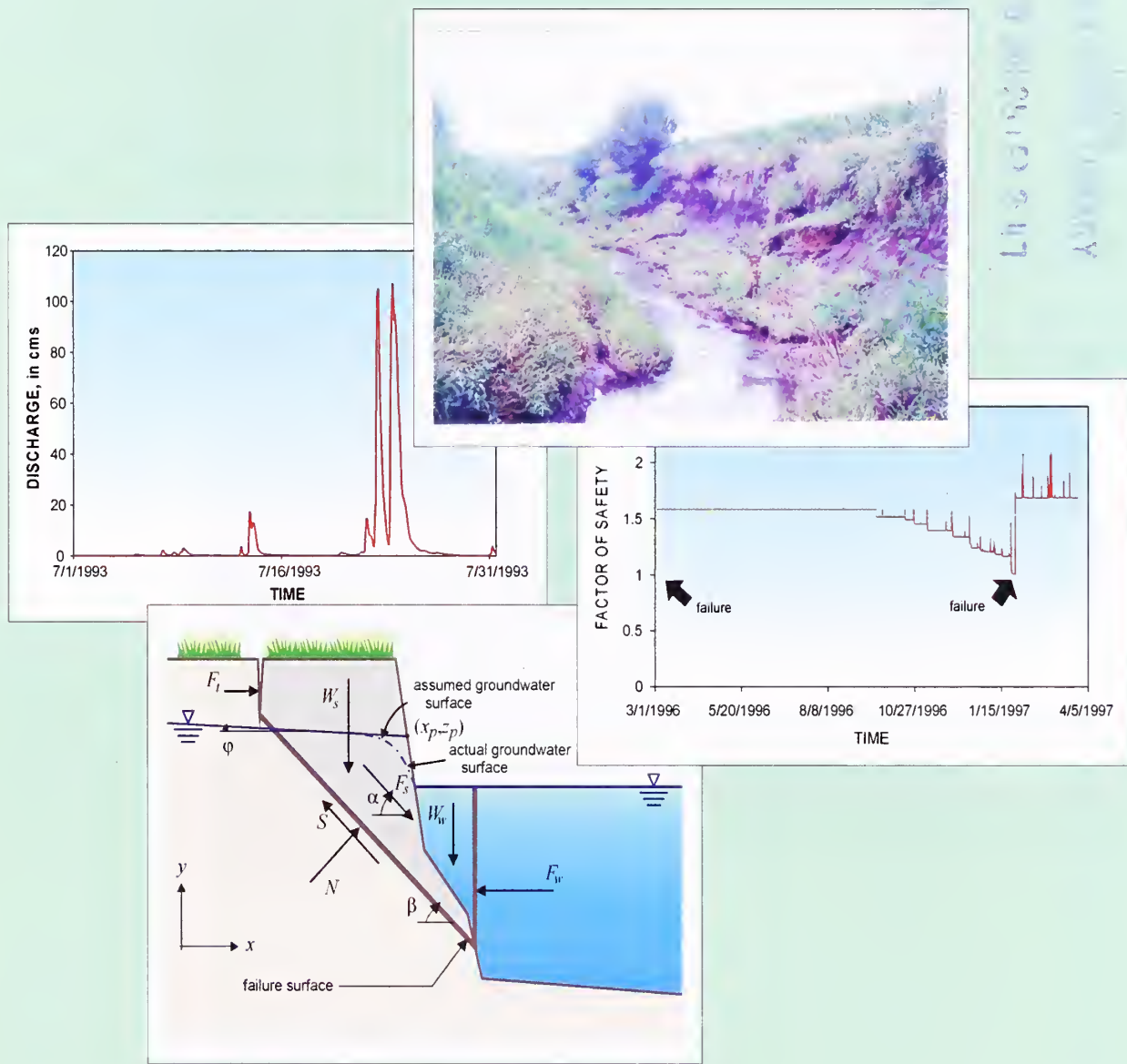
Historic, Archive Document

Do not assume content reflects current scientific knowledge, policies, or practices.



CONCEPTS – Conservational Channel Evolution and Pollutant Transport System

Stream Corridor Version 1.0



Eddy J. Langendoen

Research Report No. 16

December, 2000

USDA-ARS National Sedimentation Laboratory
P.O. Box 1157
Oxford, MS 38655



Acknowledgments

Developing a comprehensive channel evolution model cannot be the work of just a single person. Many people have been instrumental in developing the science and code behind CONCEPTS. I would like to thank the U.S. Department of Agriculture-Agricultural Research Service-National Sedimentation Laboratory (USDA-ARS-NSL), Oxford, Mississippi, for giving me the opportunity to develop CONCEPTS. I would like to acknowledge Carlos Alonso, Research Leader of the Channel and Watershed Processes Research Unit (CWPRU) of NSL for his guidance; my colleagues of CWPRU, Sean Bennett, Ron Bingner, Roger Kuhnle, and Andrew Simon for their scientific contributions and valuable knowledge on hydrology, hydraulics, sediment transport, and channel morphology; Heath Trost for testing CONCEPTS and preparing most input data; the financial support of the Lower Platte South Natural Resources District, Lincoln, Nebraska, Papio-Missouri River Natural Resources District, Omaha, Nebraska, and U.S. Army Corps of Engineers, Vicksburg District; and Fred Theurer of the USDA Natural Resources Conservation Service, National Water and Climate Center for supporting and guiding the AGNPS 98 project of which CONCEPTS is a part.

The data at Goodwin Creek were collected by CWPRU. The data at the Goodwin Creek Bendway site were collected by Brian Bell, Steve Darby, Mark Griffith, Joe Murphrey, Keith Parker, and Andrew Simon of NSL. The data at the Little Salt Creek, Lancaster County, Nebraska were collected by Brian Bell, Andrea Curini, John Massey, and Andrew Simon of NSL, Gregory Hanson of the USDA-ARS Hydraulic Engineering Unit at the Plant Science and Water Conservation Research Laboratory, Stillwater, Oklahoma, and David Rus, Phil Soenksen, and Vincent Walczyk of the USGS Water Resources Division, Lincoln, Nebraska.

Finally, I would like to thank Carlos Alonso, Sean Bennett, Andrew Simon, Francisco Simões of the US Department of the Interior, Bureau of Reclamation, Technical Service Center, Sedimentation and River Hydraulics Group, and Fred Theurer for reviewing the report and providing beneficial comments and discussions.

Table of Contents

Introduction	1
Background	1
Purpose and Capabilities	1
Limits of Application	2
System Requirements	3
Overview of Manual	3
Part 1 Model Description	5
Chapter 1 Flow Hydraulics	7
Theory	7
<i>Governing Equations</i>	<i>9</i>
Open-Channel Flow	9
Hydraulic Structures	11
Culvert	11
Bridge Crossing	14
Drop Structure	16
Generic Structure	17
Implementation of Hydraulics Submodel	17
<i>Representation of Stream Cross-Section and Stream Corridor</i>	<i>17</i>
Corridor	17
Cross Section	17
Flow Resistance	20
Computation of Flow Variables	22
Discretization	24
Generalized Preissmann Scheme	24
Approximations of Governing Equations of Open-Channel Flow	25
Solution Method	29
Double Sweep Algorithm	29
Treatment of External Boundary Conditions	30
Treatment of Internal Boundary Conditions	30
One-Equation Diffusion Wave Model	31
Chapter 2 Sediment Transport and Bed Adjustment	33
Theory	33
<i>Sediment Transport</i>	<i>33</i>

<i>Governing Equations</i>	35
Mass Balance	35
Non-Equilibrium Adjustment of Cohesionless Bed-Material Transport ...	35
Entrainment and Deposition of Cohesive Bed-Material	37
Mixing Layer	38
Sediment Transport Capacity	39
Laursen (1958)	42
Yang (1973)	43
Meyer-Peter and Mueller (1948)	43
Fall Velocity	44
Implementation of Bed-Material Transport Submodel	44
<i>Computation of Fractional Sediment Concentration</i>	44
Noncohesive Streambed	44
Cohesive Streambed	46
<i>Computation of Variations in Streambed Elevation</i>	46
Cross Section Evolution	47
<i>Mixing Layer Composition</i>	47
<i>Boundary Conditions</i>	49
External Boundary Conditions	49
Internal Boundary Conditions	49
Chapter 3 Bank Erosion and Channel Widening	51
Theory	51
<i>Fluvial Erosion Process</i>	52
Osman and Thorne Method	54
<i>Mass Wasting Process</i>	55
Streambank Stability Analysis	58
Pore-Water Pressure	60
Factor of Safety without Seepage	61
Factor of safety with Seepage	62
Factor of safety for Layered Streambanks	63
Inclination of the Failure Surface	63
<i>Implementation of the Channel-Widening Submodel</i>	64
<i>Fluvial Erosion</i>	64
<i>Mass Wasting</i>	64
Part 2 Data Specification	67
Chapter 4 Input Data	69
Run Control Data	69

<i>Block 1</i>	69
<i>Block 2</i>	72
<i>Block 3</i>	73
Output at a Certain Location and for a Certain Runoff Event	73
Time-Series Output at a Certain Location	73
Output for a Certain Runoff Event along a Section of the Modeling Reach	75
Cross Section Data	76
<i>General Data (Block 1)</i>	76
<i>Streambed Data Block (Block 4)</i>	80
<i>Streambank Data Block (Blocks 3 and 5)</i>	81
<i>Floodplain Data Block (Blocks 2 and 6)</i>	82
Hydraulic Structure Data	82
<i>Culvert</i>	83
<i>Bridge Crossing</i>	83
<i>Drop Structure</i>	83
<i>Generic Structure</i>	86
Dynamic Upstream Boundary Conditions	88
Chapter 5 Output Data	89
Output Data File Specification	89
<i>Output at a Certain Location and for a Certain Runoff Event</i>	89
Initial Data	90
Runoff Event Related Data	91
<i>Time-Series Output at a Certain Location</i>	93
Initial Data	93
Continuous Data	96
<i>Output for a Certain Runoff Event along a Section of the Modeling Reach</i>	96
Initial Data	96
Runoff Event Related Data	98
Processing of Output Data Files	99
<i>Output at a Certain Location and for a Certain Runoff Event</i>	99
<i>Time-Series Output at a Certain Location</i>	101
<i>Output for a Certain Runoff Event along a Section of the Modeling Reach</i>	101
Part 3 Sample Applications	107
Chapter 6 Goodwin Creek, Mississippi	109

Study Area	109
Application	112
<i>Hydraulics</i>	119
<i>Morphology</i>	121
Chapter 7 Goodwin Creek Bendway, Mississippi	123
Study Area	123
Application	125
Chapter 8 Little Salt Creek, Nebraska	139
Study Area	139
<i>Channel Geometry</i>	141
<i>Hydrographs</i>	142
<i>Bed-Material Properties</i>	143
<i>Bank-Material Properties</i>	143
Application	143
References	155

List of Figures

Figure 1.1	Cross-stream variations caused by: (a) bars, (b) constrictions, and (c) obstructions.	.8
Figure 1.2	Definition sketch of hydraulic variables used in the governing equations: a) cross-sectional view and b) longitudinal view.	10
Figure 1.3	Flow types at culverts: inlet control, inlet and outlet control, and uniform flow. The numbers 1, 2, and 3 indicate sections used in the structure's dynamic equation.	12
Figure 1.4	Flow at bridge crossings: (a) top view of bridge crossing showing a flow contraction at section 2; and lateral views of (b) Low Flow Class A and (c) Low Flow Class B. The numbers 1, 2, and 3 indicate sections used in the structure's dynamic equation.	15
Figure 1.5	Flow at a drop structure: (a) free overfall and (b) submerged flow. The numbers 1, 2, and 3 indicate sections used in the structure's dynamic equation.	16
Figure 1.6	Representation of a stream corridor as reaches and nodes (arrows depict information exchanged among adjacent nodes).	18
Figure 1.7	Projection of a meandering stream corridor onto a straight line.	19
Figure 1.8	Representation of cross section geometry.	20
Figure 1.9	Example of roughness elements on a cross section: trees and grasses on the floodplain, grasses on the left bank, and rocks and sediment particles on the bed.	21
Figure 1.10	Segmentation of flow area to compute effective friction factor. Method 1 uses vertical boundaries between the subsections. Method 2 uses vertical boundaries between floodplain and bank sections, and boundaries between bed and bank sections that bisect the angle between bed and bank profiles.	21
Figure 1.11	Flow area, conveyance, equivalent hydraulic radius, and equivalent Manning n as a function of flow depth for the cross section shown in Figure 1.9. Manning n values assigned to the sections are: floodplain $n=0.20$, left bank $n=0.08$, bed and right bank $n=0.03$.	23
Figure 1.12	Preissmann scheme in $x-t$ space: •, node with known values of the dependent variables Q and y ; o, node with unknown values of Q and y ; and +, point at which the dependent variables and their derivatives are approximated.	24
Figure 2.1	Multi-layer approximation of sediment transport.	34
Figure 2.2	Modes of sediment transport: bed load and suspended load.	34
Figure 2.3	Definition sketch of sediment transport variables.	36
Figure 2.4	Progress of sediment mass C toward equilibrium sediment mass \hat{C} for the case of constant flow conditions.	36
Figure 2.5	The erosion rate of a cohesive streambed as a function of bed shear stress.	38

Figure 2.6 Measured (Brownlie, 1981) versus computed (SEDTRA) sediment transport capacity. The black line is the line of perfect agreement and the magenta line is the regression line.	41
Figure 2.7 Function $\mathcal{J}(u_*/\omega)$ in Laursen's approach (Laursen, 1958).	42
Figure 2.8 Solution of advection equation in $x-t$ space.	45
Figure 2.9 Changes in elevation of the streambed: a) erosion of a partly wetted bed, b) erosion of a fully wetted bed, c) deposition on a partly wetted bed, and d) deposition on a fully wetted bed. The darker, shaded area denotes deposited or eroded sediments. .	47
Figure 2.10 Sorting of graded bed-material within the mixing layer: a) erosion, sediment particles from surface layer mix with material from substrate layers 1 and 2; and b) deposition, part of the surface layer becomes new substrate layer 1.	48
Figure 3.1 Critical shear stress τ_e versus SAR for different soil salt concentrations and dielectric dispersion values (modified from Arulanandan <i>et al.</i> , 1980).	54
Figure 3.2 Bank failure mechanisms: a) rotational failure, b) planar failure, c) cantilever failure, and d) piping or sapping failure.	57
Figure 3.3 Definition sketch of forces acting on a streambank.	59
Figure 3.4 Representation of fluvial erosion. The highlighted area is scoured by the flow, steepening the bank.	64
Figure 3.5 Possible failure block geometries for the case where the number of elevations at which the factor of safety is evaluated, N_e , equals four. Sample values of factor of safety are given for each failure block geometry. Here, factor of safety is smallest for block #2, and smaller than unity. Hence, the streambank fails along the respective slip surface.	65
Figure 4.1 Shape of a generic structure (a) and rating curve (b). S_i is side slope and z_i is starting elevation of wall segment i . h_i is breakpoint depth in the rating curve.	87
Figure 5.1 "Text Import Wizard – Step 1 of 3" window.	100
Figure 5.2 "Text Import Wizard – Step 2 of 3" window.	100
Figure 5.3 "Text Import Wizard – Step 2 of 3" window with break lines added.	101
Figure 5.4 View of Microsoft® Excel spreadsheet after importing output data file.	102
Figure 5.5 "Text Import Wizard – Step 2 of 3" window with break lines added.	102
Figure 5.6 Example plot of temporal changes in cross-section geometry.	103
Figure 5.7 Example plot of temporal changes in bed-material composition.	103
Figure 5.8 View of Microsoft® Excel spreadsheet after importing time-series output data file.	104
Figure 5.9 Example plot of the progression of factor of safety of the right streambank.	104
Figure 5.10 "Text Import Wizard – Step 2 of 3" window with break lines added.	105
Figure 5.11 View of Microsoft® Excel spreadsheet after importing profile output data file.	106

Figure 5.12 Example plot of temporal changes in thalweg profile.	106
Figure 6.1 Map of the Goodwin Creek Watershed.	110
Figure 6.2 Plan map of the 3.86 km study length of Goodwin Creek showing cross sections and flume locations.	111
Figure 6.3 The 14 reaches along Goodwin Creek for which bed-material samples were collected. Bed material median sizes for the reaches are: 1) 1.0 mm, 2) 1.4 mm, 3) 4.4 mm, 4) 6.9 mm, 5) 3.5 mm, 6) 6.7 mm, 7) 3.9 mm, 8) 1.1 mm, 9) 1.4 mm, 10) 7.3 mm, 11) 1.4 mm, 12) 0.5 mm, 13) 2.4 mm, and 14) 7.4 mm.	112
Figure 6.4 Run control data file used in the simulation of the lower 3.5 km of Goodwin Creek, Mississippi.	113
Figure 6.5 A sample cross section data file used in the simulation of the lower 3.5 km of Goodwin Creek, Mississippi.	115
Figure 6.6 Part of the discharge data file used in the simulation of the lower 3.5 km of Goodwin Creek, Mississippi.	118
Figure 6.7 Simulated storm rating-curves at the outlet of the modeling reach.	120
Figure 6.8 Simulated changes in profiles of: thalweg elevation ((a) scenario 1 and (b) scenario 2) and d_{50} ((c) scenario 1 and (d) scenario 2).	121
Figure 6.9 Simulated changes in geometry of cross section C45-1: (a) scenario 1 and (b) scenario 2.	122
Figure 7.1 Photo of the Goodwin Creek Bendway study site. Flow is from right to left.	124
Figure 7.2 Plan view of the Goodwin Creek Bendway field study site. The surveyed cross sections are shaded red.	125
Figure 7.3 Run control data file used in the simulation of the Goodwin Creek Bendway field study site.	126
Figure 7.4 A sample cross section data file used in the simulation of the Goodwin Creek Bendway field study site.	130
Figure 7.5 Part of the discharge data file used in the simulation of the Goodwin Creek Bendway field study site.	133
Figure 7.6 Comparison of observed and simulated bank failures at the Goodwin Creek Bendway field study site: (a) cross section 6 and (b) cross section 8.	136
Figure 7.7 Predicted factor of safety for the right banks of cross sections 6 and 8.	137
Figure 8.1 Map of Little Salt Creek, Lancaster County, Nebraska.	140
Figure 8.2 View of Little Salt Creek and wetlands upstream of Raymond Road.	141
Figure 8.3 Streambank failure along Little Salt Creek north of Raymond Road.	141
Figure 8.4 Run control data file used in the simulation of the long term stability of Little Salt Creek, Nebraska.	144

Figure 8.5 A sample cross section data file used in the simulation of the long-term stability of Little Salt Creek, Nebraska.	147
Figure 8.6 Part of the discharge data file used in the simulation of the long-term stability of Little Salt Creek, Nebraska.	150
Figure 8.7 Simulated evolution of the thalweg profile, Little Salt Creek, for a 30-year period.	151
Figure 8.8 Computed changes in cross section geometry at selected cross sections along Little Salt Creek for a 30-year period: (a) cross section at model kilometer 0.29 upstream of Raymond, (b) cross section at model kilometer 2.93 upstream of Mill Road, and (c) cross section at model kilometer 6.98 near Bluff Road.	152
Figure 8.9 Simulated evolution of the thalweg profile, Little Salt Creek, for a 30-year period and the streambed controlled at each bridge crossing.	153

List of Tables

Table 2.1	Sediment size fractions and corresponding transport equations.....	40
Table 4.1	Input data in block #1 of run control data.....	70
Table 4.2	Values assigned to the different processes that can be accounted for by the bank stability analysis.	71
Table 4.3	Link types to be used with CONCEPTS.	72
Table 4.4	Input data in block #2 of run control data. The user has to repeat this block for each link.....	72
Table 4.5	Input data to request output at a certain cross section and for a certain runoff event. Lines 2 through $4 + N_s$ are repeated N_{lc} times.	73
Table 4.6	Parameters that can be output for a certain runoff event and cross section.....	74
Table 4.7	Input data to request time-series output at a certain cross section. Lines 2 through $4 + N_{ts}$ are repeated N_{lc} times.	74
Table 4.8	Parameters that can be output as time series.	75
Table 4.9	Input data to request output for a certain runoff event along a section of the modeling reach. Lines 2 through $4 + N_s$ are repeated N_p times.....	76
Table 4.10	Parameters that can be output for a certain runoff event along a section of the modeling reach.....	76
Table 4.11	Makeup of cross section data input file.	77
Table 4.12	Data block #1 of the cross section data input file.....	77
Table 4.13	Values of the roughness coefficient n (Chow, 1959).	77
Table 4.14	Input block #4 with streambed data. Lines $14 + N_n$ through $32 + N_n$ are repeated N_{la} times.....	80
Table 4.15	Input block #3 and #5 with streambank data.	81
Table 4.16	Input block #2 and #6 with floodplain data.	82
Table 4.17	Input parameters common to the different types of structures.	82
Table 4.18	Input data for culverts.	83
Table 4.19	USFHWA (1985) chart and scale numbers for pipe and box culverts.	84
Table 4.20	Entrance loss coefficients for pipe and box culverts.	85
Table 4.21	Input data for bridge crossings.	85
Table 4.22	Yarnell's pier shape coefficient for various pier shapes.....	86
Table 4.23	Input data for drop structures.....	86

Table 4.24 Input data for generic structures.	86
Table 4.25 Layout of each record in the upstream boundary conditions file.	88

List of Symbols

Uppercase variables

variable	meaning	unit
A	flow area	m^2
A_b	cross-sectional area of the mixing layer	m^2
$A_j - J_j, S_j, T_j$	coefficients in discretized flow equations	
A_s	cross-sectional area of the surface or active layer	m^2
B	top width	m
C	volumetric sediment mass	m^2
\hat{C}	equilibrium volumetric sediment mass or carrying capacity of the flow	m^2
C_{1-5}	coefficients	
C_f	friction-loss coefficient	
C_L	energy-loss coefficient	
C_p	pier-shape coefficient	
C_Q	the rate of lateral inflow into a reach as a fraction of the discharge at the inlet	$1/\text{m}$
C_t	total volumetric sediment mass	m^2
D	height of culvert barrel (page 13)	m
D	diffusion coefficient (page 32)	m^2/s
D	deposition rate (Chapter 2)	m^2/s
E	entrainment rate	m^2/s
F	Froude number	
F	factor of safety	
F_s	seepage force per unit channel length	N/m
F_t	hydrostatic force per unit channel length exerted by water in the tension crack on the failure block	N/m
F_w	hydrostatic force per unit channel length exerted by surface water on the vertical section of the slip surface	N/m
H	headwater upstream of structure (Chapter 1)	m

Uppercase variables (continued)

variable	meaning	unit
H	height of failure block (Chapter 3)	m
J	number of cross sections in schematized stream corridor	
K	conveyance	m^3/s
L	distance between cross sections (page 18)	m
L	length of slip surface (Chapter 3)	m
L_c	length of culvert barrel	m
N	total normal force per unit channel length at the base of the failure block	N/m
\bar{N}	effective force normal to the failure plane per unit channel length acting on the base of the failure block	N/m
N_b	bank stability number	
N_c	Courant number	
N_e	number of elevations along the height of a streambank at which CONCEPTS evaluates factor of safety	
N_l	number of links comprising the simulated stream corridor	
N_{la}	number of soil layers comprising the streambed	
N_{lc}	number of locations at which output is requested	
N_n	number of points making up streambed, streambank, or floodplain	
N_p	number of profiles for which output is requested	
N_{rs}	number of segments comprising a rating curve	
N_s	number of storm events for which output is requested	
N_{se}	number of segments comprising the walls of a generic structure	
N_t	time-step reduction factor for diffusion equation	
N_{ts}	number of time series for which output is requested	
N_x	number of cross sections in a subreach	
Q	discharge	m^3/s
R	hydraulic radius	m
R_e	equivalent hydraulic radius	m
S	shear force at the base of the failure block per unit channel length	N/m

Uppercase variables (continued)

variable	meaning	unit
S_b	bed slope	m/m
S_c	slope of culvert barrel	m/m
S_f	friction slope	m/m
S_u	sediment flux from subsurface layers to surface layer	m^2/s
T	time-of-rise of flood wave (Chapter 1)	s
T	time scale representing the rate of adjustment of sediment mass to equilibrium sediment mass (Chapter 2)	s
U_w	pore-water force acting on the base of the failure block per unit channel length	N/m
V_w	volume eroded from the streambank per unit channel length	m^3/m
\dot{W}	actual rate of bank erosion	m/s
\dot{W}_i	initial rate of bank erosion	m/s
W_s	weight of failure block per unit channel length	N/m
W_w	weight of surface water on the failure block per unit channel length	N/m

Lowercase variables

variable	meaning	unit
a	thickness of surface or active layer	m
c	celerity of flood wave (Chapter 1)	m/s
c	point sediment concentration (Chapter 2)	ppmw
c	cohesion (Chapter 3)	Pa
c'	effective cohesion	Pa
\hat{c}	kinematic-wave celerity	m/s
c_a	apparent cohesion	Pa
c_d	developed cohesion	Pa
d	particle diameter	m
d	depth below soil surface (page 61)	m
\bar{d}	mean sediment size	m

Lowercase variables (continued)

variable	meaning	unit
d_{50}	sediment size for which 50% of the sediment mixture is finer	m
d_c	critical sediment-particle diameter	m
e	erosion-rate constant	m/s
f	flow variable (page 24)	
f_k	ratio between sediment mass entering the stream corridor and the sediment-carrying capacity of the flow at the inlet	
f_t	ratio between tension crack height and thickness of soil layer with negative earth pressures	
g	gravitational acceleration	m^2/s
\mathbf{g}	gravitational acceleration vector $(0,0,-g)^T$	m^2/s
h	flow depth	m
h	total hydraulic head (page 60)	m
h_d	hydraulic depth	m
i	hydraulic gradient	m/m
j	space index	
k	sediment-size class	
m	ratio between actual change in bed elevation at the outlet and that computed	
n	Manning roughness coefficient	$\text{s}/\text{m}^{1/3}$
n	time index (superscript)	
n'	Manning grain-roughness coefficient	$\text{s}/\text{m}^{1/3}$
n_e	equivalent Manning roughness coefficient	$\text{s}/\text{m}^{1/3}$
p	fraction of sediment available for transport	
q	lateral inflow of water into the stream corridor	m^2/s
q_s	lateral volumetric inflow of sediment into the stream corridor	m^2/s
r	Meyer-Peter and Mueller's ratio of grain roughness and bed roughness	
r_u	pore-water pressure ratio	
t	time	s
u	flow velocity	m/s

Lowercase variables (continued)

variable	meaning	unit
u_a	pore-air pressure	Pa
u_w	pore-water pressure	Pa
u_*	shear velocity	m/s
x	space coordinate in horizontal direction	m
x_p	horizontal coordinate of intersect of phreatic surface and bank face	m
y	stage	m
z	space coordinate in vertical direction	m
z_p	vertical coordinate of intersect of phreatic surface and bank face	m
z_t	thickness of layer with negative earth pressure	m
z_{tc}	height of the tension crack	m

Symbols

variable	meaning	unit
α	coefficient of power function representing a flow variable (page 23)	
α	angle of seepage force (Chapter 3)	°
α_L	step-length constant	
β	exponent of power function representing a flow variable (page 23)	
β	angle of failure plane (Chapter 3)	°
β^b	fractional content by volume of a sediment-size class in the streambank	
β^s	fractional content by volume of a sediment-size class in the surface layer	
β^u	fractional content by volume of a sediment-size class in the subsurface layer	
γ	specific weight of water	N/m ³
γ_b	soil bulk unit weight	N/m ³
γ_s	specific weight of sediment	N/m ³
Δ	increment	
ε	rate constant	1 / $\sqrt{\text{Pa}}$

Symbols (continued)

variable	meaning	unit
ε_f	erosion rate of cohesive flocs	m/s
θ	temporal weighting factor (Chapter 1)	
θ	Shields parameter (Chapter 2)	
θ_c	critical Shields parameter	
λ	porosity of streambed	
ν	kinematic viscosity	m^2/s
ρ	density of water	kg/m^3
σ	contraction ratio	
$\hat{\sigma}$	contraction ratio $1 - \sigma$	
$\bar{\sigma}$	total-stress tensor	Pa
σ_n	total stress normal to the base of the failure block	Pa
τ	shear stress	Pa
τ'	bed shear stress due to grain resistance	Pa
τ_b	bed shear stress	Pa
τ_c	critical tractive stress	Pa
τ_d	threshold bed shear stress below which deposition of cohesive sediments occurs	Pa
τ_e	shear strength of bed material	Pa
ϕ	angle of internal friction	°
ϕ'	effective angle of internal friction	°
ϕ^b	angle indicating increase in shear strength for an increase in matric suction	°
χ	hiding coefficient	
Ψ	matric-suction force acting on slip surface per unit channel length	N/m
ψ	spatial weighting factor	
ω	particle fall velocity	m/s

Introduction

Background

The Conservational Channel Evolution and Pollutant Transport System (CONCEPTS) is a computer model that simulates open-channel hydraulics, sediment transport, and channel morphology. CONCEPTS, version 1.0, incorporates unique advances on alluvial channel evolution made by scientists at the U.S. Department of Agriculture, Agricultural Research Service, National Sedimentation Laboratory (NSL) in Oxford, Mississippi. Presently, there are two versions of CONCEPTS available that consider different scales of stream systems:

- watershed-scale stream network, and
- reach-scale stream corridor.

This document **only** describes the technology and input specifications of the stream-corridor version of CONCEPTS. You may find information on the watershed-scale version of CONCEPTS on the NSL's website at URL:

<http://www.sedlab.olemiss.edu/AGNPS2001/Concepts/concepts.html>

You can download both versions of CONCEPTS from the above URL.

The basic components of CONCEPTS are channel hydraulics, channel morphology, and transport of sediments and contaminants. CONCEPTS version 1.0 does not include the transport of contaminants.

Purpose and Capabilities

The overall objective of the ongoing work on CONCEPTS is to develop an integrated stream-riparian corridor model to be used in conjunction with watershed-scale analysis, for evaluating the long-term effectiveness of proposed corridor rehabilitation designs. This modeling capability is a critical need for hydraulic engineers, fluvial geomorphologists, landscape architects, and stream ecologists involved in stream rehabilitation projects. These projects are usually challenged by the lack of integrated design tools to evaluate the long-term stability of reconstructed stream corridors. This model is an integral component of the suite of modeling tools incorporated into the AGNPS98 technology at NSL supported by the U.S. Department of Agriculture, Natural Resources Conservation Service (<http://www.sedlab.olemiss.edu/AGNPS.html>).

Version 1.0 of CONCEPTS simulates unsteady, one-dimensional flow, graded-sediment transport, and bank-erosion processes in stream corridors. It can predict the dynamic response of flow and sediment transport to instream

hydraulic structures. It computes channel evolution by tracking bed changes and channel widening. Bank erosion accounts for basal scour and mass wasting of unstable cohesive banks. CONCEPTS simulates transport of cohesive and cohesionless sediments, both in suspension and on the bed, and selectively by size classes. CONCEPTS includes channel-boundary roughness varying along a cross section, for example due to varying vegetation patterns.

CONCEPTS can be used to evaluate the efficiency of instream grade-control structures to reduce sediment yield and to stabilize streams. CONCEPTS can evaluate location and sizing alternatives of grade-control structures.

CONCEPTS can be used to evaluate the design of specific stream corridor rehabilitation measures used for stream stability and habitat improvement.

CONCEPTS version 2.0, already under development, will incorporate the simulation of riparian buffers, vegetated streambanks, and the onset of channel meandering due to the deposition of alternate bars.

Limits of Application

CONCEPTS assumes or is limited to the following:

- gradually-varying, one-dimensional flow;
- four types of instream hydraulic structures:
 - pipe and box culverts,
 - bridge crossings with a trapezoidal cross section,
 - drop structures with a trapezoidal cross section,
 - generic structures with a multi-segment trapezoidal cross section.
- straight channels or channels of very low sinuosity;
- different hydraulic roughness for bed, banks, and floodplains;
- total load sediment transport;
- homogeneous cohesionless or cohesive bed-material in transverse direction;
- 13 pre-defined sediment particle-size classes;
- non-equilibrium transport of cohesionless bed-material;
- linear erosion rate of cohesive bed material;
- consolidation of deposited cohesive sediments is unavailable;
- homogeneous cohesive bank material;
- linear lateral-erosion rate of the bank toe based on excess shear stress;
- slab or planar type of bank failure;
- (quasi-) hydrostatic groundwater pressure in streambank;
- metric system of units.

System Requirements

To use CONCEPTS you need a PC with a Microsoft Windows® 95 or later operating system. Hard disk and memory usage will vary depending on the size of the problem. The CONCEPTS executable file requires approximately 600 KB of hard disk space. Input files for typical applications require one to two MB of hard disk space, used mainly by the discharge data file. Depending on the output options specified by the user, the combined hard disk usage of the output files may vary between a couple of MB to a couple of GB. A minimum of 32 MB of RAM is recommended.

Overview of Manual

This manual presents the computer model CONCEPTS, specifically:

- Part 1, scientific basis;
- Part 2, data needs; and
- Part 3, sample applications.

Chapters 1 through 3 include the scientific basis and cover hydraulics, sediment-transport mechanics, and streambank erosion. Formulations of these components and their numerical implementation are presented.

Chapters 4 and 5 include the format of the input and output data files. Chapter 5 also presents a method to produce graphs from the output data using Microsoft® Excel.

Chapters 6 through 8 present applications of CONCEPTS to channels in northern Mississippi and eastern Nebraska.

Introduction

Part 1

MODEL DESCRIPTION

FLOW HYDRAULICS

This chapter presents the flow hydraulics submodel of CONCEPTS. You will find the scientific basis of the mathematical formulations of one-dimensional flow in open channels and at hydraulic structures used by CONCEPTS. Further, you will find the numerical implementation of the mathematical model, which will help you in selecting suitable user-defined parameters incorporated in the mathematical formulations.

Theory

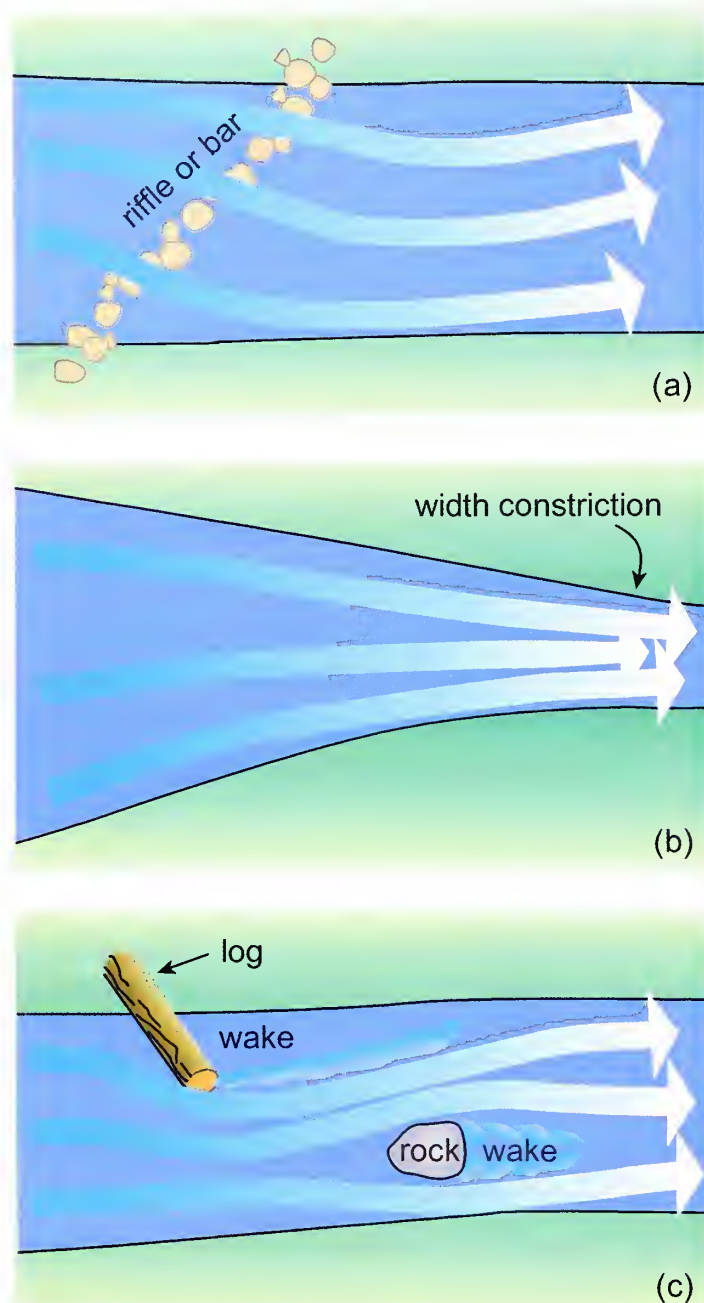
CONCEPTS assumes the flow in stream systems to be *one dimensional* along the centerline of the channel. It neglects cross-stream variations induced by cross-section geometrical features such as riffles and pointbars (Figure 1.1a), constrictions or expansions (Figure 1.1b), and obstructions such as woody debris or rocks (Figure 1.1c).

Various one-dimensional flow routing methods exist. They are commonly known as (Fread, 1996):

- lumped flow routing or hydrologic routing, and
- distributed flow routing or hydraulic routing models.

Lumped flow routing methods compute the flow as a function of time at one location along the stream, e.g. Muskingum and level-pool routing methods. *Distributed flow routing* methods compute the flow as a function of time simultaneously at a series of cross sections along the stream. Lumped flow routing methods are computationally more efficient, whereas distributed flow routing methods are most accurate. Lumped flow routing methods cannot predict backwater upstream of hydraulic structures and channel confluences.

Figure 1.1 Cross-stream variations caused by: (a) bars, (b) constrictions, and (c) obstructions.



CONCEPTS uses a distributed flow routing method to accurately model the effects of instream hydraulic structures on stream corridor rehabilitation designs.

Governing Equations

Open-Channel Flow

The *Saint Venant equations* describe unsteady, gradually-varying one-dimensional open-channel flow. Cunge *et al.* (1980) give an extensive overview of these equations. The Saint Venant equations consist of a continuity equation representing mass conservation of water and a momentum equation representing the conservation of fluid momentum.

The *continuity equation* reads

$$B \frac{\partial y}{\partial t} + \frac{\partial Q}{\partial x} = q \quad (1.1)$$

where y is stage, Q is discharge, B is flow top width, q is lateral flow into the channel per unit length of channel (e.g., overland flow or groundwater return flow), x is distance along the channel, and t is time. The *momentum equation* is

$$\frac{\partial Q}{\partial t} + \frac{\partial}{\partial x} \left(\frac{Q^2}{A} \right) + gA \left(\frac{\partial y}{\partial x} + S_f \right) = 0 \quad (1.2)$$

where A is flow area, g is gravitational acceleration, and S_f is friction slope.

The friction slope is defined as

$$S_f = \frac{Q^2}{K^2} = \frac{n^2 Q^2}{A^2 R^{4/3}} \quad (1.3)$$

where K is conveyance, R is hydraulic radius, and n is Manning roughness coefficient. The cross-sectional average flow velocity used hereafter is defined as $u = Q/A$. Figure 1.2 shows a definition sketch of the above variables.

The variables stage, y , and discharge, Q , are the *dependent variables*. The dependent variables are those that are determined by the solution method. Time, t , and distance, x , are the *independent variables*. All other variables are functions of the independent or dependent variables.

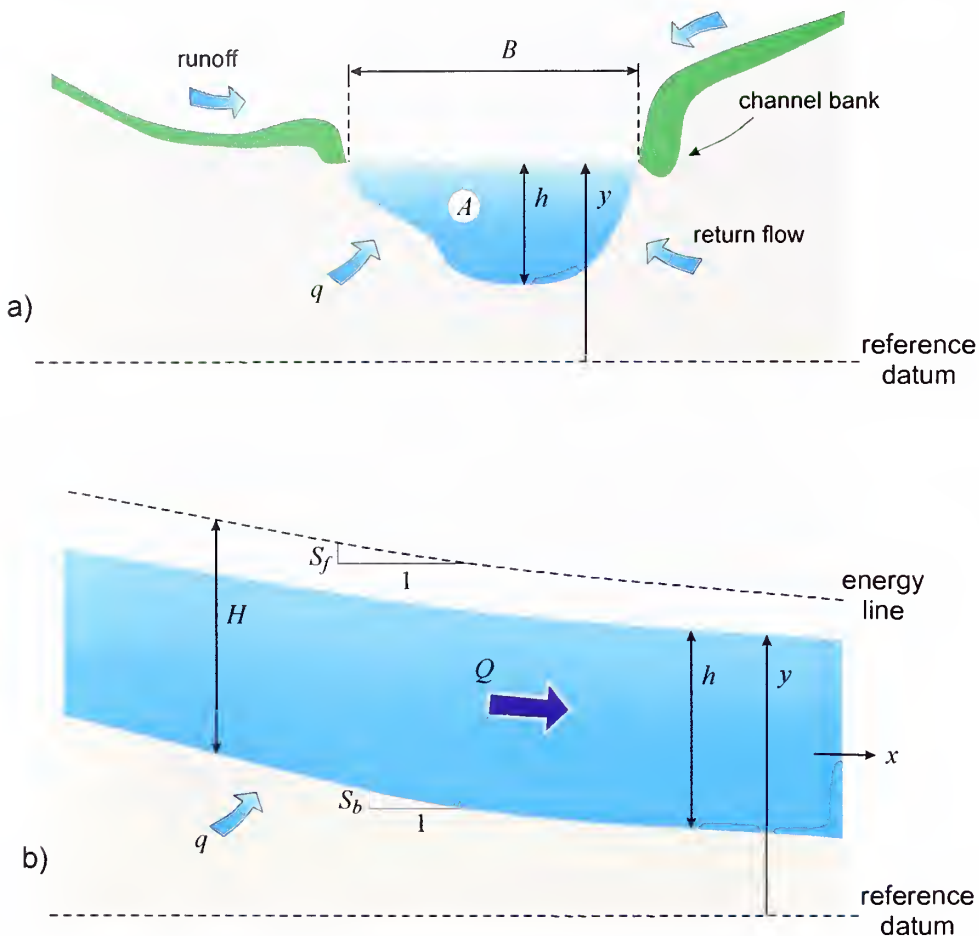
The Saint Venant equations are also known as the *dynamic wave model*. If we neglect the inertia terms in (1.2), the first and second term on the left-hand side of (1.2), for example when Froude number is small, (1.2) simplifies to

$$\frac{\partial y}{\partial x} + S_f = 0 \quad (1.4)$$

Equations (1.1) and (1.4) are known as the *diffusion wave model*. The diffusion wave model is computationally more efficient than the dynamic wave model. Also, omitting the nonlinear convective acceleration, the second term in (1.2), results in a more robust numerical model. The numerical approximation of the convective acceleration term may produce erroneous solutions or even fail to calculate a solution.

Ponce *et al.* (1978) postulated the following applicability criterion for the diffusion wave model:

Figure 1.2 Definition sketch of hydraulic variables used in the governing equations: a) cross-sectional view and b) longitudinal view.



$$T \geq \frac{15}{S_b} \sqrt{\frac{h}{g}} \quad (1.5)$$

where T is time-of-rise of the flood wave, h is flow depth, and S_b is bed slope. The flow depth and bed slope are reach-averaged values. Depending on criterion (1.5) CONCEPTS automatically switches between the dynamic and diffusion wave models.

Along a watercourse you will find two types of boundaries:

- *external boundaries*, the upstream and downstream extremities of the stream corridor; and
- *internal boundaries*, locations where the flow is rapidly varied rather than gradually varied, hence the St. Venant equations are not applicable.

Example internal boundaries are hydraulic structures, rapids, etc. The following section discusses the representation of hydraulic structures in CONCEPTS.

Hydraulic Structures

Structures can act as *controls* or *transitions*, changing local rating curves. Since sediment transport is directly related to the local velocities, hydraulic structures will not only affect discharge and stage hydrographs but also sediment movement in stream channels. For example, grade-control structures reduce channel grade by creating backwater and inducing upstream deposition, and downstream scour.

Presently, there are four types of structures included in CONCEPTS-1.0:

- culvert,
- bridge crossing,
- drop structure, and
- generic structure.

The generic structure can be any structure for which a rating curve is available.

To guarantee an efficient solution method, the mathematical representation of the flow at hydraulic structures has to be equivalent to that of open-channel flow, that is, equations (1.1) and (1.2). To model the flow at structures CONCEPTS uses *continuity* and *dynamic equations*, which establish a relation between discharges and stages upstream and downstream of the structure.

The *continuity equation*

$$\frac{\partial Q}{\partial x} = 0 \quad (1.6)$$

states that discharge across the structure is constant. Thus, the discharge upstream of the structure equals that downstream of the structure. The continuity equation is the same for all types of structures.

The *dynamic equation* describes the flow at the structure by relating the discharge through the structure to the stages upstream and downstream of the structure. Because flow pattern varies among different types of structures, each structure has a different dynamic equation.

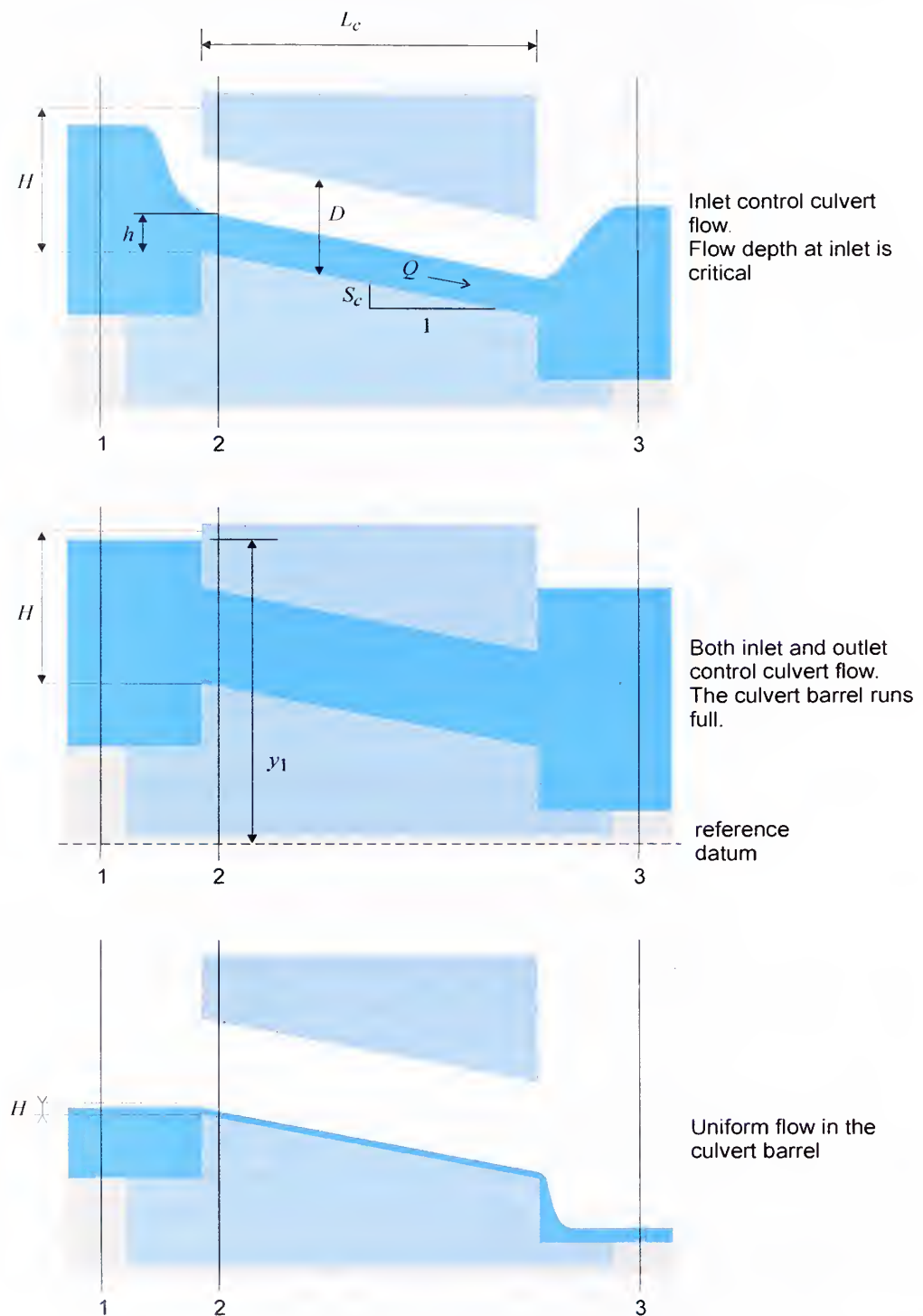
Culvert

CONCEPTS-1.0 models two culvert shapes: *pipe* culverts and *box* culverts. Various flow types characterize the flow through culverts. Bodhaine (1968) classifies culvert flow into six flow types on the basis of location of the control section and the relative heights of the headwater and tailwater elevations. CONCEPTS distinguishes three flow types (see also Figure 1.3):

- flow controlled by the culvert inlet;
- flow controlled by both culvert inlet and outlet; and
- uniform flow in the culvert barrel.

The latter flow type is a representation of culvert flow at base flow conditions.

Figure 1.3 Flow types at culverts: inlet control, inlet and outlet control, and uniform flow. The numbers 1, 2, and 3 indicate sections used in the structure's dynamic equation.



In the case of *inlet control* flow, the capacity of the culvert opening limits the capacity of the culvert. The flow in the culvert entrance is critical. The US Federal Highway Administration (USFHWA, 1985) has published

nomographs that estimate the *headwater* upstream of the culvert for a given discharge at the culvert.

The discharge at the inlet (section 2, referred to as a subscript in the equation below) is then

$$Q_2 = A_2 \sqrt{\frac{gA_2}{B_2}} \quad (1.7)$$

where the flow area and top width are for critical depth.

The US Federal Highway Administration (1985) distinguishes two headwater equations; one in the case where the inlet is not submerged and another in the case where the inlet is submerged. When the *inlet is not submerged* the headwater equation is

$$H_1 = h_2 + \frac{u_2^2}{2g} + D(C_1 \tilde{Q}_2^{C_2} - C_3 S_c) \quad (1.8)$$

and when the *inlet is submerged*

$$H_1 = D(C_4 \tilde{Q}_2^2 + C_5 - C_3 S_c) \quad (1.9)$$

where H is total head, u is velocity, D is height of the culvert barrel, S_c is slope of the culvert barrel, $\tilde{Q} = Q/(A_c \sqrt{D})$ in which A_c is the area of the culvert barrel, and C_1 through C_5 are coefficients depending on inlet and outlet characteristics, that is the type of culvert (USFHWA, 1985).

Equations (1.7) through (1.9) provide a framework to relate discharge at the culvert to stage upstream of the culvert at section 1.

If the tailwater elevation causes the culvert barrel to run full, both *culvert inlet and outlet control* the flow through the culvert. The dynamic equation then reads

$$Q_2 = A_2 \sqrt{\frac{2g(y_1 - y_3)}{C_L}} \quad (1.10)$$

where C_L is an energy-loss coefficient that is a combination of entrance, exit, and friction losses. Table 4.20 shows entrance loss coefficients given by USFHWA (1985). For a sudden expansion of flow, such as in a typical culvert, the exit loss coefficient is normally set to unity. In general, exit loss coefficients can vary between 0.3 and 1.0. The exit loss coefficient should be reduced as the transition becomes less abrupt. The friction loss coefficient, C_f , is calculated as

$$C_f = 2gL_c \frac{n^2}{R_2^{4/3}} \quad (1.11)$$

where L_c is the length of the culvert barrel, and R_2 is the hydraulic radius of the flow in the culvert barrel.

The flow depth in the culvert barrel is very small for the case of base flow in the channel. To improve the robustness of the solution algorithm CONCEPTS assumes *uniform flow* in the culvert. The *Manning equation* then gives discharge as

$$Q_2 = \frac{1}{n} A_2 R_2 \sqrt{S_c} \quad (1.12)$$

The shape of the culvert is defined by the USFHWA *chart and scale* numbers. The chart and scale number refer to a series of nomographs in USFHWA (1985). Table 4.19 lists the chart and scale numbers for pipe and box culverts.

Bridge Crossing

CONCEPTS distinguishes two, ‘low-flow conditions’ flow types at bridge crossings. *Low-flow conditions* exist when the free surface of the water is not in contact with the lower chord of the bridge deck. Henderson (1966) terms these *flow types A* and *B* (see Figure 1.4).

Class A Flow occurs when the flow through the bridge opening is subcritical. *Class B Flow* or “choked” flow occurs when the flow in the bridge opening is critical. The transition from class A to B and vice versa is a function of the contraction ratio σ , which is the ratio of the width of the bridge opening to the total width of the bridge crossing. Equating specific momentum at section 2 and section 3 yields the *limiting contraction ratio*

$$\sigma = \frac{(2 + 1/\sigma)^3 F_3^4}{(1 + 2F_3^2)^3} \quad (1.13)$$

where F is the flow Froude number.

From experiments on *Class A flow*, Yarnell (1934a, 1934b) obtained the following relation between the change in water-surface elevation across the bridge and the downstream Froude number

$$\frac{y_1 - y_3}{h_3} = C_p F_3^2 (C_p + 5F_3^2 - 0.6)(\hat{\sigma} + 15\hat{\sigma}^4) \quad (1.14)$$

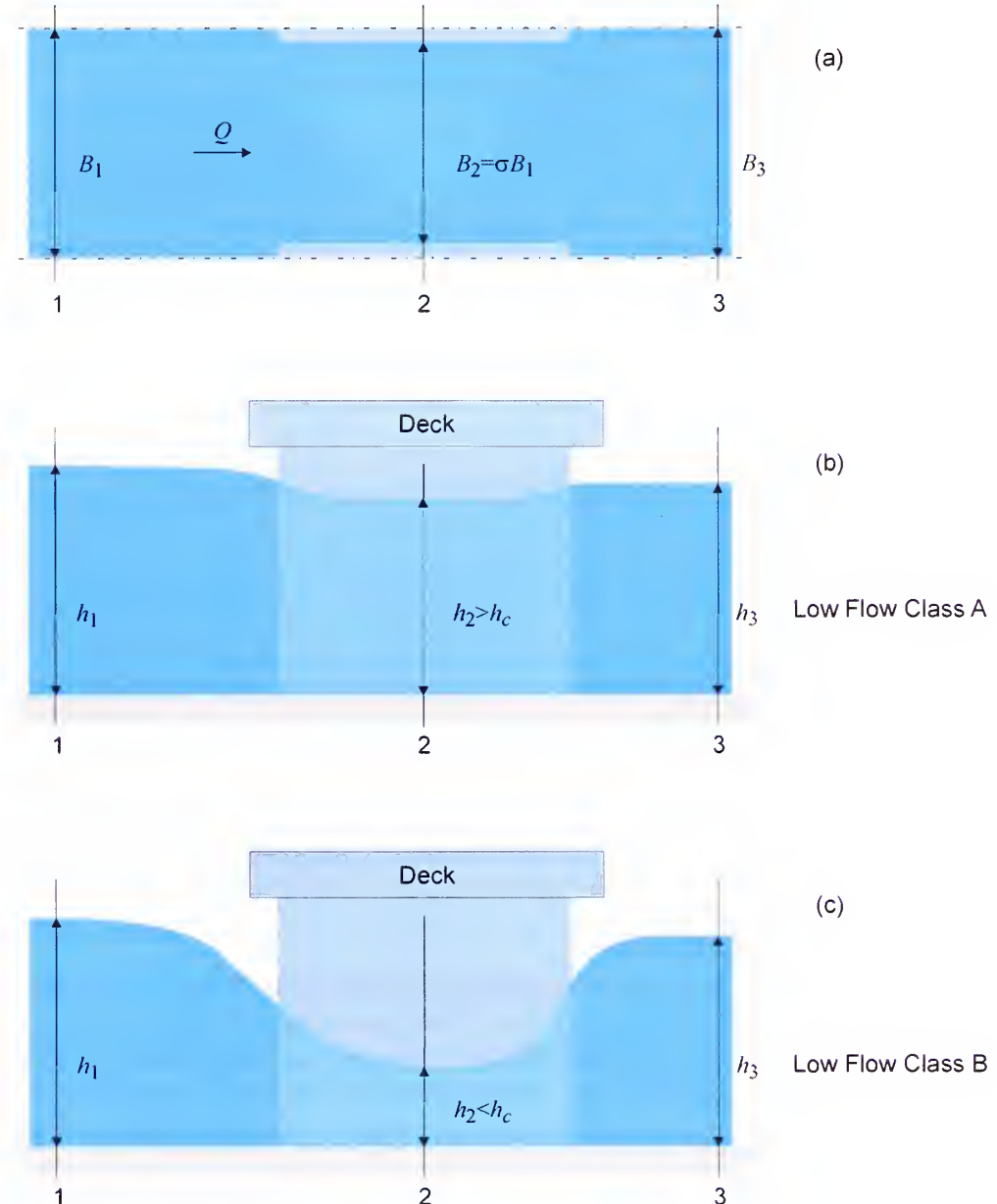
where C_p is a pier-shape coefficient, and $\hat{\sigma} = 1 - \sigma$. From (1.14) we can derive a relation between discharge at the bridge and upstream and downstream stages

$$Q_2 = A_3 \sqrt{0.1gh_3(C_p - 0.6) + \sqrt{0.01(C_p - 0.6)^2 + \frac{y_1 - y_3}{5h_3C_p(\hat{\sigma} + 15\hat{\sigma}^4)}}} \quad (1.15)$$

Table 4.22 lists values of the pier shape coefficient for various pier shapes.

Class B Flow is similar to inlet-control culvert flow. Therefore the governing equations are (1.7) and the headwater equation

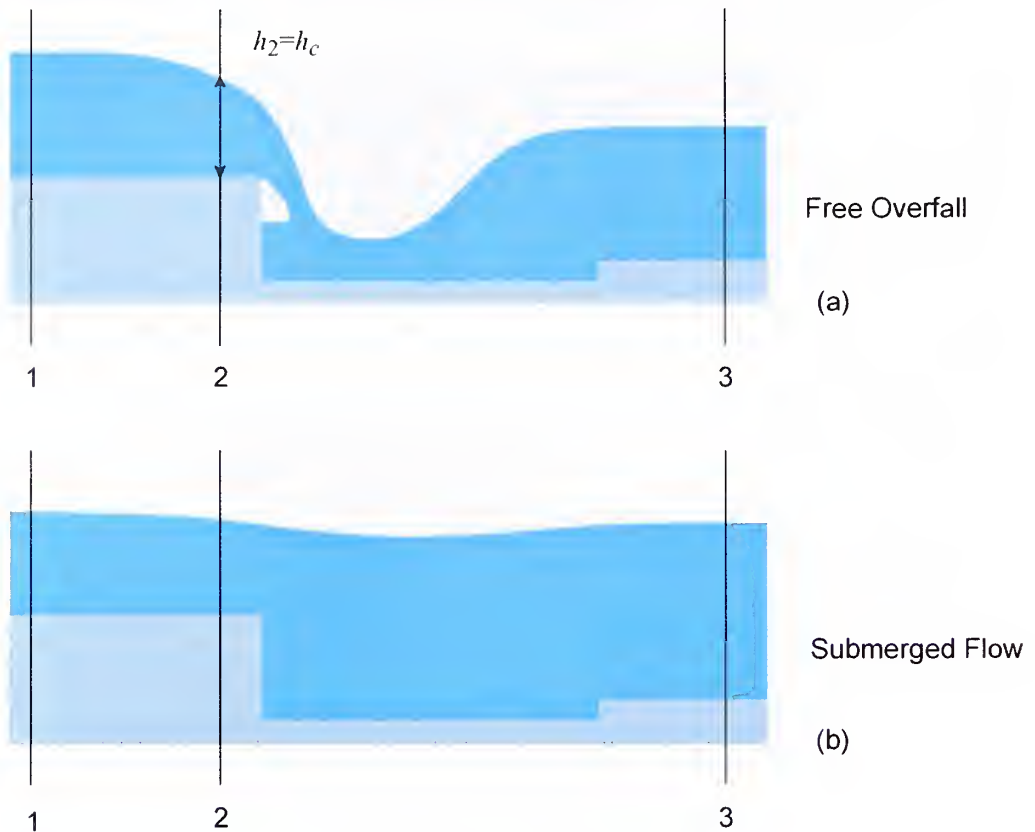
Figure 1.4 Flow at bridge crossings: (a) top view of bridge crossing showing a flow contraction at section 2; and lateral views of (b) Low Flow Class A and (c) Low Flow Class B. The numbers 1, 2, and 3 indicate sections used in the structure's dynamic equation.



$$H_1 = h_2 + \frac{u_2^2}{2g} + C_{L_p} \frac{1}{2g} \left(\frac{Q}{A} \right)_3^2 \quad (1.16)$$

where \$C_{L_p}\$ is an energy-loss coefficient depending on pier shape. For square-ended piers \$C_{L_p} = 0.35\$ and for rounded ends \$C_{L_p} = 0.18\$. The above values of energy loss are for a pier length-width ratio of four; longer piers increase the loss. Hendersen (1966) states that the amount of increase is approximately 5% and 10% for 7:1 (length:width) and 13:1 piers respectively, with rounded ends.

Figure 1.5 Flow at a drop structure: (a) free overfall and (b) submerged flow. The numbers 1, 2, and 3 indicate sections used in the structure's dynamic equation.



For the square-ended piers the backwater was slightly less for longer piers than for the 4:1 pier.

Drop Structure

CONCEPTS distinguishes two flow types at drop structures based on the *degree of submergence* of the drop structure (see Figure 1.5). The flow at the brink of the drop structure is a *free (ventilated) overfall* for low tailwater elevations, and is, therefore, critical. The drop structure becomes *submerged* for high tailwater elevations resulting in a non-ventilated overfall condition.

In the case of *critical flow* the governing equations are (1.7) and an expression for the headwater

$$H_1 = h_2 + \frac{u_2^2}{2g} + C_{L_d} \frac{1}{2g} \left(\frac{Q}{A} \right)_1^2 \quad (1.17)$$

where C_{L_d} is an energy-loss coefficient representing entrance losses.

In the case of a *submerged* drop structure, both upstream and downstream flow conditions control the flow at the drop structure. CONCEPTS uses (1.10) to compute discharge. Future versions of CONCEPTS will incorporate an

improved description of this flow type based on the work of Wu and Rajaratnam (1996,1998).

Generic Structure

A generic structure is any structure for which a rating curve is available. The governing equations are the *rating curve*

$$Q_2 = Q(h_2) \quad (1.18)$$

and the *headwater equation*

$$H_1 = h_2 + \frac{u_2^2}{2g} + C_{L_g} \frac{1}{2g} \left(\frac{Q}{A} \right)_1^2 \quad (1.19)$$

where C_{L_g} is an energy-loss coefficient representing entrance losses at the generic structure.

Implementation of Hydraulics Submodel

Representation of Stream Cross-Section and Stream Corridor

Corridor

The *stream corridor* is schematized as *reaches* connecting *cross sections* (Figure 1.6). A reach is a *stream segment* that transfers information between two cross sections. A cross section is a *node* that holds hydraulic information. The information transferred between cross sections tells CONCEPTS how the flow at one cross section relates to the flow at its upstream and downstream cross section.

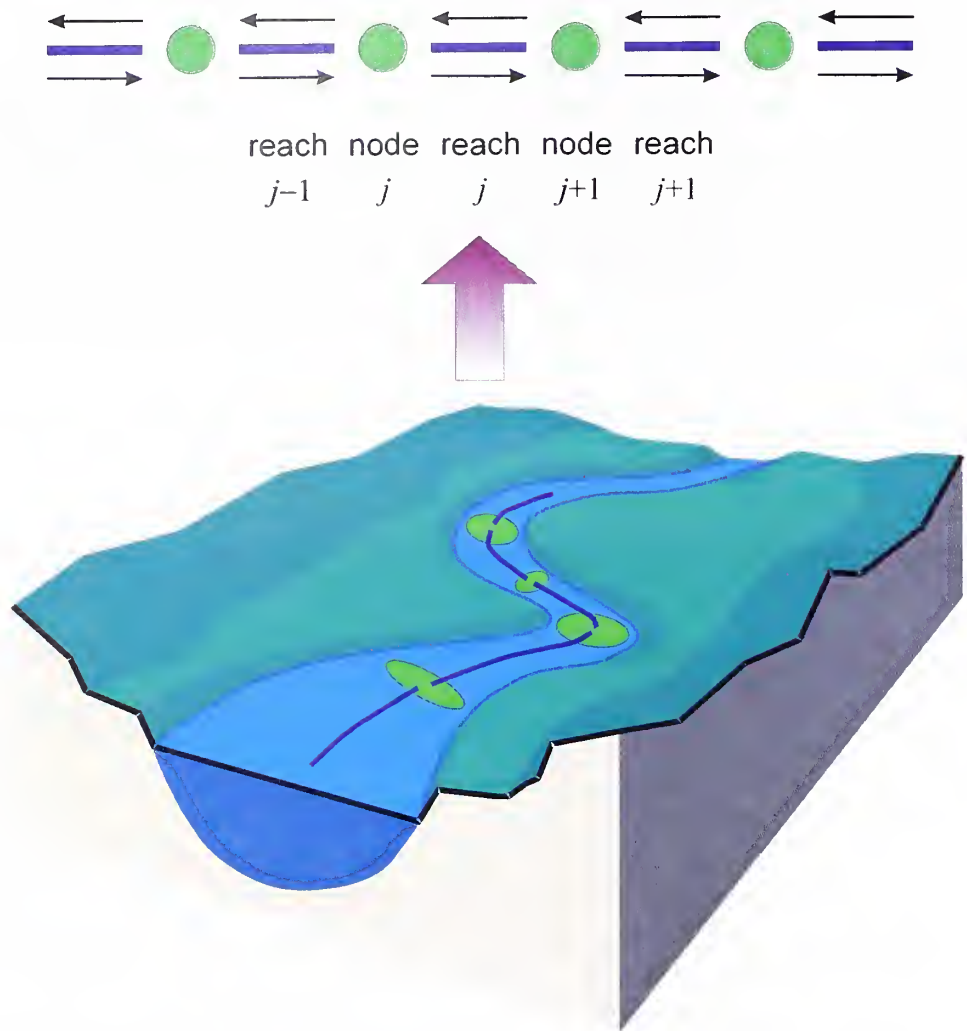
CONCEPTS assumes that the channel is straight. A sinuous stream therefore needs to be mapped to a straight line (Figure 1.7). CONCEPTS does not require any data to be entered for reaches. CONCEPTS automatically determines reach profile and length from river kilometer and thalweg elevation of its upstream and downstream cross sections.

Cross Section

Cross sections specify the boundary geometry of the stream corridor. Cross sections characterize the flow-carrying capability of the stream and its adjacent floodplain. They should extend across the entire floodplain and should be perpendicular to the anticipated flow lines.

Cross sections are required at representative locations throughout the stream corridor. They must accurately represent the streamwise changes in flow, bed slope, shape, flow-resistance characteristics, and bank- and bed-material geotechnical properties (i.e., cohesion, angle of internal friction, soil-water properties, etc.). Where abrupt changes occur, several cross sections should be

Figure 1.6 Representation of a stream corridor as reaches and nodes (arrows depict information exchanged among adjacent nodes).



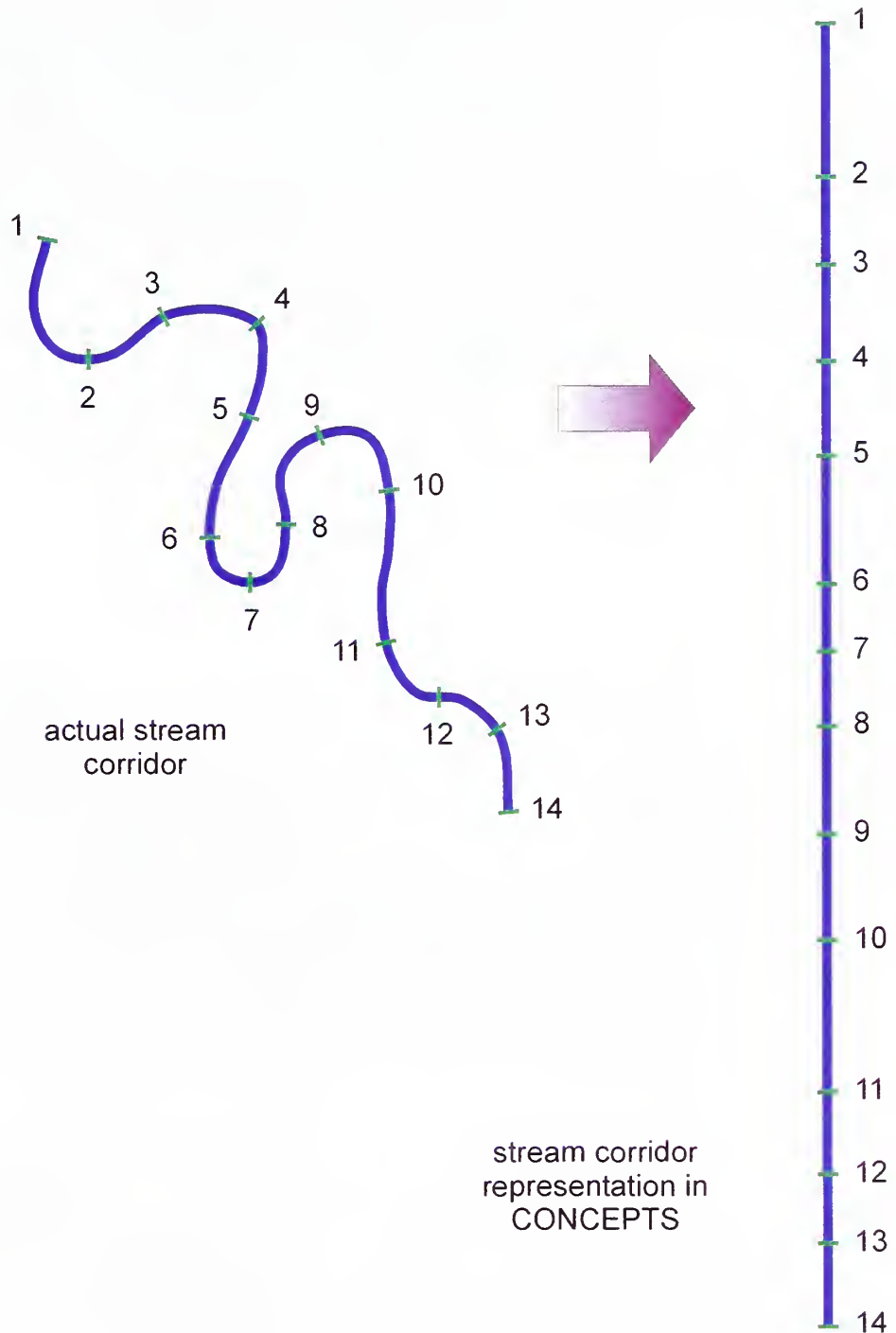
used to describe the change. Fread (1988) gives the following maximum computational space step or distance between cross sections, Δx :

$$\Delta x \leq \frac{cT}{20} \quad (1.20)$$

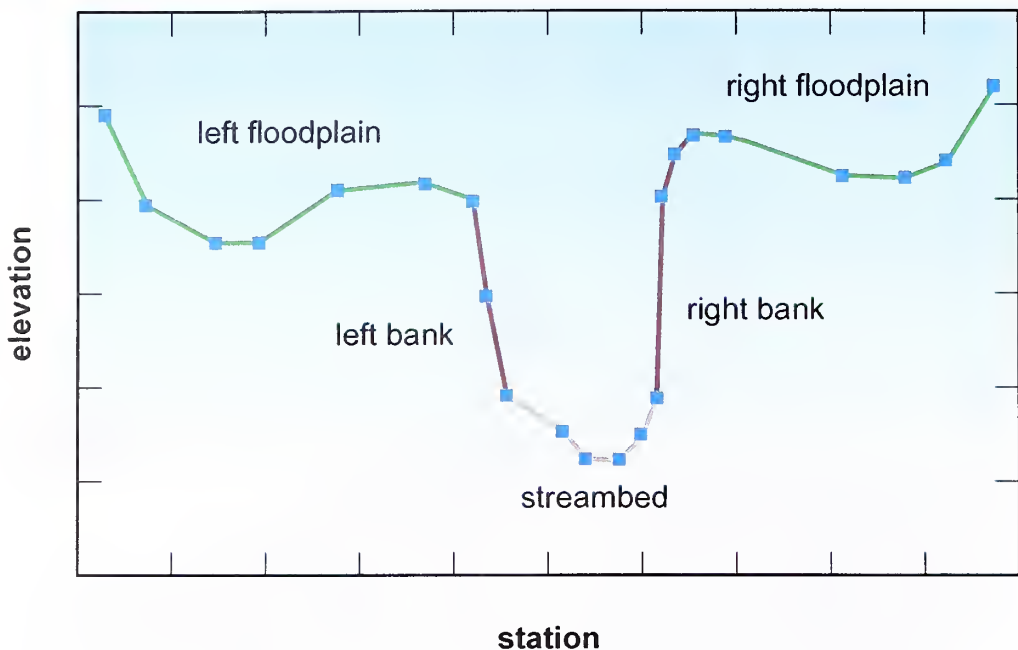
where c is celerity of the flood wave propagating through the stream corridor. Basco (1987) states that the ratio of flow area at successive cross sections should not be smaller than 0.635 or larger than 1.576. This condition results in the following approximation for the maximum space step (Fread, 1988):

$$\Delta x < \frac{L}{1 + 2|A_j - A_{j+1}|/\hat{A}} \quad (1.21)$$

where $\hat{A} = A_{j+1}$ for a contracting reach and $\hat{A} = A_j$ for an expanding reach, and L is the original distance between adjacent cross sections at space indices j and $j+1$.

Figure 1.7 Projection of a meandering stream corridor onto a straight line.

Each cross section is identified by a cross section label and a river kilometer. In CONCEPTS-1.0 river kilometer has to increase in streamwise direction. Station and elevation describe the profile of the cross section (Figure 1.8). Station values must increase from left to right. The user needs to identify left floodplain, left bank, streambed, right bank, and right floodplain.

Figure 1.8 Representation of cross section geometry.

Flow Resistance

CONCEPTS uses *Manning n* to parameterize the *resistance to flow* in a watercourse. Manning *n* represents the effect of roughness elements on the floodplain, channel banks, and bed (Figure 1.9). Also, small eddy losses due to mild expansion and contraction of reaches as well as river bend losses are often included as components of the Manning *n*.

Manning *n* varies with the magnitude of flow. For example, as flow increases and more portions of the bank and overbank become flooded, the vegetation at these elevations causes an increase in the resistance to flow. There are some basic references available for estimating *n* values: e.g., Cowan (1956), Chow (1959), USSCS (1975), USFHWA (1979), Coon (1998). Table 4.13 lists *n* values for various types of channels from Chow (1959).

CONCEPTS allows the user to input different Manning *n* values for streambed, left and right banks, and left and right floodplains. It uses the method of Garbrecht (1990) to compute an *equivalent friction factor* for the wetted section of the cross section. The flow area comprises sections affected only by either left floodplain, left bank, channel bed, right bank, or right floodplain (see Figure 1.10). The user can select from two methods to divide the sections:

- Method 1. The boundaries between the sections are vertical.
- Method 2. The boundaries between floodplain and bank sections are vertical, and those between bank and bed sections bisect the angle between bed and bank profile.

Figure 1.9 Example of roughness elements on a cross section: trees and grasses on the floodplain, grasses on the left bank, and rocks and sediment particles on the bed.

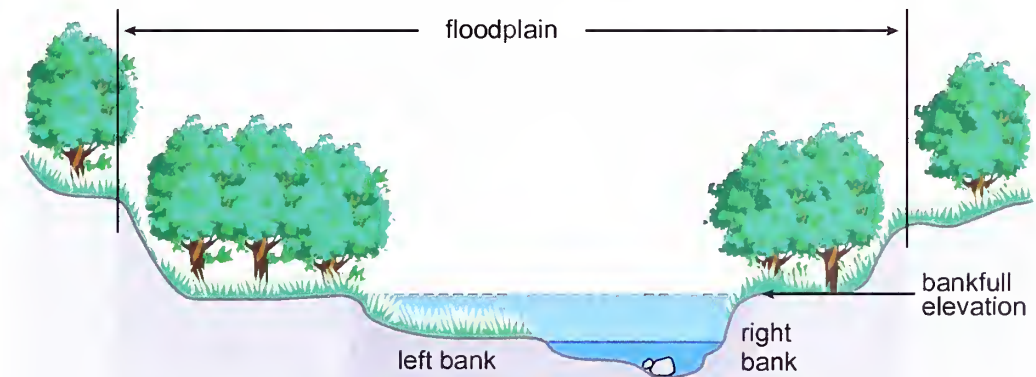
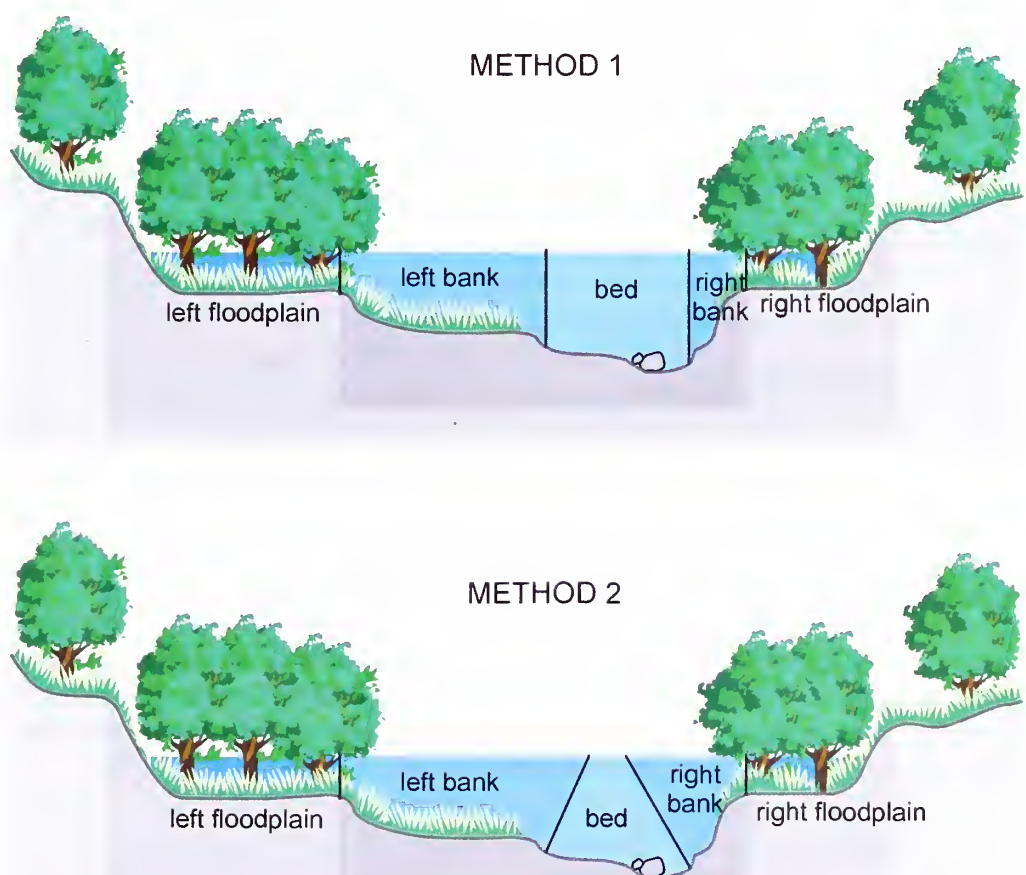


Figure 1.10 Segmentation of flow area to compute effective friction factor. Method 1 uses vertical boundaries between the subsections. Method 2 uses vertical boundaries between floodplain and bank sections, and boundaries between bed and bank sections that bisect the angle between bed and bank profiles.



We compute the equivalent roughness, n_e , as

$$n_e = \frac{AR_e^{2/3}}{K} \quad (1.22)$$

where flow area A and conveyance K are calculated as a summation of the flow area and conveyance of each section (left floodplain, left bank, bed, right bank, right floodplain)

$$A = \sum_{\text{sections}} A_i \quad (1.23a)$$

$$K = \sum_{\text{sections}} K_i = \sum_{\text{sections}} \frac{1}{n_i} A_i R_i \quad (1.23b)$$

and the equivalent hydraulic radius R_e is a conveyance-weighted average over the sections

$$R_e = \frac{1}{K} \sum_{\text{sections}} K_i R_i \quad (1.23c)$$

Equations (1.22) through (1.23c) assure continuity and a smooth increase in total conveyance as the water surface rises above overbank elevation. For the case of uniform flow, the equivalent one-dimensional representations (1.22) and (1.23c) of roughness and hydraulic radius yield the same total discharge as that obtained by summing the flow rates of each section (two-dimensional approach). The equivalent hydraulic radius is not necessarily a monotonous increasing function of flow depth. A decrease may occur as flow moves from predominantly main channel to predominantly overbank flow.

Figure 1.11 shows flow area, conveyance, equivalent hydraulic radius, and equivalent Manning n for the cross section shown in Figures 1.9 and 1.10, and using ‘Method 2’ (cf. Figure 1.10) to segment the cross section. The following n values were assigned to the sections: left floodplain, 0.20; left bank, 0.08; bed, 0.03; right bank, 0.03; and right floodplain, 0.20. In this case equivalent hydraulic radius is a monotonous increasing function of flow depth because the floodplain is relatively narrow.

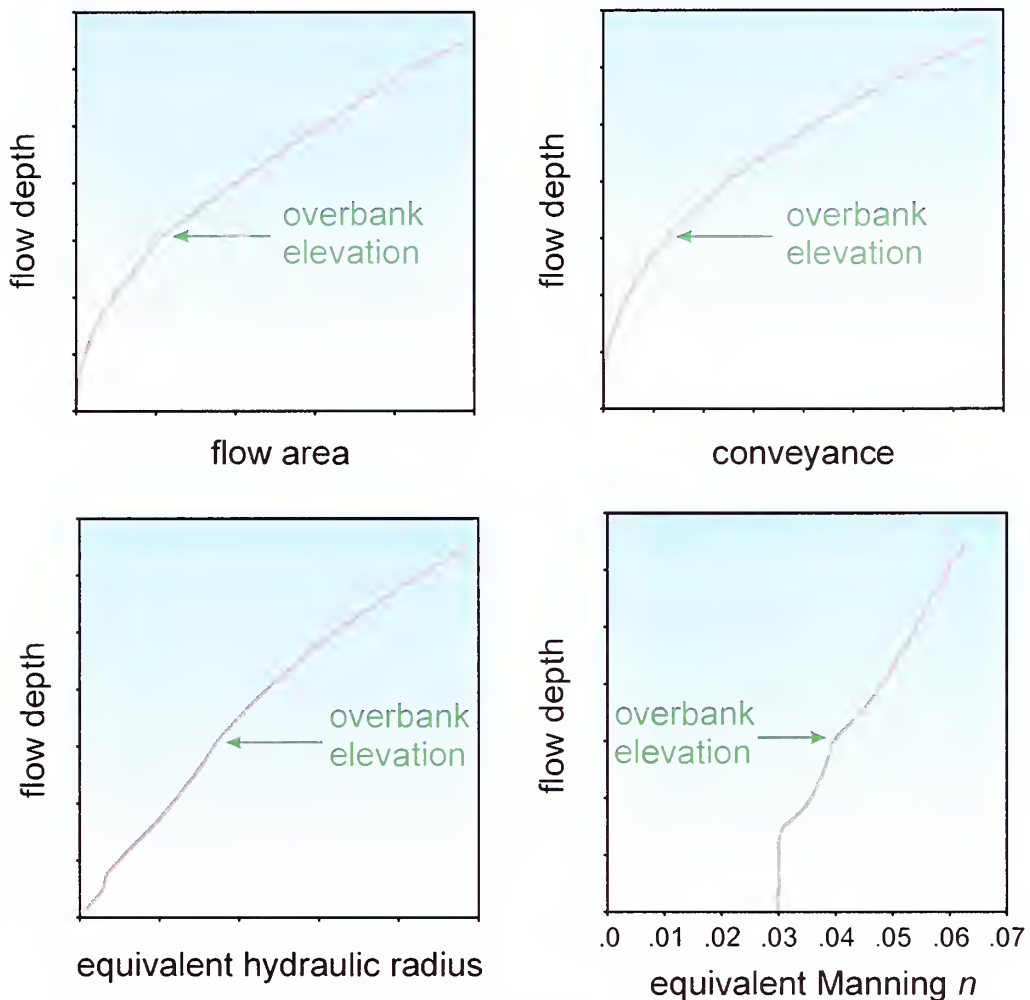
Computation of Flow Variables

The flow variables: flow area, hydraulic radius, wetted perimeter, top width, conveyance, and Manning n vary with flow depth, and have to be updated when flow depth changes during a runoff event. It is computationally time-consuming to recalculate these flow variables at each time step. There exist two methods to represent the flow variables:

- 1** look-up tables, and
- 2** power functions.

Look-up tables store values of flow variables at a series of flow depths that range from zero at the channel bed to the flow depth at the valley elevation.

Figure 1.11 Flow area, conveyance, equivalent hydraulic radius, and equivalent Manning n as a function of flow depth for the cross section shown in Figure 1.9. Manning n values assigned to the sections are: floodplain $n=0.20$, left bank $n=0.08$, bed and right bank $n=0.03$.



Finding the depth interval in the look-up table that contains a given flow depth and interpolating provide the values of flow variables.

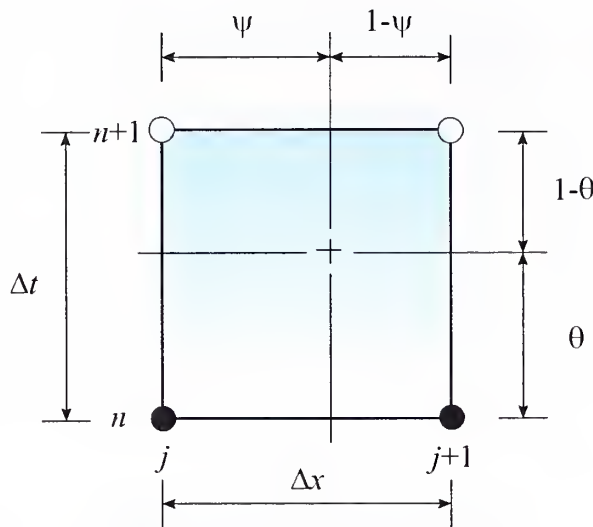
Power functions represent the flow variables as (Garbrecht, 1990)

$$\text{flow variable} = \alpha h^\beta \quad (1.24)$$

where α and β are coefficient and exponent of the power function, respectively. Power functions may accurately represent flow variables if they vary monotonically with depth, as Figure 1.11 depicts. However, the values of flow variables may locally vary markedly if the cross-sectional profile is quite irregular, which cannot be represented by power functions. Also, hydraulic radius may decrease when the water surface rises above the overbank elevation, before increasing further.

Look-up tables are more accurate than power functions and are, therefore, used by CONCEPTS.

Figure 1.12 Preissmann scheme in x - t space: ●, node with known values of the dependent variables Q and y ; ○, node with unknown values of Q and y ; and +, point at which the dependent variables and their derivatives are approximated.



Discretization

Generalized Preissmann Scheme

There exist many approaches to approximate the system of governing equations: (1.1) and (1.2) for the dynamic wave model and (1.1) and (1.4) for the diffusion wave model. CONCEPTS uses the *generalized Preissmann scheme* (Abbott and Basco, 1989). The advantages of the Preissmann scheme are among others:

- It has been extensively used by many scientists with good results.
- It is simple, robust, and compact.
- It allows a variable spatial grid.
- It is implicit in time.

This scheme is also known as the *box implicit scheme* because of the way it approximates the hydraulic variables (see Figure 1.12). *Implicit time integration* allows large time steps, reducing the computational effort associated with long-term simulations.

The generalized Preissmann scheme approximates any variable f and its spatial and temporal derivatives as (see Figure 1.12):

$$f(x, t) = \theta[\psi f_{j+1}^{n+1} + (1 - \psi)f_j^{n+1}] + (1 - \theta)[\psi f_{j+1}^n + (1 - \psi)f_j^n] \quad (1.25a)$$

$$\frac{\partial}{\partial t} f(x, t) = \psi \frac{f_{j+1}^{n+1} - f_{j+1}^n}{\Delta t} + (1 - \psi) \frac{f_j^{n+1} - f_j^n}{\Delta t} \quad (1.25b)$$

$$\frac{\partial}{\partial x} f(x, t) = \theta \frac{f_{j+1}^{n+1} - f_j^{n+1}}{\Delta x} + (1 - \theta) \frac{f_{j+1}^n - f_j^n}{\Delta x} \quad (1.25c)$$

where j is space index denoting the location of a cross section, n is time index denoting a time level, and θ ($0 \leq \theta \leq 1$) and ψ ($0 \leq \psi \leq 1$) are temporal and spatial weighting factors, respectively to provide model flexibility with respect to numerical stability and convergence of the solution. Setting the spatial weighting factor $\psi = 0.5$ reduces the scheme to Preissmann's original scheme (Preissmann, 1961).

Approximations of Governing Equations of Open-Channel Flow

It is convenient to express temporal variations of hydraulic variables in *variations of the dependent variables* stage and discharge, for example the flow area at cross section j and time level $n+1$ reads

$$A_j^{n+1} = A_j^n + \left(\frac{\partial A}{\partial y} \right)_j^n \Delta y_j + \left(\frac{\partial A}{\partial Q} \right)_j^n \Delta Q_j \quad (1.26)$$

where the differential changes in stage and discharge are $\Delta y = y^{n+1} - y^n$ and $\Delta Q = Q^{n+1} - Q^n$, respectively.

Substituting the above approximations of variables and their derivatives in the governing equations of open-channel flow (1.1) through (1.3) yields a *nonlinear* system of equations. We can *linearize* the equations by assuming that the differential changes in stage and discharge are much smaller than the respective values of stage and discharge. Consequently, we obtain a system of *finite difference continuity* and *momentum equations* expressed in the unknown quantities Δy_j , Δy_{j+1} , ΔQ_j , and ΔQ_{j+1} of the form:

$$A_j \Delta y_j + B_j \Delta Q_j + C_j \Delta y_{j+1} + D_j \Delta Q_{j+1} = E_j \quad (1.27a)$$

$$F_j \Delta y_j + G_j \Delta Q_j + H_j \Delta y_{j+1} + I_j \Delta Q_{j+1} = J_j \quad (1.27b)$$

where the coefficients A_j through J_j are flow-depending coefficients. The coefficients A_j through E_j are:

$$A_j = \frac{1 - \Psi}{\Delta t} B_j^n \quad (1.28a)$$

$$B_j = -\frac{\theta}{\Delta x} \quad (1.28b)$$

$$C_j = \frac{\Psi}{\Delta t} B_{j+1}^n \quad (1.28c)$$

$$D_j = \frac{\theta}{\Delta x} \quad (1.28d)$$

$$\begin{aligned} E_j = & -\frac{\Psi}{\Delta t}[A_{j+1}^* - A_{j+1}^n] - \frac{1-\Psi}{\Delta t}[A_j^* - A_j^n] \\ & - \frac{\theta}{\Delta x}[Q_{j+1}^* - Q_j^*] - \frac{1-\theta}{\Delta x}[Q_{j+1}^n - Q_j^n] \end{aligned} \quad (1.28e)$$

In the case of the dynamic wave model the coefficients F_j through J_j are:

$$\begin{aligned} F_j = & -\frac{2\theta(1-\Psi)}{\Delta x} \frac{u_j^n}{(h_d)_j^n} [Q_{j+1}^n - Q_j^n] \\ & + \frac{\theta}{\Delta x} \left[B_j^n (\Psi(u_{j+1}^n)^2 + (1-\Psi)(u_j^n)^2) \right. \\ & \left. + 2(1-\Psi) \frac{(u_j^n)^2}{(h_d)_j^n} (A_{j+1}^n - A_j^n) \right] \\ & + g \frac{\theta}{\Delta x} [(1-\Psi)B_j^n(y_{j+1}^n - y_j^n) - (\Psi A_{j+1}^n + (1-\Psi)A_j^n)] \\ & - g\theta \left[2(1-\Psi)(\Psi A_{j+1}^n + (1-\Psi)A_j^n) \frac{(S_f)_j^n}{K_j^n} \left(\frac{\partial K}{\partial y} \right)_j^n \right. \\ & \left. - (1-\Psi)B_j^n [\Psi(S_f)_{j+1}^n + (1-\Psi)(S_f)_j^n] \right] \end{aligned} \quad (1.28f)$$

$$\begin{aligned} G_j = & \frac{1-\Psi}{\Delta t} - \frac{2\theta}{\Delta x} \left[(\Psi u_{j+1}^n + (1-\Psi)u_j^n) - (1-\Psi) \frac{Q_{j+1}^n - Q_j^n}{A_j^n} \right] \\ & - \frac{2\theta(1-\Psi)}{\Delta x} (A_{j+1}^n - A_j^n) \frac{(u_j^n)^2}{Q_j^n} \\ & + 2g\theta(1-\Psi)(\Psi A_{j+1}^n + (1-\Psi)A_j^n) \frac{(S_f)_j^n}{Q_j^n} \end{aligned} \quad (1.28g)$$

$$H_j = -\frac{2\theta\Psi}{\Delta x} \frac{u_{j+1}^n}{(h_d)_{j+1}^n} (Q_{j+1}^n - Q_j^n) \quad (1.28h)$$

$$\begin{aligned} & -\frac{\theta}{\Delta x} \left[B_{j+1}^n (\Psi(u_{j+1}^n)^2 + (1-\Psi)(u_j^n)^2) \right. \\ & \left. - 2\Psi \frac{(u_{j+1}^n)^2}{(h_d)_{j+1}^n} (A_{j+1}^n - A_j^n) \right] \end{aligned}$$

$$+ g\theta [\Psi B_{j+1}^n (y_{j+1}^n - y_j^n) + (\Psi A_{j+1}^n + (1-\Psi)A_j^n)]$$

$$\begin{aligned} & -g\theta \left[2\Psi(\Psi A_{j+1}^n + (1-\Psi)A_j^n) \frac{(S_f)_{j+1}^n}{K_{j+1}^n} \left(\frac{\partial K}{\partial y} \right)_{j+1}^n \right. \\ & \left. - \Psi B_{j+1}^n (\Psi(S_f)_{j+1}^n + (1-\Psi)(S_f)_j^n) \right] \end{aligned}$$

$$I_j = \frac{\Psi}{\Delta t} + \frac{2\theta}{\Delta x} \left[(\Psi u_{j+1}^n + (1-\Psi)u_j^n) + \Psi \frac{Q_{j+1}^n - Q_j^n}{A_{j+1}^n} \right] \quad (1.28i)$$

$$- \frac{2\theta\Psi}{\Delta x} (A_{j+1}^n - A_j^n) \frac{(u_{j+1}^n)^2}{Q_{j+1}^n}$$

$$+ 2g\theta\Psi(\Psi A_{j+1}^n + (1-\Psi)A_j^n) \frac{(S_f)_{j+1}^n}{Q_{j+1}^n}$$

$$\begin{aligned}
J_j = & -\frac{1-\Psi}{\Delta t}(\mathcal{Q}_j^* - \mathcal{Q}_j^n) - \frac{\Psi}{\Delta t}(\mathcal{Q}_{j+1}^* - \mathcal{Q}_{j+1}^n) \\
& - \frac{2}{\Delta x}[\theta(\Psi u_{j+1}^* + (1-\Psi)u_j^*) + (1-\theta)(\Psi u_{j+1}^n + (1-\Psi)u_j^n)] \\
& \times [(1-\theta)(\mathcal{Q}_{j+1}^n - \mathcal{Q}_j^n) + \theta(\mathcal{Q}_{j+1}^* - \mathcal{Q}_j^*)] \\
& + [\theta(\Psi(u_{j+1}^*)^2 + (1-\Psi)(u_j^*)^2) + (1-\theta)(\Psi(u_{j+1}^n)^2 + (1-\Psi)(u_j^n)^2)] \\
& \times \frac{1}{\Delta x}[(1-\theta)(A_{j+1}^n - A_j^n) + \theta(A_{j+1}^* - A_j^*)] \\
& - g[\theta(\Psi A_{j+1}^* + (1-\Psi)A_j^*) + (1-\theta)(\Psi A_{j+1}^n + (1-\Psi)A_j^n)] \\
& \times \left\{ \frac{1}{\Delta x}[(1-\theta)(y_{j+1}^n - y_j^n) + \theta(y_{j+1}^* - y_j^*)] \right. \\
& + \left[\theta(\Psi(S_f)_{j+1}^* + (1-\Psi)(S_f)_j^*) \right. \\
& \left. \left. + (1-\theta)(\Psi(S_f)_{j+1}^n + (1-\Psi)(S_f)_j^n) \right] \right\}
\end{aligned} \tag{1.28j}$$

where $h_d = A/B$ is hydraulic depth.

In the case of the diffusion wave model the coefficients F_j through J_j are:

$$F_j = -\theta \left[\frac{1}{\Delta x} + 2(1-\Psi) \frac{(S_f)_j^n}{K_j^n} \left(\frac{\partial K}{\partial y} \right)_j^n \right] \tag{1.28k}$$

$$G_j = 2\theta(1-\Psi) \frac{(S_f)_j^n}{\mathcal{Q}_j^n} \tag{1.28l}$$

$$H_j = \theta \left[\frac{1}{\Delta x} - 2\Psi \frac{(S_f)_{j+1}^n}{K_{j+1}^n} \left(\frac{\partial K}{\partial y} \right)_{j+1}^n \right] \tag{1.28m}$$

$$I_j = 2\theta\Psi \frac{(S_f)_{j+1}^n}{\mathcal{Q}_{j+1}^n} \tag{1.28n}$$

$$\begin{aligned}
J_j = & -\frac{\theta}{\Delta x}(y_{j+1}^* - y_j^*) - \frac{1-\theta}{\Delta x}(y_{j+1}^n - y_j^n) \\
& - \theta[\psi(S_f)_{j+1}^* + (1-\psi)(S_f)_j^*] \\
& - (1-\theta)[\psi(S_f)_{j+1}^n + (1-\psi)(S_f)_j^n]
\end{aligned} \tag{1.28o}$$

We must solve (1.27a) and (1.27b) iteratively to advance the solution from time t^n to time t^{n+1} . The superscript * in (1.28e), (1.28j), and (1.28o) denotes that the flow variable is evaluated using the solution obtained in the latest iteration step.

Solution Method

Double Sweep Algorithm

The system of finite difference equations (1.27a), (1.27b), (1.39a), and (1.39b) forms a pentadiagonal matrix. CONCEPTS successively applies the *double sweep method* or Thomas algorithm to solve the pentadiagonal matrix (Roache, 1977). The computed increments Δy and ΔQ are used to update the flow variables at time t^* , and consequently the coefficients E_j and J_j . The iteration method is stopped when the solutions of y and Q have converged, that is $\Delta h \rightarrow 0$ and $\Delta Q \rightarrow 0$. The paragraphs below briefly discuss the implementation.

We introduce the auxiliary variables S_j and T_j to linearly relate the unknown differential increments Δy_j and ΔQ_j as:

$$\Delta Q_j = S_j \Delta y_j + T_j \tag{1.29}$$

Substituting (1.29) into (1.27a) and (1.27b), and eliminating Δy_j yields

$$\Delta Q_{j+1} = S_{j+1} \Delta y_{j+1} + T_{j+1} \tag{1.30}$$

where

$$S_{j+1} = \frac{(F_j + G_j S_j) C_j - (A_j + B_j S_j) H_j}{(A_j + B_j S_j) I_j - (F_j + G_j S_j) D_j} \tag{1.31a}$$

$$T_{j+1} = \frac{(J_j - G_j T_j)(A_j + B_j S_j) - (E_j - B_j T_j)(F_j + G_j S_j)}{(A_j + B_j S_j) I_j - (F_j + G_j S_j) D_j} \tag{1.31b}$$

In the first, *forward sweep* we apply (1.31a) and (1.31b) recursively, with j varying from 1 to $J-1$ with J being the number of cross sections of the schematized stream corridor. The upstream boundary conditions specify the values of S_1 and T_1 . After completion of the first sweep, the calculated values of S_J and T_J and the downstream boundary condition enable the computation of Δy_J and ΔQ_J . In the second, *backward sweep* we compute Δy_j from

$$\Delta y_j = \frac{(E_j - B_j T_j) - (C_j \Delta y_{j+1} + D_j \Delta Q_{j+1})}{(A_j + B_j S_j)} \quad (1.32)$$

and ΔQ_j from (1.29) by applying the equations recursively, with j varying from $J-1$ to 1.

Treatment of External Boundary Conditions

Discharge hydrographs, $Q_1 = Q(t)$, are imposed at the *upstream boundary* of the stream corridor. The coefficients S_1 and T_1 read

$$S_1 = 0 \text{ and } T_1 = Q_1^{n+1} - Q_1^n \quad (1.33)$$

At the *downstream boundary* a *rating curve* is imposed. The user can specify a *rating curve* when one is available, or CONCEPTS can calculate a *loop-rating curve* based on local flow conditions. The user-specified rating curve has the form of a multi-segment power function:

$$Q = f(h) = \begin{cases} \alpha_1 h^{\beta_1} & h \leq h_1 \\ \alpha_2 h^{\beta_2} & h_1 < h \leq h_2 \\ \dots & \dots \\ \alpha_{N_{rs}} h^{\beta_{N_{rs}}} & h > h_{N_{rs}-1} \end{cases} \quad (1.34)$$

where N_{rs} is the number of segments comprising the rating curve, and α_i , β_i , and h_i are coefficient, exponent, and breakpoint of rating curve segment i . If there is only one segment, h_1 should be set to a very large number.

A loop-rating boundary condition allows the unsteady wave to pass the outlet with minimal disturbance of the outlet itself. We assume the following relation between discharge and stage at the outlet

$$Q = f(h) = K(h) \sqrt{S_f} \quad (1.35)$$

Rewriting the momentum equation (1.2) yields an expression for the friction slope in (1.35)

$$S_f = -\left[\frac{\partial y}{\partial x} + \frac{1}{gA} \left(\frac{\partial Q}{\partial t} + \frac{\partial}{\partial x} \left(\frac{Q^2}{A} \right) \right) \right] \quad (1.36)$$

In the case of the diffusion wave model we only retain the water surface slope in (1.36). We approximate (1.36) as

$$S_f = -\left[\frac{y_J^n - y_{J-1}^n}{\Delta x} + \frac{1}{gA_J^n} \left(\frac{Q_J^n - Q_{J-1}^{n-1}}{\Delta t} + \frac{(Q^2/A)_J^n - (Q^2/A)_{J-1}^n}{\Delta x} \right) \right] \quad (1.37)$$

The flow depth increment at the outlet is then

$$\Delta y_J = \frac{T_J + Q_J^n - f^n}{\frac{df}{dy} - S_J} \quad (1.38)$$

Treatment of Internal Boundary Conditions

Similar to the open-channel flow equations, we express the approximated continuity and dynamic equations of flow at hydraulic structures in terms of differential changes of the dependent variables:

$$\Delta Q_1 - \Delta Q_3 = Q_3^n - Q_1^n \quad (1.39a)$$

$$\Delta Q_1 - \frac{\partial f}{\partial y_1} \Delta y_1 - \frac{\partial f}{\partial y_3} \Delta y_3 = f^n - Q_1^n \quad (1.39b)$$

where f represents the dynamic equation of the structure. Equations (1.39a) and (1.39b) are equivalent to (1.27a) and (1.27b).

We can derive analytical expressions of the derivatives of f with respect to y_1 and y_3 . However, if the *structure* is a *control*, that is the flow at the structure is critical, this approach is not very robust. In this case we approximate the derivative of f with respect to y_1 as

$$\frac{\partial f}{\partial y_1} = \frac{2\Delta Q}{y_1(Q + \Delta Q) - y_1(Q - \Delta Q)} \quad (1.40)$$

where $y_1(Q)$ is the headwater equation and ΔQ is a pre-set discharge increment.

One-Equation Diffusion Wave Model

The Preissmann scheme applied to the dynamic wave or diffusion-wave model will predict unrealistic solutions of the dependent variables when there are large increases of discharge and flow depth at the upstream end of a computational section (e.g., when a flood wave enters the computational section). We can readily show this through the discretized continuity equation from which we obtain the following expression for the differential change of stage at the downstream end of a reach Δy_{j+1} :

$$\frac{\Psi}{\Delta t} B_{j+1}^n \Delta y_{j+1} = -\frac{1-\Psi}{\Delta t} B_j^n \Delta y_j + \frac{\theta}{\Delta x} (\Delta Q_j - \Delta Q_{j+1}) - \frac{1}{\Delta x} (Q_{j+1}^n - Q_j^n) \quad (1.41)$$

When a flood wave enters the reach, Δy_j and ΔQ_j are positive and may be quite large. Assuming $\Delta Q_{j+1} \approx 0$ and $Q_{j+1}^n - Q_j^n \approx 0$, Δy_{j+1} is negative and quite large. As a consequence, the predicted flow depth h_{j+1} may become negative. If this condition occurs, CONCEPTS switches to the ‘one-equation’ diffusion wave model.

We can reformulate the diffusion wave model as a single equation in either discharge or stage by eliminating one of the dependent variables. We can

eliminate stage by taking the derivative of (1.1) with respect to x and subtracting the derivative of (1.4) with respect to t . This yields the *one-equation diffusion wave model*:

$$\frac{\partial \underline{Q}}{\partial t} + c \frac{\partial \underline{Q}}{\partial x} - D \frac{\partial^2 \underline{Q}}{\partial x^2} = \hat{c} q \quad (1.42)$$

where the celerity \hat{c} is

$$\hat{c} = \frac{\underline{Q}}{BK} \frac{dK}{dh} \quad (1.43)$$

which is also known as the kinematic wave celerity, the celerity c is

$$c = \hat{c} + \frac{D \partial B}{B \partial x} \quad (1.44)$$

and the diffusion coefficient

$$D = \frac{\underline{Q}}{2BS_f} \quad (1.45)$$

CONCEPTS uses a fractional step method (e.g., see Yanenko, 1971) to integrate (1.42). In the first step we employ the *method of characteristics* (Abbott, 1966) to integrate the advection term and add lateral inflow

$$\frac{\partial \underline{Q}}{\partial t} + c \frac{\partial \underline{Q}}{\partial x} = \hat{c} q \quad (1.46)$$

the solution of which is the initial condition for the integration of the diffusion term

$$\frac{\partial \underline{Q}}{\partial t} = D \frac{\partial^2 \underline{Q}}{\partial x^2} \quad (1.47)$$

for which we use an *explicit, central finite-difference scheme* (e.g., see Abbott and Basco, 1989). If $\Delta t > 0.5\Delta x^2/D$, we iteratively integrate (1.47) using a time step $\Delta t/N_t$, where the coefficient $N_t \geq 2\Delta t D / \Delta x^2$. The above method ensures that discharge is always positive and its peak attenuates in streamwise direction.

Finally, differential changes in water-surface elevation are computed as

$$\Delta y = \frac{\Delta Q}{\frac{dK}{dy} \sqrt{S_f}} \quad (1.48)$$

CONCEPTS also switches to the one-equation diffusion wave model if $\Delta Q/Q > O(1)$ or $\Delta y/y > O(1)$.

SEDIMENT TRANSPORT AND BED ADJUSTMENT

This chapter presents the one-dimensional sediment transport and river-bed evolution submodel used in CONCEPTS-1.0. You will find a brief description of the conceptual basis for the mathematical formulations of sediment transport in alluvial channels and how streamwise variations in sediment transport affect the evolution of the streambed. This chapter also gives a detailed presentation of the numerical approximation of the mathematical model of streambed evolution.

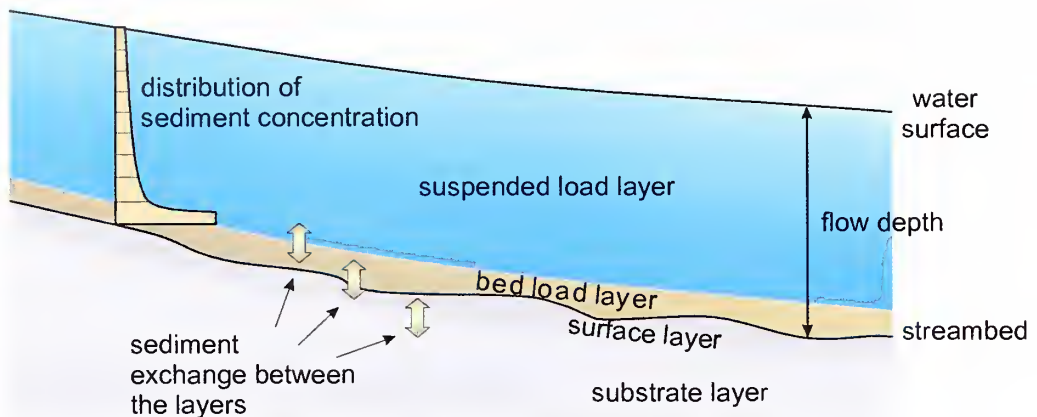
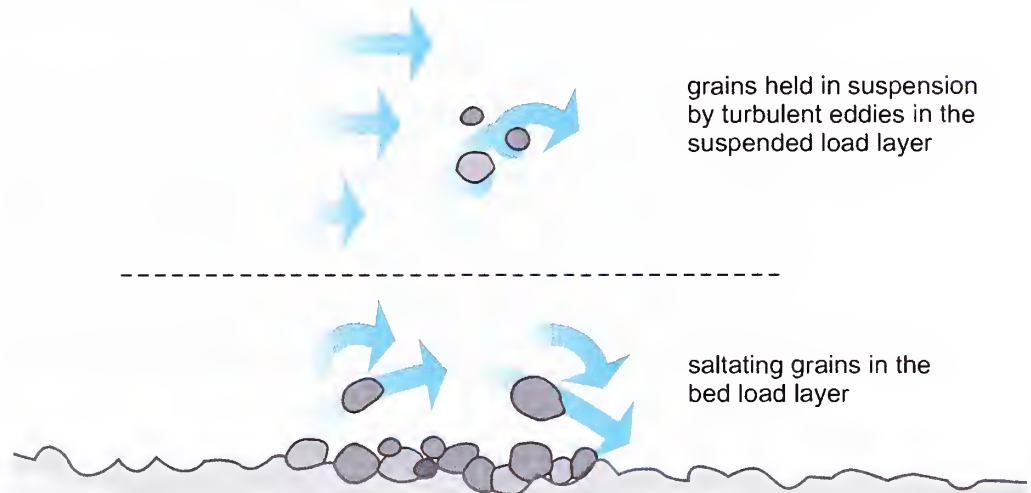
Theory

Sediment Transport

Sediment transport rates are a function of flow hydraulics, bed composition, and upstream sediment supply. The composition of the channel bed may change as particles are eroded from or deposited on the bed, thereby changing flow hydraulics and fractional transport rates.

To model these physical processes, one commonly distinguishes two layers across the water column and one or more layers covering the streambed (see Figure 2.1; e.g., Armanini and Di Silvio, 1988; van Niekerk *et al.*, 1992). The two layers across the water column are (see Figure 2.2):

- 1 a layer near the bed where sediment particles roll, slide, or saltate, and are transported as *bed load*, and
- 2 a layer spanning the remainder of the water column where particles are in suspension and are transported as *suspended bed-material load* or *wash load*.

Figure 2.1 Multi-layer approximation of sediment transport.**Figure 2.2** Modes of sediment transport: bed load and suspended load.

Sediment particles exchange between the bed and suspended load layers and the bed. Governing equations for each layer and empirical expressions of the fluxes between the layers and the bed enable us to compute the sediment transport rates in each layer. Conversely, we can combine the suspended and bed load layers into a single *total load* layer. The fluxes between the transporting layers disappear and only the sediment flux between the bed and fluid remains.

This *two-layer approach* may be a more accurate description of sediment transport mechanics because of the difference in suspended and bed load transport modes. However, the expressions for the sediment fluxes between the layers are empirical and are mainly derived from data acquired from sand-bed

rivers and flume experiments (e.g., Garcia and Parker, 1991). The *one-layer approach* cannot distinguish the different behavior of sediment particles in the suspended and bed loads. However, it is computationally more efficient because of its simplicity, which is important for long-term simulations of the evolution of stream systems. CONCEPTS, therefore, characterizes the sediment transport as total load.

The sediment flux between streambed and overlying fluid not only depends on flow conditions and size fractions available in the bed or transported by the flow, but also on the interparticle forces in the presence of clay particles on the streambed. The entrainment rate of sediment particles on *cohesive* streambeds markedly differs from that of *cohesionless* streambeds.

Governing Equations

Mass Balance

Mass conservation of sediment by size fraction is

$$\frac{\partial C_k}{\partial t} + \frac{\partial u C_k}{\partial x} = E_k - D_k + q_{s_k} \quad (2.1)$$

where t is time, x is distance along the channel centerline, u is flow velocity, E is entrainment rate of particles from the bed, D is deposition rate of particles onto the bed, q_s is rate of sediment inflow from streambanks and fields adjacent to the channel, the subscript k denotes the k -th size class, and C is the sediment mass with dimension length². The sediment mass C is defined as:

$$C = \frac{1}{1 \times 10^6 \gamma_s} \int_A c dA \quad (2.2)$$

where c is point concentration in ppm by weight, γ_s is specific weight of sediment, and γ is specific weight of water.

Figure 2.3 shows a definition sketch of the variables used to determine sediment transport. *Temporal variations in bed-material area* are given by

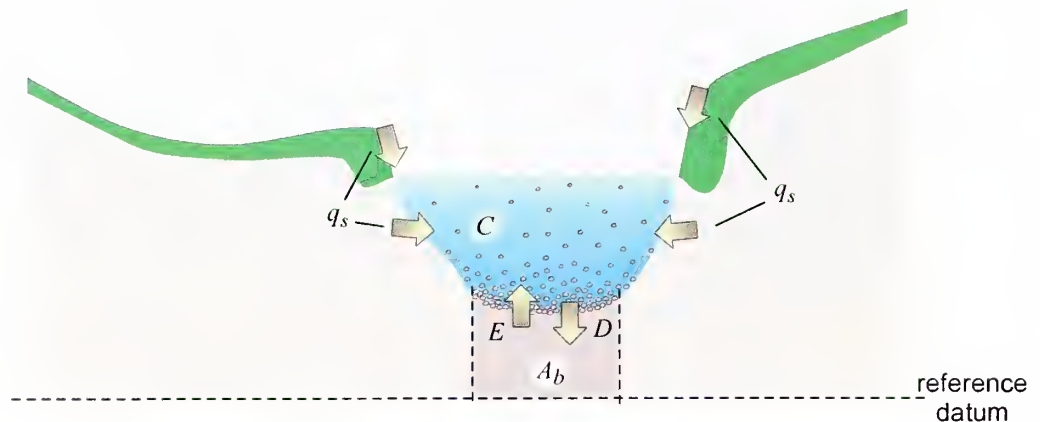
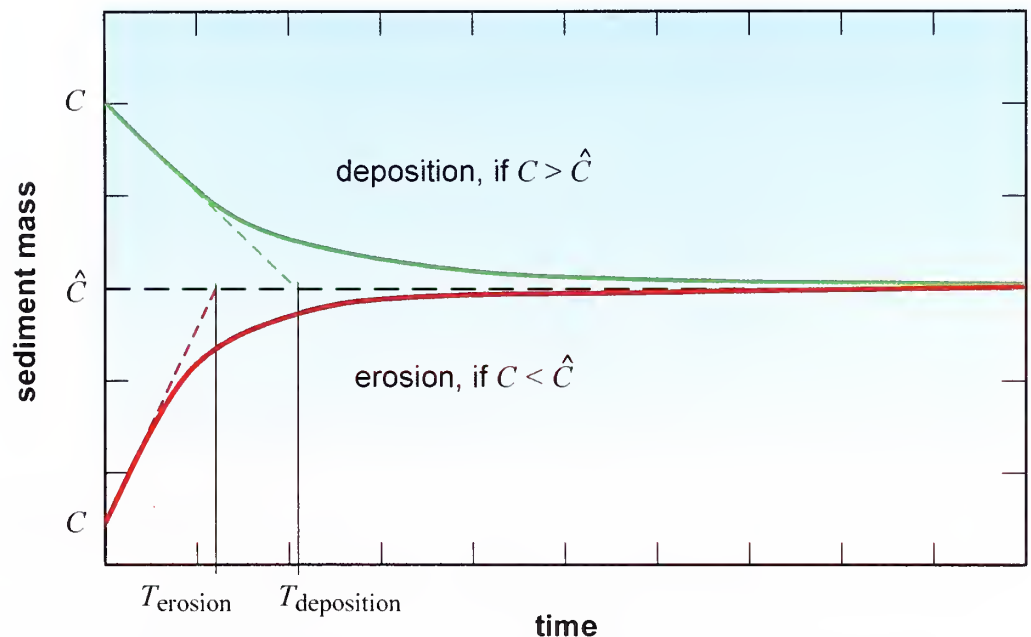
$$(1 - \lambda) \frac{\partial A_{b_k}}{\partial t} = D_k - E_k \quad (2.3)$$

where λ is porosity and A_b is cross-sectional area of the mixing layer.

The entrainment and deposition rates differ for cohesive and cohesionless bed material and, thus, are computed using different methods.

Non-Equilibrium Adjustment of Cohesionless Bed-Material Transport

For *cohesionless* streambeds we use the formulation proposed by Bennett (1974) analogous to that of Foster and Meyer (1972) who assume that the local

Figure 2.3 Definition sketch of sediment transport variables.**Figure 2.4** Progress of sediment mass C toward equilibrium sediment mass \hat{C} for the case of constant flow conditions.

erosion or deposition rate is proportional to the difference between the sediment transport rate and sediment transport capacity:

$$E_k - D_k = \frac{1}{T_k} (\hat{C}_k - C_k) \quad (2.4)$$

where T is a time scale representing the adjustment rate of the sediment mass C to \hat{C} , which is the *equilibrium sediment mass* and is a function of local, instantaneous flow conditions. Figure 2.4 shows an example of how C approaches \hat{C} for the case of erosion and deposition under constant flow conditions. Various formulations of T exist in literature. For particles transported in *suspension*, Armanini and Di Silvio (1988) suggest

$$\frac{T\omega}{h} = \frac{a}{h} + \left(1 - \frac{a}{h}\right) \exp\left[-1.5\left(\frac{a}{h}\right)^{-1/6} \frac{\omega}{u_*}\right] \quad (2.5)$$

where ω is particle fall velocity, h is flow depth, a is thickness of the surface or active layer, and u_* is shear velocity. For sediment particles transported as *bed load*, Phillips and Sutherland (1989) propose

$$T = \alpha_L(\theta - \theta_c)d/u \quad (2.6)$$

where α_L is step-length constant, θ is Shields parameter, θ_c is critical Shields parameter, and d is particle diameter. Phillips and Sutherland (1989) experimentally found $4000 < \alpha_L < 9000$.

CONCEPTS employs formulation (2.5). Although (2.5) was not derived for sediment particles transported as bed load, it correctly tends to $C = \hat{C}$ because $T \ll \Delta x/u$ for coarse particles, where Δx is the space step used by CONCEPTS.

Entrainment and Deposition of Cohesive Bed-Material

The transport, deposition, and erosion processes of *cohesive* sediments are extremely complex due to their highly varying properties and, therefore, behavior when their environment changes. Cohesive beds in incised channels may be very firm and highly consolidated. Ariathurai and Arulanandan (1978) give *erosion rate* as

$$E = eB\left(\frac{\tau_b}{\tau_e} - 1\right) \quad (2.7)$$

where e is erosion-rate constant, B is wetted width of streambed, τ_b is bed shear stress, and τ_e is shear strength of the bed material (see Figure 2.5). The erosion-rate constant and bed shear-strength vary with type of sediment, water content, total salt concentration, ionic species in the water, pH, and temperature (Mehta *et al.*, 1989). For soft (water content well above 100%), partially consolidated beds, Parchure and Mehta (1985) found the erosion rate to be

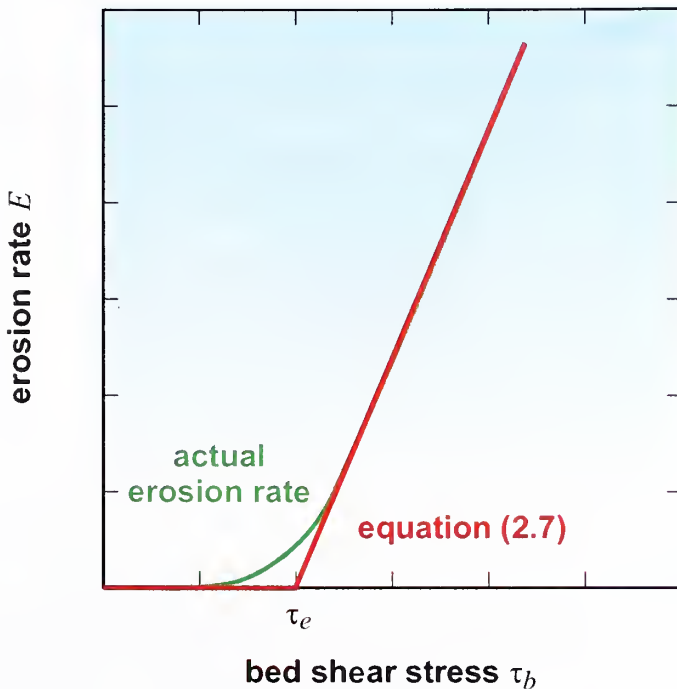
$$E = \varepsilon_f B \exp(\varepsilon \sqrt{\tau_b - \tau_e}) \quad (2.8)$$

where ε_f is floc erosion rate and ε is a rate constant. When the excess shear stress becomes large, the bed may fail at some plane below the surface and clumps of material are mass eroded. Once entrained, CONCEPTS breaks up the clumps into their primary particles, which are then transported as wash load (clay and fine silt particles) or become part of the bed-material load.

The *deposition rate* is commonly given by Krone's (1962) formulation:

$$D = B\omega c\left(1 - \frac{\tau_b}{\tau_d}\right) \quad (2.9)$$

Figure 2.5 The erosion rate of a cohesive streambed as a function of bed shear stress.



where τ_d is the shear stress below which sediment particles in transport begin to deposit. The term in between parentheses in (2.9) is the probability of particles sticking to the bed and not being re-entrained by the flow. CONCEPTS sets the deposition rate to zero if $\tau_b > \tau_d$.

Once deposited, cohesive particles or aggregates undergo consolidation and thixotropic effects. This results in a vertical stratification of the bed with respect to density and shear strength, with both properties typically increasing with depth (Mehta *et al.*, 1982). These processes are complex and highly varying in space and time. A simple description of these processes is not yet available. CONCEPTS, therefore, assumes that a deposited layer of cohesive particles has the same characteristics as the bed surface.

Mixing Layer

For graded bed material the sediment-transport rates depend on the bed-material composition, which itself depends on historical erosion and deposition rates. Hirano (1971) divided the bed into a *surface* or *active layer* and a *substrate* or *subsurface layer*. These layers constitute the so-called mixing layer (see also Figure 2.1). Sediment particles are continuously exchanged between flow and the surface layer. Sediment particles exchange between surface layer and substrate when the bed scours or fills. The *volumetric fraction content* by size class in the surface layer is determined by the following mass conservation equation:

$$\frac{\partial \beta_k^s A_s}{\partial t} = D_k - E_k + S_{u_k} \quad (2.10)$$

where β_k^s is the fractional content by volume of size class k in the surface layer ($\sum_k \beta_k = 1$), A_s is the area of the surface layer, and S_u is the sediment flux from the substrate to the surface layer given by:

$$S_{u_k} = \beta_k^* \left(\frac{\partial A_s}{\partial t} - \frac{\partial A_b}{\partial t} \right) \quad (2.11)$$

The term within parentheses divided by the active bed width is the downward displacement of the lower boundary of the surface layer, and

$$\beta_k^* = \begin{cases} \beta_k^s & \text{if } S_u \leq 0 \\ \beta_k^u & \text{if } S_u > 0 \end{cases} \quad (2.12)$$

where β_k^u is the fractional content by volume of size class k in the subsurface layer.

The thickness of the surface or active layer is associated with the time scale under consideration, here the time step Δt of the time-integration scheme (Rahuel *et al.*, 1989). For very small time scales, the surface layer can be considered as a thin layer containing particles susceptible to entrainment into the flow due to a momentary increase in the bed shear stress. If the time scale is of the order of the time it takes for a bed form to traverse its own wavelength, the thickness of the surface layer is approximately the height of the bed form. For very long time scales during which considerable changes in bed level elevation may occur, the surface layer thickness is related to the thickness of the layer of material eroded or deposited.

Scientists have considered the surface layer thickness to be a function of dune height or water depth (Armanini and Di Silvio, 1988; Rahuel *et al.*, 1989), or grain size (Borah *et al.*, 1982; van Niekerk *et al.*, 1992; Cui *et al.*, 1996). CONCEPTS sets the thickness of the surface layer to 10% of the flow depth. Rahuel *et al.* (1989) propose a thickness of the surface layer between 10% and 20% of the flow depth. Armanini and Di Silvio (1988) suggest a minimum thickness of the surface layer of 5% of the flow depth.

Sediment Transport Capacity

The flow *sediment transport capacity* is the transported sediment load under equilibrium conditions (uniform flow and $E = D$, that is, no net erosion or deposition). CONCEPTS uses a modification of the sediment transport capacity predictor SEDTRA developed by Garbrecht *et al.* (1996). SEDTRA calculates the total sediment transport by size fraction for twelve predefined size classes ($0.01 \text{ mm} < d < 50 \text{ mm}$) with a suitable transport equation for

Table 2.1 Sediment size fractions and corresponding transport equations.

size class	upper bound (mm)	representative diameter (mm)	description	transport equation
1	0.010		clay - very fine silt	wash load
2	0.025	0.016	fine - medium silt	Laursen
3	0.065	0.040	medium - coarse silt	Laursen
4	0.250	0.127	fine sand	Laursen
5	0.841	0.458	medium - coarse sand	Yang
6	2.000	1.297	very coarse sand	Yang
7	3.364	2.594	very fine gravel	Meyer-Peter & Mueller
8	5.656	4.362	fine gravel	Meyer-Peter & Mueller
9	9.514	7.336	fine gravel	Meyer-Peter & Mueller
10	16.000	12.338	medium gravel	Meyer-Peter & Mueller
11	26.909	20.749	coarse gravel	Meyer-Peter & Mueller
12	38.055	32.000	coarse gravel	Meyer-Peter & Mueller
13	50.000	43.713	very coarse gravel	Meyer-Peter & Mueller

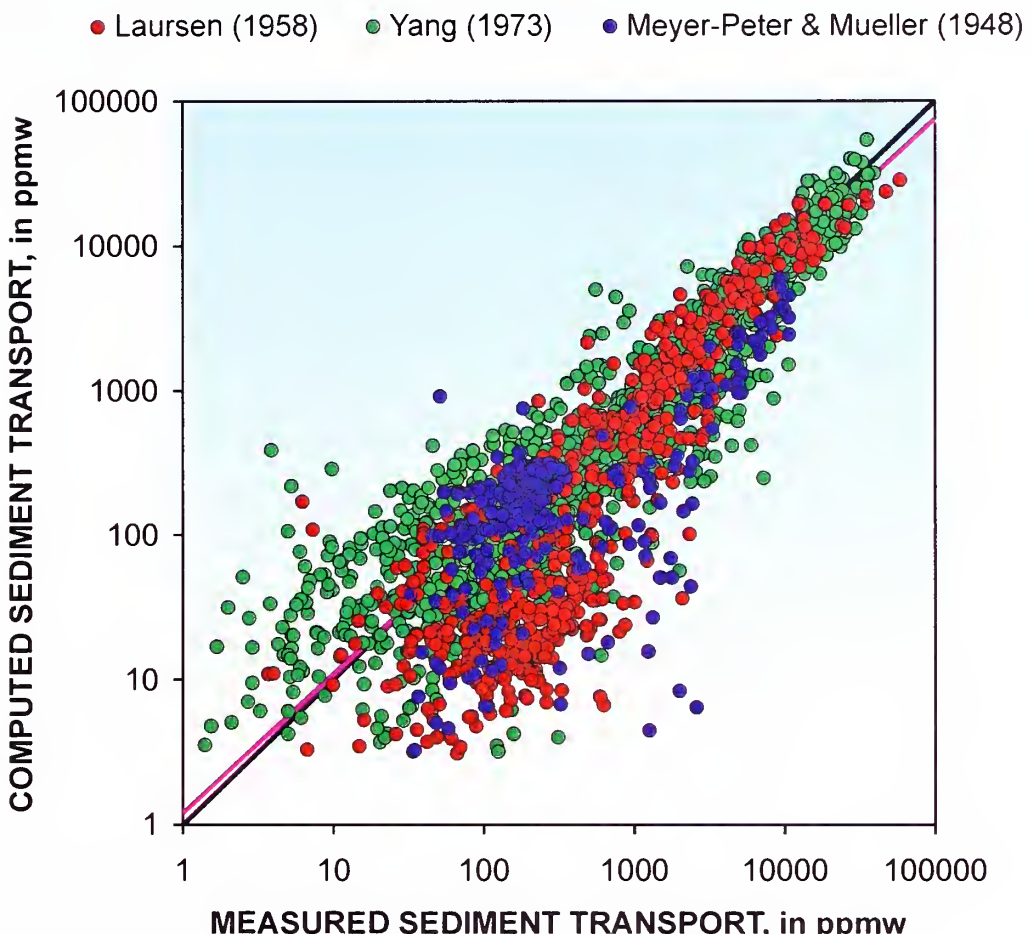
each size fraction: Laursen (1958) for *silt* size classes, Yang (1973) for *sand* size classes, and Meyer-Peter and Mueller (1948) for *gravel* size classes. We have added a thirteenth sediment size class for sediment particles smaller than 10 µm. Once entrained, the flow carries this size class as wash load without deposition. Table 2.1 lists the 13 size classes and their transport equations. SEDTRA takes into account the interdependence between size fractions for initiation of motion by a *critical sediment diameter* for each size fraction that is a function of the sediment mixture.

The Shields curve is a reliable predictor of the flow strength necessary for the initiation of cohesionless particles with a narrow size range. For sediments with a widely graded size distribution, however, the differences in the critical flow strength tend to be significantly reduced. Widely graded sediment beds tend to increase the critical flow strength for initiation of the sizes finer than the mean size and decrease the critical flow strength of the sizes coarser than the mean size. To account for the effect of the mixture on the critical flow strength of the individual size fractions, SEDTRA defines the critical diameter for initiation of each of the twelve size fractions as (Kuhnle *et al.*, 1996)

$$d_{c,k} = d_k \left(\frac{\bar{d}}{d_k} \right)^\chi \quad (2.13)$$

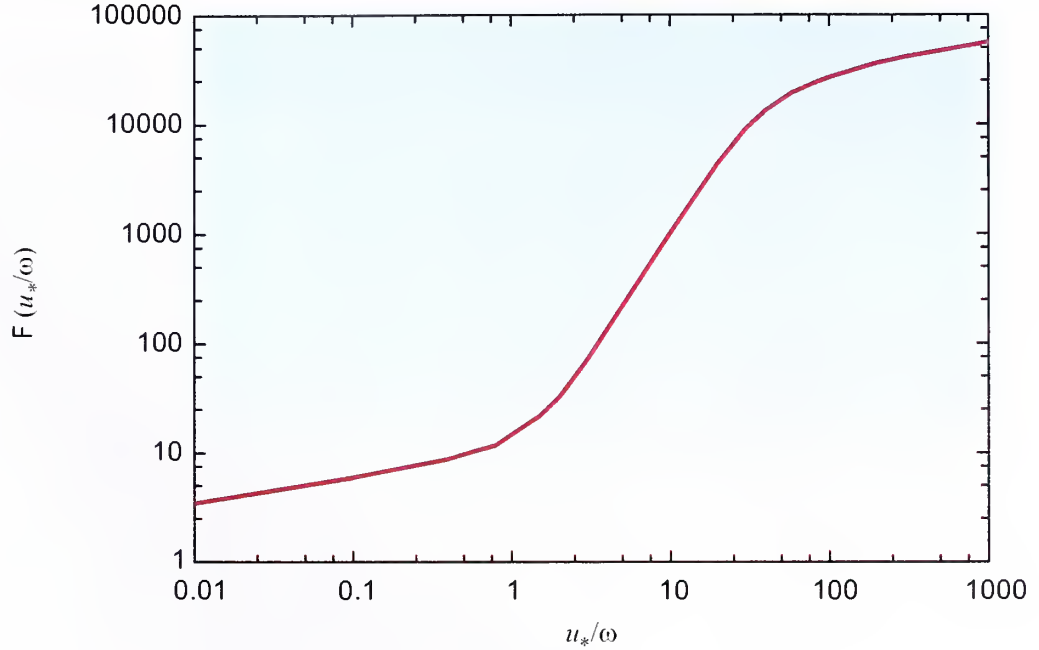
where \bar{d} is the mean size of the bed material, and χ is a hiding coefficient. The hiding coefficient ranges from 0 to 1. For $\chi = 1$, the mean size of the sediment is the critical diameter for all size fractions and all fractions tend to move at the same flow strength. For $\chi = 0$, each size fraction behaves independently of the others and the d_k for each size fraction is used to calculate flow strength at which motion begins.

Figure 2.6 Measured (Brownlie, 1981) versus computed (SEDTRA) sediment transport capacity. The black line is the line of perfect agreement and the magenta line is the regression line.



Extensive testing of SEDTRA found it to be applicable to channels with widely graded sediment distributions and to channel networks with variable sediment characteristics (Garbrecht *et al.*, 1996). Garbrecht *et al.* (1996) tested SEDTRA against Brownlie's (1981) data set. These data consist of 5,263 laboratory and 1,764 field measurements made under equilibrium or near-equilibrium conditions and a wide range of channel, flow, and bed-material characteristics. Garbrecht *et al.* (1996) did not use data having one or more of the following values for testing: water temperature above 35 Celsius, sediment specific gravity other than between 2.4 and 2.8, energy slopes less than 0.00001, gradation greater than 1.5 (laboratory data) or 2.0 (field data), and channel width-to-depth ratios less than 5.

Figure 2.6 shows total measured versus total computed sediment transport. About 80% of the computed laboratory data are within a factor of two of the measured values, and about 90% within a factor of three. About 55% of the computed field data are within a factor of three, and about 70% within a factor of 5. The regression line plots closely to the line of perfect agreement, r^2 equals 0.85.

Figure 2.7 Function $\mathcal{J}(u_*/\omega)$ in Laursen's approach (Laursen, 1958).

The following sections present the transport equations in SEDTRA. The point concentration c is related to sediment mass C by (2.2). SEDTRA applies transport equations (2.15), (2.17), and (2.19) to individual particle-size classes. The total sediment mass, C_t , is defined as:

$$C_t = \sum_k p_k C_k \quad (2.14)$$

where p_k is the fraction of sediment in the k -th size class available for transport. The fraction p_k depends on β_k^s and the fraction of sediment in the k -th size class entering the reach from upstream and the streambanks.

Laursen (1958)

SEDTRA uses Laursen's (1958) transport equation in the form as given in Vanoni (1975)

$$c = 0.01 \gamma \left(\frac{d}{h} \right)^{7/6} \left(\frac{\tau'}{\tau_c} - 1 \right) F \left(\frac{u_*}{\omega} \right) \quad (2.15)$$

where the shear velocity $u_* = \sqrt{ghS_f}$, g is gravitational acceleration, S_f is friction or energy slope, τ_c is critical tractive force as given by (2.13), and F is a function of the parameter u_*/ω , see Figure 2.7. Laursen (1958) used the Manning-Strickler equation to express the bed shear stress τ' due to grain resistance as

$$\tau' = \frac{\rho u^2}{58} \left(\frac{d_{50}}{h} \right)^{1/3} \quad (2.16)$$

where d_{50} is the sediment size for which 50% of the mixture is finer.

Yang (1973)

Yang (1973) assumed sediment concentration to be related to unit stream power uS_f . From analysis of laboratory data, Yang found

$$\begin{aligned} \log c &= 5.435 - 0.286 \log \frac{\omega d}{v} - 0.457 \log \left(\frac{u_*}{\omega} \right) \\ &\quad + \left(1.799 - 0.409 \log \frac{\omega d}{v} - 0.314 \log \frac{u_*}{\omega} \right) \log \left(\frac{uS_f}{\omega} - \frac{(uS_f)_c}{\omega} \right) \end{aligned} \quad (2.17)$$

where v is kinematic viscosity, and $(uS_f)_c$ is critical unit stream power. The critical dimensionless unit stream power is the product of the friction slope and critical dimensionless velocity (u_c/ω) , where

$$\frac{u_c}{\omega} = \begin{cases} \frac{2.5}{\log(u_*d_c/v) - 0.06} + 0.66 & \text{for } 1.2 < \frac{u_*d_c}{v} < 70 \\ 2.05 & \text{for } 70 \leq \frac{u_*d_c}{v} \end{cases} \quad (2.18)$$

Meyer-Peter and Mueller (1948)

Meyer-Peter and Mueller (1948) proposed the following relation for bed load transport

$$c = \frac{8 \times 10^6 \gamma_s u_* d_c}{\rho q} (r^{3/2} \theta - 0.047) \quad (2.19)$$

where ρ is water density, q is unit discharge, r is the ratio of bed roughness and grain roughness Strickler coefficients, and θ is Shields parameter:

$$\theta = \frac{\gamma R S_f}{(\gamma_s - \gamma) d_c} \quad (2.20)$$

The ratio r is determined as

$$r^{3/2} = \left(\frac{n'}{n_e} \right)^2 \quad (2.21)$$

where Mueller determined the grain roughness as

$$n' = \frac{d_{90}^{1/6}}{26} \quad (2.22)$$

Fall Velocity

Equations (2.5), (2.9), (2.15), and (2.17) require the fall velocity ω . CONCEPTS uses the fall velocities provided by the U.S. Interagency Committee on Water Resources, Subcommittee on Sedimentation (USICWR, 1963). USICWR (1963) determined fall velocity for various sediment sizes and shapes under different water temperatures. CONCEPTS, however, only uses the fall velocities for well-rounded natural sediment particles.

USICWR (1963) established these fall velocities for particles falling by themselves in still water. However, the presence of other particles, turbulence within the flow, and particle density will all affect fall velocity, but CONCEPTS version 1.0 does not account for them.

Implementation of Bed-Material Transport Submodel

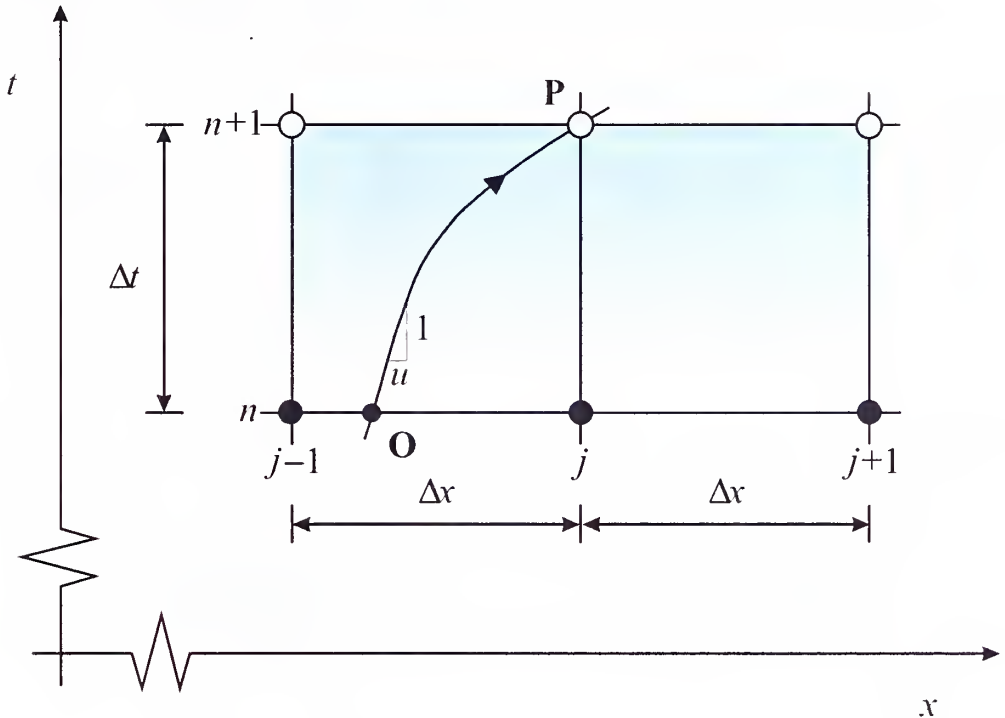
Computation of Fractional Sediment Concentration

Noncohesive Streambed

The sediment transport equation (2.1) is an *advection equation* with a *source term* representing a net erosion from or deposition on the bed of sediment particles and a lateral inflow of eroded bank material and eroded soil carried by lateral runoff. Bank erosion rates are computed by the streambank component of CONCEPTS (see Chapter 3 on “Bank Erosion and Channel Widening”). Runoff sediment yield is user-supplied input data.

There exists much literature on methods that have been developed to integrate the advection equation. Though the character of the advection equation with constant coefficients is well understood, its numerical integration may be quite difficult, especially if the solution displays large gradients (e.g., Hirsch, 1988). Also, if the coefficient in the advection term is varying, as is velocity in (2.1), the complexity of the numerical integration increases. Further, one may use a stable scheme to integrate the advection equation, however, to obtain a *diverging* solution because of the behavior of the *source term*. If the ratios $\Delta t/T$ and $\Delta x/uT$, where Δt is time step, are much larger than unity, the discretized source term is much larger in magnitude than the discretized unsteady and advection terms. Therefore, the source term controls the sediment concentration, and any solution method of the advection equation will be either unstable or inaccurate. The source term has to be approximated by an implicit method to assure a stable solution (LeVeque and Yee, 1990). Alternatively, we can employ a *fractional step method* (Yanenko, 1971), and solve the following system of equations:

$$\frac{\partial C_k}{\partial t} + \frac{\partial u C_k}{\partial x} = q_{s_k} \quad (2.23a)$$

Figure 2.8 Solution of advection equation in x - t space.

$$\frac{dC_k}{dt} = \frac{1}{T_k} (\hat{C}_k - C_k) \quad (2.23b)$$

The *advection equation* (2.23a) is solved first. Its solution is used as initial condition of the *initial value problem* (2.23b).

The behavior of sediment mass C can be studied in x - t space (see Figure 2.8).

The characteristic projected backwards from point P intersects the $t = t^n$ line at point O. Thus, sediment particles travel from point O to point P in a time step $\Delta t = t^{n+1} - t^n$. Neglecting the source term we simply have $C_P = C_O$.

Including the source term, C will adjust itself from C_O , approaching a value of C_P at a rate given by timescale T . In the above analysis we neglected lateral inflow of sediments.

CONCEPTS solves (2.23a) by the *method of characteristics* to obtain an *intermediate solution* C^* :

$$C_{k,j}^* = \begin{cases} (1 - N_c) C_{k,j}^n + N_c C_{k,j-1}^n + q_{s_k} \Delta t & \text{for } N_c \leq 1 \\ \left(1 - \frac{1}{N_c}\right) C_{k,j-1}^* + \frac{1}{N_c} C_{k,j-1}^n + q_{s_k} \Delta t & \text{for } N_c > 1 \end{cases} \quad (2.24)$$

where $N_c = u\Delta t/\Delta x$ is the *Courant number*. The discretization scheme (2.24) is first order in space and time, and therefore may be quite diffusive if longitudinal gradients of sediment concentration are large.

The intermediate solution $C_{k,j}^*$ is the *initial condition* for solving the *ordinary differential equation* (2.23b). Many methods are available to solve (2.23b) numerically, e.g., see Gear (1971) or Lambert (1973). However, if we assume that both \hat{C}_k and T are constant during the time step Δt , we obtain the following analytical solution

$$C_{k,j}^{n+1} = \hat{C}_{k,j} + (C_{k,j}^* - \hat{C}_{k,j}) \exp(-\Delta t/T) \quad (2.25)$$

Equation (2.25) yields $C_{k,j}^{n+1} = \hat{C}_{k,j}$ for coarse sediment particles ($T \ll \Delta t$), and $C_{k,j}^{n+1} = C_{k,j}^*$ for very fine particles (say wash load, $T \rightarrow \infty$).

Cohesive Streambed

In the case of a cohesive streambed, (2.7) and (2.9) comprise the source and sink terms, respectively. Equation (2.23b) then reads

$$\frac{dC_k}{dt} = E_k - D_k \quad (2.26)$$

which is solved by the well-known *forward Euler method* (e.g., Celia and Gray, 1992)

$$(C_k)_j^{n+1} = (C_k)_j^* + \Delta t((E_k)_j^* - (D_k)_j^*) \quad (2.27)$$

where

$$(E_k)_j^* = B \left[\frac{\frac{1}{2}[(\tau_b)_j^n + (\tau_b)_j^{n+1}]}{(\tau_e)_j} - 1 \right] \quad (2.28a)$$

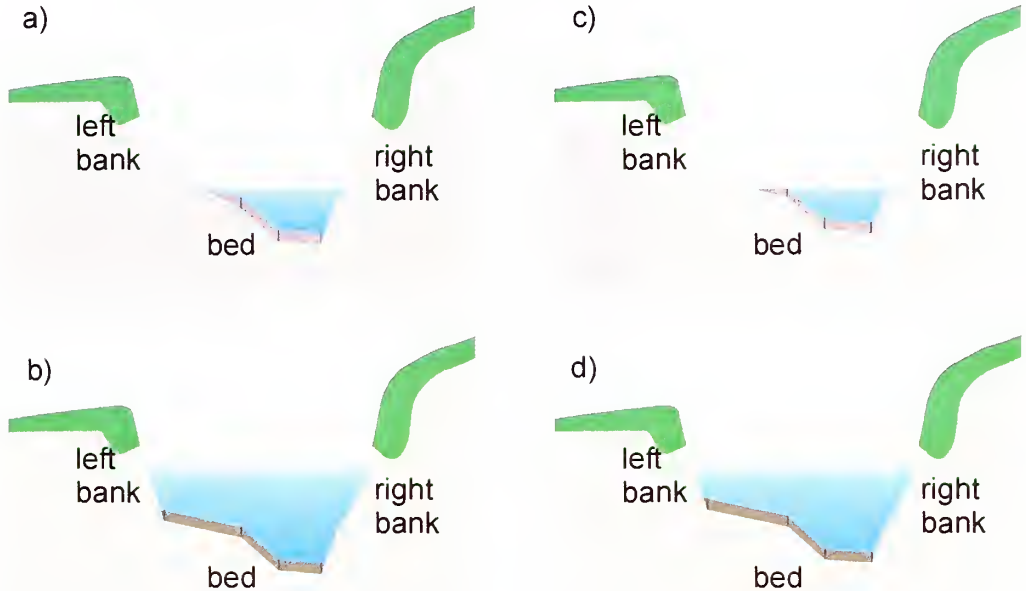
$$(D_k)_j^* = B \omega_k c_k \left[1 - \frac{\frac{1}{2}[(\tau_b)_j^n + (\tau_b)_j^{n+1}]}{(\tau_d)_j} \right] \quad (2.28b)$$

Computation of Variations in Streambed Elevation

The relation describing change in bed material area (2.3) is equivalent to (2.23b) and (2.26). Therefore, the change in bed material storage per unit length of channel, ΔA_{b_k} , equals the difference between the intermediate sediment concentration and that at t^{n+1} :

$$\Delta A_{b_k} = (A_{b_k})_j^{n+1} - (A_{b_k})_j^n = \frac{1}{1-\lambda} [(C_k)_j^* - (C_k)_j^{n+1}] \quad (2.29)$$

Figure 2.9 Changes in elevation of the streambed: a) erosion of a partly wetted bed, b) erosion of a fully wetted bed, c) deposition on a partly wetted bed, and d) deposition on a fully wetted bed. The darker, shaded area denotes deposited or eroded sediments.



Cross Section Evolution

CONCEPTS uses the change in bed-material storage (2.29) to update the elevation of cross-sectional nodes along the wetted part of the bed, see Figure 2.9. Figures 2.9a and 2.9b show the change in bed elevation for the case of erosion of a partly wetted bed and a fully wetted bed, respectively. Figures 2.9c and 2.9d show the change in bed elevation for the case of deposition on a partly wetted bed and a fully wetted bed.

CONCEPTS shifts the bed profile up and down parallel to the original bed profile without changing the bank profile. In the case of a partly wetted bed, a new point at the intersection of water surface and bed profile is inserted.

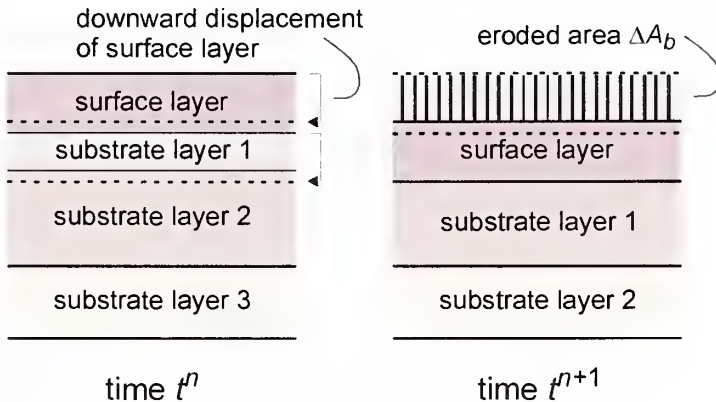
Mixing Layer Composition

CONCEPTS vertically divides the bed into a surface layer and several subsurface layers, which reflect historical deposition of sediment particles on the streambed or the undisturbed streambed. CONCEPTS keeps track of the different compositions of surface and subsurface layers. Rewriting the mass conservation equation of the surface layer (2.10) using (2.3) and (2.11) yields

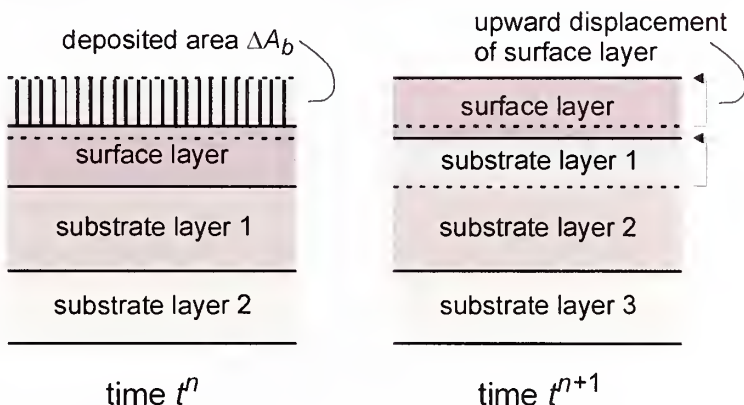
$$\frac{\partial \beta_k^s A_s}{\partial t} = (1 - \lambda) \frac{\partial A_{b_k}}{\partial t} + \beta_k^* \left(\frac{\partial A_s}{\partial t} - \frac{\partial A_b}{\partial t} \right) \quad (2.30)$$

Figure 2.10 Sorting of graded bed-material within the mixing layer: a) erosion, sediment particles from surface layer mix with material from substrate layers 1 and 2; and b) deposition, part of the surface layer becomes new substrate layer 1.

a) bed erosion



b) sediment deposition



We assume that β_k^* is constant during a time step Δt , thus

$$(\beta_k^s)^{n+1} = \frac{1}{A_s^{n+1}} [(\beta_k^s A_s)^n + (1 - \lambda) \Delta A_{b_k} + (\beta_k^*)^n (\Delta A_s - \Delta A_b)] \quad (2.31)$$

Figure 2.10 shows the mixing of sediment particles with those in subsurface layers if erosion occurs and the initiation of new subsurface layers if deposition occurs. Entrainment of sediment particles from the surface layer and its ensuing downward displacement causes particles from subsurface layers to be mixed with those in the surface layer (2.10a).

Deposition of sediment particles on the bed leads to an upward displacement of the surface layer and the initiation of new subsurface layers (2.10b).

Boundary Conditions

CONCEPTS requires boundary conditions at the upstream and downstream boundaries of the channel, and at hydraulic structures. The upstream and downstream boundaries are also known as *external boundaries*, whereas boundaries such as hydraulic structures are known as *internal boundaries*.

External Boundary Conditions

At the upstream boundary the user must supply the sediment discharge by size class entering the channel. This is done by entering (see also sections “Run Control Data” and “Dynamic Upstream Boundary Conditions” in Chapter 4, “Input Data”):

- 1 sediment load as a fraction, f_k , of the local sediment-carrying capacity of the flow:

$$f_k = \frac{C_k}{\bar{C}_k} \quad (2.32)$$

or,

- 2 a time series of sediment load (in kg/s), $C_k = C_k(t)$, in the file with upstream boundary conditions.

The solution method (2.24), (2.25), and (2.29) does not require a downstream boundary condition. However, this means that only processes occurring in the modeling reach determine the evolution of the outlet. This may lead to inaccurate results. The user has the option to adjust the predicted change (2.29) in bed elevation as

$$\Delta A_{b_k} = (1 - m) \Delta A_{b_k} \quad (2.33)$$

where m ($0 \leq m \leq 1$) is a user-specified modifier. If $m = 0$, no control, CONCEPTS does not adjust the predicted change in bed elevation. If $m = 1$, full control, CONCEPTS keeps the bed elevation at the outlet constant throughout the simulation.

Internal Boundary Conditions

At hydraulic structures the sediment transport rate is a function of the supply of sediment and the elevation of the upstream invert of the structure. If the upstream invert of the structure is located above the channel thalweg, CONCEPTS deposits that part of the sediment load transported as bed load just upstream of the structure. Based on the following criterion:

$$\frac{u_*}{\omega_k} < 0.47 \quad (2.34)$$

CONCEPTS determines the size classes k that are carried mainly as bed load and are deposited. The sediment particles in the other size classes pass through the structure without depositing. This process stops once the thalweg elevation

Sediment Transport and Bed Adjustment

reaches the elevation of the upstream invert of the structure. At this point all sediment is passed through the structure without depositing.

BANK EROSION AND CHANNEL WIDENING

This chapter presents the stream-width adjustment submodel of CONCEPTS-1.0. The conceptual basis for the mathematical characterization of streambank-erosion processes are discussed, followed by the numerical implementation of the mathematical model.

Theory

Channel-width adjustment occurs in a wide variety of geomorphic contexts and is usually accompanied by changes in other morphological parameters such as channel depth, roughness, bed-material composition, riparian vegetation, energy slope, and channel planform. The processes responsible for width adjustment are diverse, and the adjustment process itself displays a wide variety of spatial and temporal patterns. The ASCE Task Committee on Hydraulics, Bank Mechanics, and Modeling of River Width Adjustment lists (ASCE, 1998):

- widening by erosion of one or both banks without substantial incision;
- widening in sinuous channels by erosion of the outer bank exceeding advancement of opposite bank;
- widening in braided rivers by flows deflected around growing braid bars;
- rapid widening in degrading streams by increasing bank height and steepness;
- narrowing by formation of in-channel berms or benches at the margins;
- narrowing in sinuous channels by advancing point bars exceeding the retreat of the opposite cut bank;
- narrowing in braided channels by the abandoning of a marginal anabranch.

It is unlikely that equilibrium approaches such as regime theory, extremal hypothesis, or tractive force methods can accurately predict width adjustment over time. CONCEPTS simulates channel width adjustment by incorporating the fundamental physical processes responsible for bank retreat:

- *fluvial erosion* or entrainment of bank material particles by the flow, and
- *mass bank failure*, for example due to channel incision.

Fluvial Erosion Process

Water flowing in an alluvial channel exerts forces of drag and lift on the boundaries that tend to detach and entrain surface particles. The origin of resisting forces varies according to the grain size and the nature of electrochemical bonding that may exist between cohesive particles. Alluvial bank materials are formed primarily by fluvial deposition and are often stratified. Therefore, the characteristics and erodibility of the bank may vary with elevation. Also, floodplain deposits typically include alluvial sand and gravels, clay plugs, and strongly cohesive backswamp deposits, so that bank material properties vary spatially over relatively short distances.

In the case of *noncohesive* sands and gravels, the forces resisting erosion are generated mainly by the immersed weight of the particles. Generally, the mobility of noncohesive bank materials can be predicted using a *Shields-type entrainment function*, but this must be modified to take into account the destabilizing effect of the channel side slope.

Fine-grained bank materials, containing significant amounts of silt and clay, are to some degree *cohesive* and resist entrainment primarily through interparticle, electrochemical bonding rather than through the immersed weight of the particles. When cohesive bank materials are entrained by the flow, it is aggregates of grains (such as soil crumbs or peds that have been produced by soil-forming processes) that are detached. *Fluvial entrainment*, therefore, requires that the local boundary shear stresses exceed the *critical value to initiate motion of aggregates* or peds rather than that related to the primary soil particles. Ped size, stability, and interped bonding strength are not conservative soil properties as they depend to some degree on the local history of soil development, in general, and recent antecedent conditions of wetting and drying, in particular. It follows that the conditions of incipient motion for cohesive bank materials are complex, time-dependent, and difficult to define. *Critical boundary shear stresses* for cohesive bank soils tend to be higher than for noncohesive bank materials. As a result, erosion rates for cohesive banks are generally lower than for noncohesive banks. Once entrained, aggregates disintegrate rapidly due to corrosion at the channel boundaries and turbulent buffeting in the flow, so that most fine sediment derived from bank erosion is transported in suspension and is conventionally classified as wash load.

The *erodibility* of bank soils can be increased markedly by weakening processes such as *weathering*. The processes responsible for loosening and

detaching grains and aggregates are closely associated with soil moisture conditions at and beneath the bank surface. Swelling and shrinking of soils during repeated cycles of wetting and drying can contribute to cracking that significantly increases erodibility and reduces soil shear strength. Heaving and the growth of needle ice crystals at the bank surface, followed by collapse of ice wedges and needles during thawing of soil moisture, are highly effective in increasing the susceptibility of cohesive bank materials to fluvial erosion.

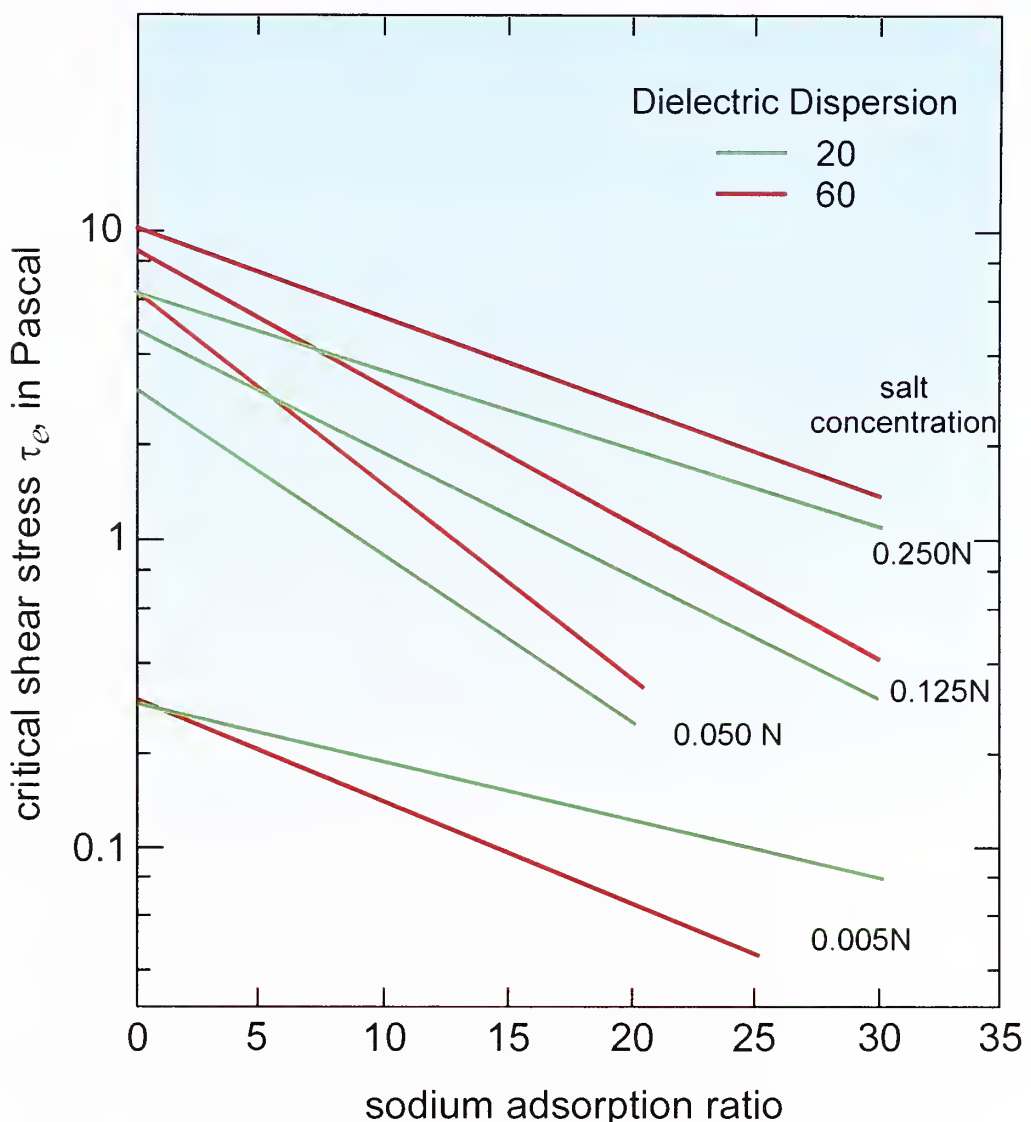
Temporal variability in the erodibility of bank soils due to the operation of weathering processes means that the effectiveness of a given flow event in eroding the bank depends not only on the magnitude and duration of a particular event but also on the antecedent conditions.

Bank vegetation locally increases the roughness of the boundary, increasing flow resistance, retarding the near-bank flow, and damping turbulence (see, among others, the early work by Kouwen *et al.*, 1969, and the more recent work by López and García, 1997). The type and density of vegetation are very important. Flexible vegetation, such as *grasses* and *shrubs*, are usually only effective in retarding the flow at low velocities. Rigid, *woody species* continue retarding the flow up to very high velocities, but may generate serious bank scour through local acceleration of flow around their trunks. For trees to be effective in reducing flow attack on the bank they must be spaced sufficiently closely (Thorne, 1990).

Vegetation can also increase the *erosion resistance* of the soil. The roots and rhizomes of plants bind the soil and introduce an ‘added’ cohesion over the intrinsic cohesion of the bank material. The *critical condition for erosion* of a vegetated bank is the *threshold of failure of the plant stems* by snapping, stem scour, or uprooting rather than that for detachment of bank material itself. This is usually associated with much higher levels of flow intensity. Further, vegetated banks are generally better drained and drier than unvegetated banks, so that the impact of *moisture-related processes* that weaken and loosen the soil is reduced. Gray and Leiser (1982) and Coppin and Richards (1990) have reviewed the effects of herbaceous vegetation in reducing flow erosivity and bank erodibility and concluded that major effects include the following:

- Foliage and plant residues intercept and absorb rainfall energy and prevent soil compaction by raindrop impact.
- Root systems physically retain soil particles.
- Near-bank velocities are retarded by increased roughness.
- Plant stems dampen turbulence to reduce instantaneous peak shear stresses.
- Roots and humus increase permeability and reduce excess pore-water pressures.
- Depletion of soil moisture reduces water-logging.

Figure 3.1 Critical shear stress τ_e versus SAR for different soil salt concentrations and dielectric dispersion values (modified from Arulanandan *et al.*, 1980).



Osman and Thorne Method

Osman and Thorne (1988) developed a method to predict the *lateral-erosion rate* at the bank toe. Osman and Thorne follow the excess shear stress approach set forth by Arulanandan *et al.* (1980). *Excess shear stress* is defined as the difference between the shear stress exerted by the flowing water on the bank, τ , and the critical shear stress, τ_e , at which the soil particles are entrained.

Arulanandan *et al.* (1980) determined the critical shear stress as a function of sodium adsorption ratio (SAR), pore-fluid salt concentration, and the dielectric dispersion as shown in Figure 3.1. Once you obtain the value of τ_e , the method consists of the following steps if $\tau > \tau_e$:

Step 1. An initial rate of lateral bank erosion \dot{W}_i is given by

$$\dot{W}_i = \frac{0.037}{\rho_s} \tau_e \exp(-1.3 \tau_e) \quad (3.1)$$

where ρ_s is mass density of the bank material.

Step 2. The rate of soil erosion is assumed to have an approximately linear increase with shear stress once the critical shear stress is exceeded. The actual erosion rate \dot{W} is then

$$\dot{W} = \dot{W}_i \left(\frac{\tau}{\tau_e} - 1 \right) \quad (3.2)$$

The lateral erosion distance during a time step Δt is

$$\Delta W = \dot{W} \Delta t \quad (3.3)$$

A lower bound of τ_e for the application of Osman and Thorne's method is 0.6 Pa. Soils with lower critical shear stresses are only weakly cohesive and will generally behave as cohesionless materials.

Mass Wasting Process

Fluvial erosion drives bank retreat directly by the removal of material from the bank toe, and indirectly causes bank retreat by triggering *mass instability*. The *stability of the bank* with regard to mass failure depends on the balance between *gravitational forces* that tend to drive the soil mass downwards and the forces of *friction* and *cohesion* that resist movement. Failure of the bank occurs when driving forces exceed resisting forces on the most critical potential *failure surface*, and the bank collapses in a gravity-induced, mass failure. This may occur as fluvial erosion of the bed next to the bank toe increases the bank height, or undercutting increases the bank angle.

The *analysis of slope stability* with respect to mass failure has been the topic of considerable research effort, primarily by geotechnical engineers, but also by geomorphologists and geophysicists. The treatment of river bank stability is generally based on research for engineered slopes and embankments.

There is a clear contrast in failure mechanics between noncohesive and cohesive materials because of significant differences in their soil mechanics. In a noncohesive bank, shear strength increases more rapidly with depth than does shear stress, so that critical conditions are more likely to occur at shallow depths. In a cohesive bank, however, shear stress increases more quickly than shear strength with increasing depth so that critical surfaces tend to be located deep within the bank.

Noncohesive materials usually fail by dislodgement and avalanching of individual particles or by shear failure along shallow, very slightly curved slip surfaces. Deep-seated failures occur in cohesive materials with a block of

disturbed, but more or less intact, bank material sliding into the channel along a curved failure surface. In banks with *shallow slope angles* (<60°), the failure surface is curved and the block tends to rotate back toward the bank as it slides, in a *rotational slip* (Figure 3.2a). *Steep banks* characteristically fail along almost *planar surfaces*, with the detached block of soil sliding downward and outward into the channel in either a planar slip or a toppling failure (Figure 3.2b).

Cantilevered or overhanging banks are generated when erosion of an erodible layer in a stratified or composite bank leads to undermining of overlying, erosion-resistant layers (Figure 3.2c). Frequently, the strength of cantilever blocks is significantly increased by root reinforcement due to riparian and floodplain vegetation and decreased by tension cracks.

Tensile forces (negative earth pressure) may develop in the upper soil layer producing cracks as a consequence. Terzaghi (1943) gives the thickness of this layer as:

$$z_t = \frac{2c}{\gamma_s} \tan(45 + \phi/2) \quad (3.4)$$

In material with little ability to withstand tensile stresses, a small cut will result in time in the development of a tension crack (with height z_{tc}) deep enough to produce instability. Commonly, assuming $z_{tc} = 0$ may lead to better agreement between observed and predicted failures (Lohnes and Handy, 1968). Tension cracks may develop at the instant bank failure is about to occur, therefore not significantly contributing to the instability of the bank.

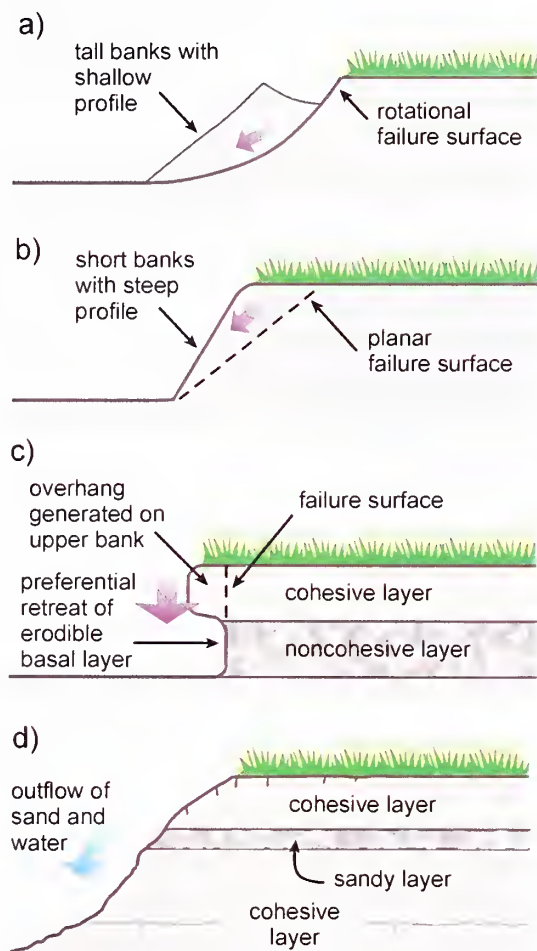
Hagerty (1990) describes streambank collapse by exfiltrating seepage, which is called *piping* or *sapping* (Figure 3.2d1-3). The outflowing water removes soil particles in the exfiltration zone. Undercut strata located above the zone of soil loss become unstable and collapse.

Whether bank failure occurs by rotational slip, toppling, or cantilever collapse, the primary force tending to move the failure block is the *weight of the block*. Fluvial erosion can increase the driving force by increasing the bank height or by increasing the bank slope angle. The weight of bank material also increases with the moisture content of the soil and failure often follows the change from submerged to saturated conditions that develops when drawdown occurs in the channel (e.g., Sands and Kapitzke, 1998).

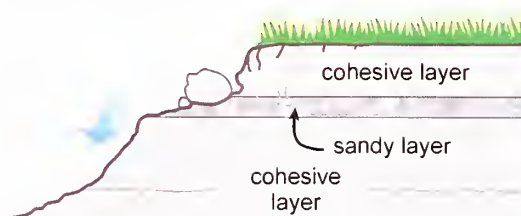
The role of *vegetation* in affecting mass bank failure and width adjustment is complex and poorly understood. Although vegetation generally reduces soil erodibility, its impact on bank stability with respect to mass failure may be either stabilizing or destabilizing. Hence, depending on the geomorphic context and dominance of either fluvial processes or mass failure, vegetation may produce either a net increase or a decrease in bank stability.

Gray and Leiser (1982) and Coppin and Richards (1990) reviewed the ways that woody vegetation may affect the balance of forces promoting and resisting

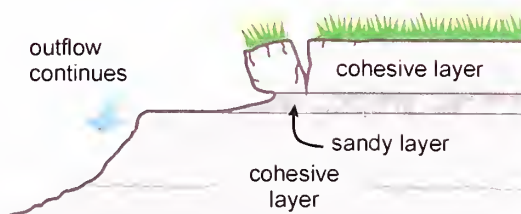
Figure 3.2 Bank failure mechanisms: a) rotational failure, b) planar failure, c) cantilever failure, and d) piping or sapping failure.



1. seepage outflow generates soil loss



2. undermined upper layer falls, blocks detached



3. failed blocks topple

mass failure. Roots mechanically reinforce soil by transferring shear stresses in the soil to *tensile stresses* in the roots, which root strength is able to resist. However, this effect operates only to the rooting depth of the vegetation, and it does not reinforce potential failure planes that pass beneath the plant rootballs. Hence, root reinforcement is negated when bank height significantly exceeds rooting depth.

Soil moisture levels are decreased by canopy interception and evapotranspiration, reducing the frequency of occurrence of saturated conditions conducive to bank collapse, or increased by stemflow (Simon and Collison, 2001). Anchored and embedded stems can act as buttress piles or arch abutments in a slope, counteracting downslope shear stresses and increasing bank stability. However, roots may also invade cracks and fissures in a soil or rock mass and thereby cause local instability by their wedging or prying action. The surcharge of weight of vegetation may significantly increase motivating forces, causing destabilization of the bank, and wind loading on tall vegetation may exert an additional and potentially critical destabilizing moment on the bank.

Streambank Stability Analysis

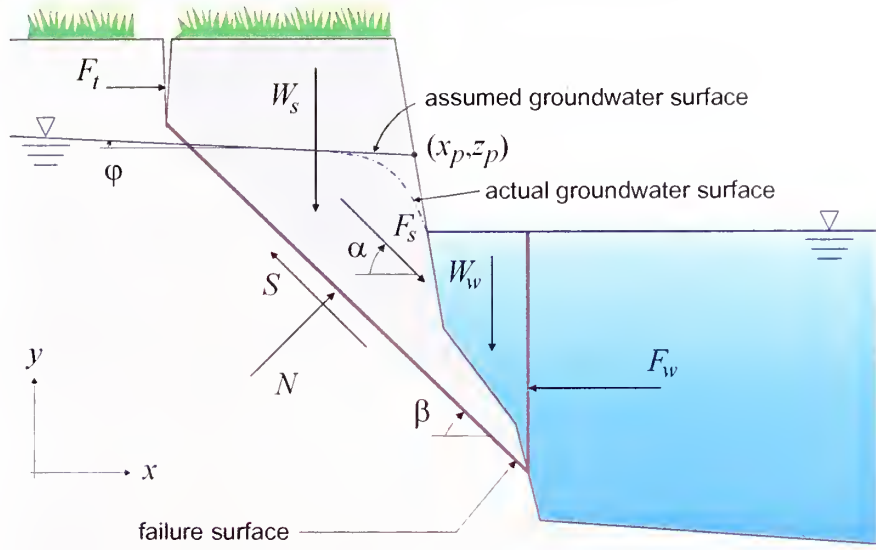
Streambank stability can be analyzed using methods developed for engineered slopes and embankments, e.g., Bishop (1955), Morgenstern and Price (1965), Terzaghi and Peck (1967), and Fredlund and Krahn (1977). These *limit equilibrium methods* are based upon static equilibriums of forces and/or moments. Simon *et al.* (1999) have presented a comprehensive stability analysis for layered streambanks based on the limit equilibrium method. They included forces due to pore-water pressures and confining pressures. We have extended their stability analysis by explicitly accounting for the seepage force in the factor of safety and implementing an alternative formulation of confining pressures, though presently for homogeneous bank material.

Following Huang (1983) the surface water on the failure block is modeled by assuming it is a material with no strength (cohesion and angle of internal friction are set to zero). Hence, the slip surface is extended vertically through the water, and a horizontal hydrostatic force is applied on the vertical portion of the slip surface (see Figure 3.3).

The forces acting on the failure block are (Figure 3.3):

- 1 the *weight of the failure block*, W_s ;
- 2 the *weight of surface water* on the failure block, W_w ;
- 3 the *hydrostatic force* exerted by surface water on the vertical slip surface, F_w ;
- 4 the *hydrostatic force* exerted by water in the tension crack, F_t ;
- 5 the *seepage force*, F_s ;
- 6 the *shear force* at the base of the failure block, S ; and

Figure 3.3 Definition sketch of forces acting on a streambank.



7 the total *normal force* at the base of the failure block, N .

The shear force acting at the base of the failure block can be written using the *shear strength equation* for either *saturated* or *unsaturated* soils (Fredlund and Rahardjo, 1993):

$$S = \frac{L}{F} (c' + (\sigma_n - u_a) \tan \phi' + (u_a - u_w) \tan \phi^b) \quad (3.5)$$

where σ_n is total stress normal to the base of the failure block, u_a is pore-air pressure, u_w is pore-water pressure, c' is the effective cohesion, ϕ' is the effective angle of internal friction associated with the normal stress state variable $(\sigma_n - u_a)$, ϕ^b is an angle indicating the increase in shear strength for an increase in matric suction $(u_a - u_w)$, L is the length of the inclined slip surface, and F is the *factor of safety* which is defined as the factor by which the shear strength parameters must be reduced in order to bring the soil mass into a state of limiting equilibrium along the assumed slip surface.

Integrating the expression of static equilibrium of a two-dimensional soil element

$$\nabla \cdot \bar{\sigma} + \gamma_b g = 0 \quad (3.6)$$

where $\bar{\sigma}$ is the total stress tensor, γ_b is bulk unit weight of the bank material, and g is the gravitational acceleration vector, over the failure block yields the following force balances in horizontal and vertical directions:

$$F_w - F_t + S \cos \beta - N \sin \beta = 0 \quad (3.7a)$$

$$W_s + W_w - S \sin \beta - N \cos \beta = 0 \quad (3.7b)$$

where β is the failure-plane angle. Setting pore-air pressures to zero (approximately true in natural soil deposits), and using $\sigma_n = N/L$ and $u_w = U_w/L$, where U_w is pore-water force acting on the slip surface, the shear force becomes

$$S = \frac{1}{F} (Lc' + N\tan\phi' + U_w \tan\phi^b) \quad (3.8)$$

Eliminating the shear force S and normal force N from (3.7a), (3.7b), and (3.8) yields the following expression for the *factor of safety*:

$$F = \frac{c'L + [(W_s + W_w)\cos\beta + (F_w - F_t)\sin\beta]\tan\phi' - U_w \tan\phi^b}{(W_s + W_w)\sin\beta - (F_w - F_t)\cos\beta} \quad (3.9)$$

For saturated soils $\phi^b = \phi'$, and (3.9) simplifies to

$$F = \frac{c'L + [(W_s + W_w)\cos\beta - U_w + (F_w - F_t)\sin\beta]\tan\phi'}{(W_s + W_w)\sin\beta - (F_w - F_t)\cos\beta} \quad (3.10)$$

Pore-Water Pressure

The *pore-water pressure* distribution within a saturated zone of a two-dimensional, semi-infinite soil mass is *hydrostatic* if the groundwater is at rest and the water density is homogeneous. We can readily calculate pore-water pressures if we know the position of the phreatic surface. If there is *groundwater flow* the pore-water pressure distribution is no longer hydrostatic because pressure gradients are needed to maintain the flow. In the following we assume a steady, uniform Darcian flow field throughout the streambank. This is a considerable approximation because of the curvature and fluctuation of the phreatic surface near the bank surface (Figure 3.3). However, it allows us to examine the effect of *seepage* on the factor of safety of a streambank in a simplified manner.

The *seepage force* F_s per unit area is defined as

$$F_s = i\gamma_w \quad (3.11)$$

where i is hydraulic gradient with $i = \sqrt{(\partial h/\partial x)^2 + (\partial h/\partial z)^2}$, i.e. i is equal to the magnitude of the change in head per unit length along a flow line, h is total hydraulic head, and γ_w is unit weight of water. The angle α (see Figure 3.3) defines the direction of the seepage force. The horizontal component of the seepage force is $F_{s_x} = |F_s| \cos\alpha$ and the vertical component of the seepage force is $F_{s_z} = -|F_s| \sin\alpha$. Equilibrium of the groundwater requires

$$\frac{\partial u_w}{\partial x} + F_{s_x} = 0 \quad (3.12a)$$

$$\frac{\partial u_w}{\partial z} + \gamma_w + F_{s_z} = 0 \quad (3.12b)$$

The pore-water distribution is linear in x and z for the case of uniform, Darcian seepage:

$$u_w = C_1x + C_2z + C_3 \quad (3.13)$$

where C_1 , C_2 , and C_3 are constants. From (3.12a) and (3.12b) it follows that $C_1 = -F_{s_x}$ and $C_2 = -(\gamma_w + F_{s_z})$. We can determine C_3 from the position (x_p, z_p) (cf. Figure 3.3) of the phreatic surface on the face of the streambank where the pore-water pressure equals zero: $C_3 = F_{s_x}x_p + (\gamma_w + F_{s_z})z_p$. The *pore-water distribution* then reads

$$u_w = \gamma_w(z_p - z) + \gamma_w|i|((x_p - x)\cos\alpha - (z_p - z)\sin\alpha) \quad (3.14)$$

where the first term on the right-hand side of (3.14) is the hydrostatic part of the distribution and the second term on the right-hand side of (3.14) is the non-hydrostatic part of the distribution due to seepage. Equating (3.14) to zero gives the position of the phreatic surface

$$z = z_p + \frac{|i|\cos\alpha}{1 - |i|\sin\alpha}(x_p - x) \quad (3.15)$$

The coordinate pair (x_p, z_p) can be selected as the top of the seepage face on the streambank.

Factor of Safety without Seepage

Herein, we derive an expression for the *factor of safety* for a streambank assuming the groundwater is at rest. Hence, the first term on the right-hand side of (3.14) represents the pore-water pressure distribution. Commonly, the *pore-water pressure ratio* r_u is used instead of pore-water pressure U_w . Bishop and Morgenstern (1960) defined the pore-water pressure ratio as

$$r_u = \frac{u_w}{\gamma_b d} \quad (3.16)$$

where d is depth below the soil surface. Integrating (3.16) we have

$U_w = r_u W_s \sec\beta$, and consequently

$$F = \frac{c'L + [((1 - r_u \sec^2\beta)W_s + W_w)\cos\beta + (F_w - F_t)\sin\beta]\tan\phi' + \Psi\tan\phi^b}{(W_s + W_w)\sin\beta - (F_w - F_t)\cos\beta} \quad (3.17)$$

where Ψ is the total negative pore-water pressure or *matric suction* along the slip surface in the unsaturated zone. Huang (1983) argued that definition (3.16) of pore-water pressure ratio is not reasonable as the term $1 - r_u \sec^2\beta$ becomes negative for larger failure plane angles. The pore-water pressure ratio $r_u \approx 0.5$

for a fully saturated failure block; if $\beta > 45^\circ$ the effective force normal to the failure plane is

$$\bar{N} = (1 - r_u \sec^2 \beta) W_s \cos \beta < 0 \quad (3.18)$$

Huang (1983) and others (e.g., Fredlund, 1995) use the concept of *buoyant weight* to overcome this problem. The pore-water pressure is used to reduce the effective stress along the failure surface by a factor $(1 - r_u)$, so

$\bar{N} = (1 - r_u) W_s \cos \beta$. Huang (1983) defined the pore-water pressure ratio as the ratio between the total pore-water pressure and the total overburden pressure:

$$r_u = \frac{\text{volume of sliding mass under water} \times \gamma_w}{\text{volume of sliding mass} \times \gamma_b} \quad (3.19)$$

We adjust (3.19) to account for the presence of surface water on the bank as follows:

$$r_u = \frac{(\text{vol. sliding mass under water} + \text{vol. surface water on bank}) \times \gamma_w}{\text{vol. sliding mass} \times \gamma_b + \text{vol. surface water on bank} \times \gamma_w} \quad (3.20)$$

where the text “vol.” means “volume of.” Introducing (3.20) into (3.9) yields

$$F = \frac{c'L + [(1 - r_u)(W_s + W_w) \cos \beta + (F_w - F_t) \sin \beta] \tan \phi' + \Psi \tan \phi^b}{(W_s + W_w) \sin \beta - (F_w - F_t) \cos \beta} \quad (3.21)$$

Defining *apparent* or *total cohesion* as (Fredlund and Rahardjo, 1993)

$$c_a = c' - \frac{1}{L}(r_u(W_s + W_w) \cos \beta \tan \phi' - \Psi \tan \phi^b) \quad (3.22)$$

the factor of safety is

$$F = \frac{c_a L + [(W_s + W_w) \cos \beta + (F_w - F_t) \sin \beta] \tan \phi'}{(W_s + W_w) \sin \beta - (F_w - F_t) \cos \beta} \quad (3.23)$$

Factor of safety with Seepage

Seepage affects the factor of safety through *apparent cohesion*. The horizontal component of the seepage force, F_{s_x} , influences the pore-water pressure distribution by tilting the phreatic surface, consequently changing the saturated area of the failure block. The vertical component of the seepage force, F_{s_z} , changes the vertical gradient of pore-water pressure. We can account for the seepage force by adjusting r_u , Ψ , and introducing an excess positive pore-water force in (3.21):

$$c_a = c' - \frac{1}{L}[(r_u + \bar{r}_u)(W_s + W_w) \cos \beta \tan \phi' + \bar{U}_w \tan \phi' - (\Psi + \bar{\Psi}) \tan \phi^b] \quad (3.24)$$

where the overbar denotes a correction of the variable due to seepage.

Factor of safety for Layered Streambanks

We can also use (3.23) to determine the stability of *layered streambanks* by using a weighted, average cohesion and angle of internal friction for the heterogeneous bank material. However, we cannot readily extend (3.23) to account for the strength of each soil in a layered streambank. In this case we have to revert to the method of slices (Fellenius, 1936).

Inclination of the Failure Surface

Darby and Thorne (1996) followed Taylor (1948), who stated that the most dangerous *failure surface* is that with the maximum *stability number*

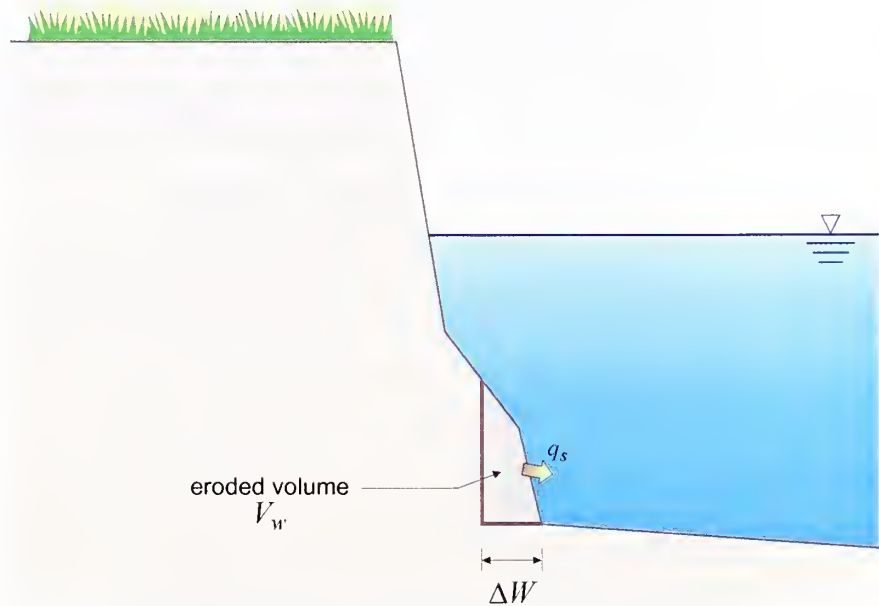
$N_b = \gamma_b H / c_d$, where H is height of failure block and c_d is developed cohesion, or equivalently the failure surface for which cohesion is fully mobilized, that is, $\partial c_d / \partial \beta = 0$. However, Darby and Thorne (1996) assumed $c_d = c'$. Effective cohesion is primarily determined by soil structure and soil moisture, and therefore may not vary much with failure plane angle. Hence, Darby and Thorne's approach of rewriting (3.21) to yield an expression for effective cohesion, and equating the derivative of this expression with respect to failure plane angle to zero, is unrealistic. Moreover, the factor of safety for the resulting failure plane angle is not a minimum.

Here, the *inclination of the failure plane* is that for which the factor of safety is minimum, that is, $\partial F / \partial \beta = 0$. Taking the derivative of (3.23) with respect to the failure plane angle gives

$$\begin{aligned} \frac{\partial F}{\partial \beta} = & \left\{ L \frac{\partial c_a}{\partial \beta} [(W_s + W_w) \sin \beta - (F_w - F_t) \cos \beta] \right. \\ & - c_a L \left[\frac{\partial (W_s + W_w)}{\partial \beta} \sin \beta + 2(W_s + W_w) \cos \beta - (F_w - F_t) \frac{\cos 2\beta}{\sin \beta} \right] \\ & \left. - \left[(W_s + W_w)^2 + (F_w - F_t) \frac{\partial (W_s + W_w)}{\partial \beta} + (F_w - F_t)^2 \right] \tan \phi' \right\} \\ & / [(W_s + W_w) \sin \beta - (F_w - F_t) \cos \beta]^2 \end{aligned} \quad (3.25)$$

Equating (3.25) to zero yields the failure plane angle.

Figure 3.4 Representation of fluvial erosion. The highlighted area is scoured by the flow, steepening the bank.



Implementation of the Channel-Widening Submodel

Fluvial Erosion

CONCEPTS uses (3.1)–(3.3) to compute lateral erosion distance at the toe of the bank, which is used to adjust the bank profile as shown in Figure 3.4. Like Osman and Thorne (1988), CONCEPTS assumes that lateral erosion produces a vertical cut on the streambank and a horizontal cut on the streambed.

CONCEPTS calculates the eroded volume per unit channel length, V_w , by determining the intersection of the vertical cut and bank profile and using ΔW . We convert the eroded volume of bank material to a lateral flux of sediment into the channel

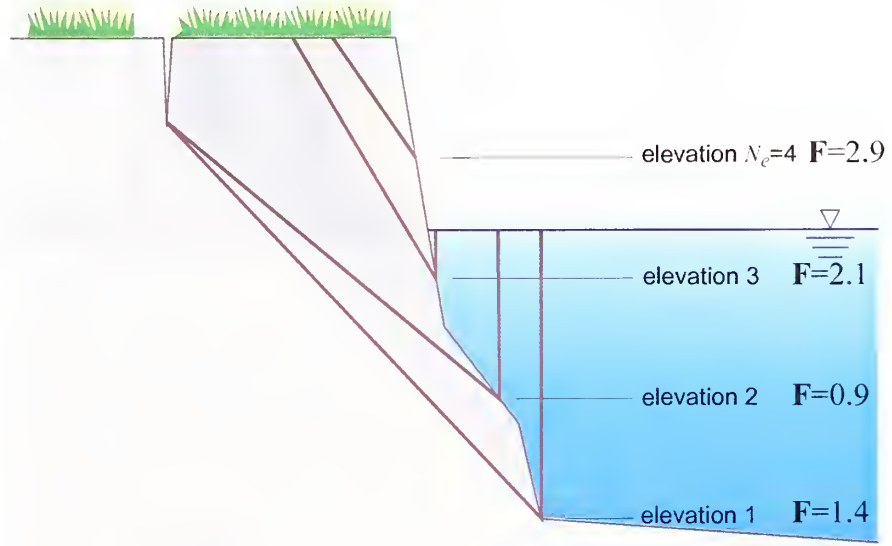
$$q_{s_k} = \frac{\beta_k^b V_w}{\Delta t} \quad (3.26)$$

in which β_k^b is fractional content by volume of size class k in the streambank. Equation (3.26) shows that the eroded volume is uniformly partitioned over the time step Δt . The lateral flux is added to the conservation of sediment mass carried by the flow (2.1).

Mass Wasting

The slip surface does not need to intersect the streambank at the toe of the bank. The bank-stability algorithm evaluates the factor of safety at N_e

Figure 3.5 Possible failure block geometries for the case where the number of elevations at which the factor of safety is evaluated, N_e , equals four. Sample values of factor of safety are given for each failure block geometry. Here, factor of safety is smallest for block #2, and smaller than unity. Hence, the streambank fails along the respective slip surface.



elevations, which are equidistantly distributed along the bank profile. The user must specify N_e as an input parameter to the model.

The bank-stability analysis is a two-step process. The algorithm firstly determines the angle of the slip surface that minimizes factor of safety at each of the N_e elevations (Figure 3.5), and consequently computes factor of safety. Finally, the algorithm selects the smallest of the N_e number of factor of safeties. The bank fails if this factor of safety is smaller than unity.

If bank failure occurs, CONCEPTS computes the volume of the failure block and converts it to a lateral flux of sediment into the channel (Simon *et al.*, 1991) as in (3.26). Field studies (Simon *et al.*, 1999) show that this is not very realistic; the failure block will break into smaller blocks and aggregates in which cohesion holds sediment particles together. A deterministic model of this process, however is not yet available.

The user specifies the depth of the tension crack as a fraction f_t of the depth of the soil layer with negative earth pressure (3.4) as:

$$z_{tc} = f_t z_t \quad (3.27)$$

Bank Erosion and Channel Widening

Part 2

DATA SPECIFICATION

INPUT DATA

This chapter presents the input data structure of CONCEPTS. CONCEPTS requires the following input files created by the user: (1) one input file with run control data, (2) one input file with discharge data at the upstream boundary of the modeling reach, (3) an input file for each cross section in the modeling reach, and (4) an input file for each hydraulic structure in the modeling reach.

Run Control Data

The run control data input file consists of three main blocks of data:

- Block 1. project related data, general data, and makeup of modeling reach
- Block 2. names of cross section and hydraulic structure files
- Block 3. output options

Block 1

Block 1 consists of $31 + N_l$ input lines, see Table 4.1, where N_l is the number of links comprising the simulated stream corridor. A link is defined as a subreach or a hydraulic structure. A subreach is a channel segment between two structures. If there are no hydraulic structures along the simulated channel, the number of links equals one because there is just one reach. If there is one hydraulic structure in the modeling reach, say a box culvert, the number of links equals three: (1) a subreach between the upstream boundary and the box culvert, (2) the box culvert itself, and (3) a subreach between the box culvert and the downstream boundary.

Line 5 contains the run identifier, which is a twelve-character string. CONCEPTS uses the run identifier to name the output files as: run identifier + ‘ ’ + number + ‘.TXT’. For example, if the run identifier is SIMULATION, then

Table 4.1 Input data in block #1 of run control data.

line number	line description	data type	unit
1-4	comment lines		
5	run identifier	string	
6	comment line		
7	project title	string	
8-9	comment lines		
10	name of discharge file	string	
11	comment line		
12	flow-related data	real/integer	m^3/s
13	comment line		
14	upstream sediment discharge option and rates	integer/real	
15	comment line		
16	fraction of fines in a cohesive bed and bed control at downstream boundary	real	
17	comment line		
18	bank-failure analysis options	integer	
19	comment line		
20	type of bed resistance formulation	integer	
21	comment line		
22	water temperature	real	$^{\circ}\text{C}$
23	comment line		
24	included submodels	integer	
25-26	comment lines		
27	simulation times	string/integer	sec
28-29	comment lines		
30	number of links N_l		
31	comment line		
32 – $32 + N_l - 1$	link IDs		

the output file names are ‘SIMULATION 050.TXT’, ‘SIMULATION 051.TXT’, etc. The numbering of the output files starts at 50. The project title on line 7 is an 80-character string.

Line 10 contains a 32-character string that is the name of the file with the flow and sediment discharge time-series at the upstream boundary of the modeling reach (see page 88). Line 12 contains: (1) baseflow discharge at the upstream boundary (m^3/s); (2) the rate of lateral inflow (C_Q) as a fraction of the discharge at the upstream boundary (m^{-1}), that is

$$q = C_Q Q_1 \quad (4.1)$$

where Q_1 is the discharge imposed at the upstream boundary; and (3) a flag indicating the type of downstream boundary condition used in the flow simulation. If the flag is zero, CONCEPTS uses the loop-rating curve (1.35). If the flag is set to one, CONCEPTS uses the user-specified rating curve (1.34).

Table 4.2 Values assigned to the different processes that can be accounted for by the bank stability analysis.

process	value
positive pore-water pressures	1
confining pressures	2
matric suction	4
seepage	8

In the latter case line 12 also contains the number of segments N_{rs} and values for h_i , α_i , and β_i for each segment by segment.

Line 14 contains a flag, which can be set to 0 or 1, indicating how sediment load is imposed at the upstream boundary. If the user sets the flag to zero, line 14 also contains the fraction f_k of the local sediment transport capacity for each of the 13 size classes (see (2.32)). Thus, if $f_k = 0.1$ for a certain size class, the flow will carry a sediment load equalling 10% of the local sediment transport capacity for that size class. If the user sets the flag to one, the sediment load is given in the file with upstream boundary conditions (line 10).

The first number on line 16 informs CONCEPTS when the streambed can be assumed cohesive or cohesionless. If the fraction of fines in the bed is larger than this input entry, the bed is assumed to be cohesive. CONCEPTS defines fines as clay and silt particles, that is, size classes 1 through 3 (see Table 2.1). The second number is the modifier m that adjusts the predicted change in bed elevation at the downstream boundary of the simulated stream corridor (see (2.33)).

Line 18 contains two integers used by the bank-stability analysis algorithm. The first number denotes the level of complexity of the stability analysis. The user specifies which physical processes need to be taken into account. The analysis distinguishes the following processes: positive pore-water pressures, confining pressures, matric suction or negative pore-water pressures, and seepage. Each process has an assigned value, see Table 4.2. The user specifies the complexity of the analysis by adding these values. For example, if the user wants to account for positive pore-water pressures (a value of 1) and for confining pressures (a value of 2), the user needs to enter a value of 3 in the input file. If the user enters zero, none of the four processes will be taken into account. The second number on line 18 is the number of possible elevations at which the slip surface may intersect the bank profile (see section on the implementation of “mass wasting”).

Line 20 contains a flag that sets the type of streambed resistance formulation. If the entered number is two (2), CONCEPTS uses the friction-factor relation proposed by Karim (1995). Karim obtained satisfactory results within the following range of variables: flow depths from 0.03 to 16.7 m, velocities from 0.32 to 3.41 m/s, energy slopes from 0.0000183 to 0.0243, median sediment sizes from 0.08 to 28.6 mm, and gradation coefficients of bed sediments from 1

Table 4.3 Link types to be used with CONCEPTS.

link type	ID
channel reach	1
pipe culvert	11
box culvert	13
bridge crossing	21
drop structure	26
generic structure	31

to 2. If the user enters a value other than two, CONCEPTS uses a constant Manning n , which is specified in the cross section data file.

Line 22 contains the water temperature ($^{\circ}\text{C}$), which CONCEPTS uses to compute water density and viscosity.

Line 24 contains three flags, which can be set at either 0 or 1. These flags determine whether CONCEPTS takes into account sediment routing and bed adjustment, streambank fluvial erosion, and streambank mass-wasting, respectively. If the user sets a flag to zero the corresponding process is not taken into account.

Line 27 contains the start time and end time of the simulation, and the time step (sec). The start and end time are 19-character strings formatted as “mm/dd/yyyy hh:mm:ss.” For example, two o’clock in the afternoon on June 7, 1999 is represented as: 06/07/1999 14:00:00.

CONCEPTS uses the integer value entered for the time step as initial time step. During the simulation the time step is automatically adjusted based on temporal variations in discharge and flow depth.

Line 30 contains the number of links. Lines 32 through $31 + N_l$ consist of the link IDs for each link in the modeling reach. Table 4.3 lists the available linktypes.

Block 2

Block 2 identifies the files that contain input data for cross sections and hydraulic structures. It consists of $3 + N_x$ lines for each link in the modeling reach, where N_x is the number of cross sections if the link is a reach and $N_x = 0$ if the link is a hydraulic structure, see Table 4.4.

If the link is a reach, line 3 contains an integer representing the number of cross sections in that reach. If the link is a hydraulic structure, line 3 contains a 32-character string representing the name of the file with the input data of the structure.

Table 4.4 Input data in block #2 of run control data. The user has to repeat this block for each link.

line number	line description	data type
1 - 2	comment lines	
3	number of cross sections, N_x , if link is a subreach name of input file if link is a hydraulic structure	integer string
4 - $3 + N_x$	name of input file for each cross section if link is a subreach	string

Table 4.5 Input data to request output at a certain cross section and for a certain runoff event. Lines 2 through $4 + N_s$ are repeated N_{lc} times.

line number	line description	data type
1	number of locations N_{lc}	integer
2	type of outputted data	integer
3	location reference	integer
4	number of storm events N_s	integer
5 - $5 + N_s - 1$	dates of storm events	string

If the link is a reach, lines 4 through $3 + N_x$ contain the names (32-character string) of the files with data related to cross sections.

Block 3

Block 3 comprises output options. There are three output categories:

- 1 output at a certain location and for a certain runoff event,
- 2 time-series output at a certain location, and
- 3 output for a certain runoff event along a section of the modeling reach.

The user needs to specify the options following the above sequence.

Output at a Certain Location and for a Certain Runoff Event

Table 4.5 lists the data the user has to enter to request output from the first category. Line 1 contains the number of locations (N_{lc}) at which output is requested, followed by the type of data on line 2. The latter is a summation of values assigned to various variables (see Table 4.6). For example, if the user wants to output peak discharge and stage, and sediment yield for a certain runoff event, the user needs to enter 21 (=1+4+16).

Line 3 contains information on the location of the cross section within the modeling reach. The user has to enter the link number and in-link cross section number, for example cross section 4 in link 1.

Table 4.6 Parameters that can be output for a certain runoff event and cross section.

outputted parameter	value
peak discharge	1
peak flow depth	2
peak stage	4
peak friction slope	8
sediment yield	16
cumulative sediment yield over all runoff events thus far	32
change in bed elevation	64
cumulative change in bed elevation over all runoff events thus far	128
lateral erosion	256
cumulative lateral erosion over all runoff events thus far	512
cross-sectional geometry	1,024
in-bank top and bottom width of cross section	2,048
bank height	4,096
not used	
characteristic particle sizes	16,384
particle size distribution	32,768

Table 4.7 Input data to request time-series output at a certain cross section. Lines 2 through $4 + N_{ts}$ are repeated N_{lc} times.

line number	line description	data type
1	number of locations N_{lc}	integer
2	type of outputted data	integer
3	location reference	integer
4	number of time series N_{ts}	integer
5 - $5 + N_{ts} - 1$	start and end times of each series	string

Line 4 contains the number of runoff events (N_s) for which output is requested at that particular cross section. Lines 5 through $N_s + 4$ contain the dates of occurrence of the runoff events.

Lines 2 through $N_s + 4$ are repeated N_{lc} times.

Time-Series Output at a Certain Location

Table 4.7 lists the data the user has to enter to request time-series output. Line 1 contains the number of locations (N_{lc}) at which output is requested, followed by the type of data on line 2. The latter is a summation of values assigned to various variables (see Table 4.8). For example, if the user wants to output discharge, stage, and factor of safety, the user needs to enter 524,297 (=1+8+524,288).

Line 3 contains information on the location of the cross section within the modeling reach. The user has to enter the link number and in-link cross section

Table 4.8 Parameters that can be output as time series.

outputted parameter	value
discharge	1
velocity	2
flow depth	4
stage	8
flow area	16
flow top width	32
wetted perimeter	64
hydraulic radius	128
conveyance	256
friction slope	512
energy head	1,024
Froude number	2,048
bed shear stress	4,096
sediment discharge (silt/sand/gravel/total)	8,192
cumulative sediment yield (silt/sand/gravel/total)	16,384
cumulative change in bed elevation	32,768
thalweg elevation	65,536
cumulative lateral erosion	131,072
not used	
factor of safety	524,288
apparent cohesion	1,048,576
pore-water force	2,097,152
matric suction force	4,194,304
weight of failure block	8,388,608
weight of water on the bank	16,777,216
horizontal component of the confining force	33,554,432
groundwater elevation	67,108,864
location of bank top	134,217,728

number, for example cross section 4 in link 1. Line 4 contains the number of time series (N_{ts}) for which output is requested at that particular cross section. Lines 5 through $N_{ts} + 4$ contain the start and end dates of the time series.

Lines 2 through $N_{ts} + 4$ are repeated N_{lc} times.

Output for a Certain Runoff Event along a Section of the Modeling Reach

Table 4.9 lists the data the user has to enter to request output for a certain runoff event along a section of the modeling reach, hereafter referred to as a *profile*. Line 1 contains the number of profiles (N_p) at which output is requested, followed by the type of data on line 2. The latter is a summation of values assigned to various variables (see Table 4.10). For example, if the user wants to output peak discharge and stage, and sediment yield for a certain storm event, the user needs to enter 67 (=1+2+64).

Table 4.9 Input data to request output for a certain runoff event along a section of the modeling reach. Lines 2 through $4 + N_s$ are repeated N_p times.

line number	line description	data type
1	number of profiles N_p	integer
2	type of outputted data	integer
3	location reference	integer
4	number of storm events N_s	integer
5 - $5 + N_s - 1$	dates of storm events	string

Table 4.10 Parameters that can be output for a certain runoff event along a section of the modeling reach.

outputted parameter	value
peak discharge	1
peak stage	2
thalweg elevation	4
cumulative change in bed elevation over all runoff events thus far	8
in-bank top width	16
bank height	32
sediment yield	64
characteristic particle sizes	128

Line 3 contains information on the locations of the first and last cross section of the profile. The user has to enter the link number and in-link cross section number, for example cross section 4 in link 1 for the first cross section and cross section 5 in link 3 for the last cross section.

Line 4 contains the number of storm events (N_s) for which output is requested for that particular section. Lines 5 through $N_s + 4$ contain the dates of occurrence of the storm events.

Lines 2 through $N_s + 4$ are repeated N_p times.

Cross Section Data

The cross section data file contains the cross-sectional geometry and parameters that may vary from cross section to cross section. CONCEPTS divides the cross section into a streambed, left and right banks, and left and right floodplains. Data blocks related to these geometric elements make up the input file, see Table 4.11.

Table 4.11 Makeup of cross section data input file.

data block	description
1	general data
2	left floodplain
3	left bank
4	streambed
5	right bank
6	right floodplain

Table 4.12 Data block #1 of the cross section data input file.

line number	line description	data type	unit
1 - 4	comment lines		
5	name of cross section	string	
6	river kilometer	real	km
7	comment line		
8	Manning <i>n</i>	real	s/m ^{1/3}
9	comment line		
10	tributary inflow	real	

General Data (Block 1)

Data block 1 consists of 10 input lines, see Table 4.12. Line 5 contains a 40-character string, which is the name of the input file. Line 6 contains the river kilometer (km) of the cross section. CONCEPTS assumes river kilometer increases in streamwise direction. Line 8 contains the Manning *n* of the total cross section. During the simulation, the equivalent friction factor (see subsection on Flow Resistance) replaces this value. Table 4.13 lists example *n* values for various types of channels from Chow (1959). Line 10 contains the discharge rate of a tributary entering the reach at this cross section. The discharge rate is defined as a fraction of the discharge at this cross section. For example, if the tributary contributes 30 percent of the discharge at the cross section, the user needs to enter 0.3.

Streambed Data Block (Block 4)

The block containing streambed data consists of $15 + N_n + 19 \times N_{la}$ lines of input (see Table 4.14), where N_n is the number of points in the bed profile and N_{la} is the number of soil layers in the bed. Line 3 contains the number of points in the bed profile (see Figure 1.8). Lines 5 through $4 + N_n$ contain the station and elevation values (m) of these points.

Table 4.13 Values of the roughness coefficient n (Chow, 1959).

Type of Channel and Description	Minimum	Normal	Maximum
Natural streams - minor streams (top width at flood stage < 100 ft)			
Streams on plain			
clean, straight, full stage, no rifts or deep pools	0.025	0.030	0.033
same as above, but more stones and weeds	0.030	0.035	0.040
clean, winding, some pools and shoals	0.033	0.040	0.045
same as above, but some weeds and stones	0.035	0.045	0.050
same as above, lower stages, more ineffective slopes and sections	0.040	0.048	0.055
same as two up, more stones	0.045	0.050	0.060
sluggish reaches, weedy, deep pools	0.050	0.070	0.080
very weedy reaches, deep pools, or floodways with heavy stand of timber and underbrush	0.075	0.100	0.150
Mountain streams, no vegetation in channel, banks usually steep, trees and brush along banks submerged at high stages			
bottom: gravels, cobbles, and few boulders	0.030	0.040	0.050
bottom: cobbles with large boulders	0.040	0.050	0.070
Natural streams - floodplains			
Pasture, no brush			
short grass	0.025	0.030	0.035
high grass	0.030	0.035	0.050
Cultivated areas			
no crop	0.020	0.030	0.040
mature row crops	0.025	0.035	0.045
mature field crops	0.030	0.040	0.050
Brush			
scattered brush, heavy weeds	0.035	0.050	0.070
light brush and trees, in winter	0.035	0.050	0.060
light brush and trees, in summer	0.040	0.060	0.080
medium to dense brush, in winter	0.045	0.070	0.110
medium to dense brush, in summer	0.070	0.100	0.160
Trees			
dense willows, summer, straight	0.110	0.150	0.200
cleared land with tree stumps, no sprouts	0.030	0.040	0.050
same as above, but with heavy growth of sprouts	0.050	0.060	0.080
heavy stand of timber, a few down trees, little undergrowth, flood stage below branches	0.080	0.100	0.120
same as above, but with flood stage reaching branches	0.100	0.120	0.160
Natural streams - major streams (top width at flood stage > 100 ft); the n value is less than that for minor streams of similar description because banks offer less effective resistance			
regular section with no boulder or brush	0.025		0.060
irregular and rough section	0.035		0.100
Excavated or dredged			

Table 4.13 Values of the roughness coefficient n (Chow, 1959). (continued)

Type of Channel and Description	Minimum	Normal	Maximum
Earth, straight, and uniform			
clean, recently completed	0.016	0.018	0.020
clean, after weathering	0.018	0.022	0.025
gravel, uniform section, clean	0.022	0.025	0.030
with short grass, few weeds	0.022	0.027	0.033
Earth winding and sluggish			
no vegetation	0.023	0.025	0.030
grass, some weeds	0.025	0.030	0.033
dense weeds or aquatic plants in deep channels	0.030	0.035	0.040
earth bottom and rubble sides	0.028	0.030	0.035
stony bottom and weedy banks	0.025	0.035	0.040
cobble bottom and clean sides	0.030	0.040	0.050
Dragline-excavated or dredged			
no vegetation	0.025	0.028	0.033
light brush on banks	0.035	0.050	0.060
Rock cuts			
smooth and uniform	0.025	0.035	0.040
jagged and irregular	0.035	0.040	0.050
Channels not maintained, weeds and brush uncut			
dense weeds, high as flow depth	0.050	0.080	0.120
clean bottom, brush on sides	0.040	0.050	0.080
same as above, highest stage of flow	0.045	0.070	0.110
dense brush, high stage	0.080	0.100	0.140
Lined or built-up channels - metal			
Smooth steel surface			
unpainted	0.011	0.012	0.014
painted	0.012	0.013	0.017
Lined or built-up channels - nonmetal			
Cement			
neat surface	0.010	0.011	0.013
mortar	0.011	0.013	0.015
Wood			
planed, untreated	0.010	0.012	0.014
planed, creosoted	0.011	0.012	0.015
unplaned	0.011	0.013	0.015
plank with battens	0.012	0.015	0.018
lined with roofing paper	0.010	0.014	0.017
Concrete			
trowel finish	0.011	0.013	0.015
float finish	0.013	0.015	0.016
finished, with gravel on bottom	0.015	0.017	0.020
unfinished	0.014	0.017	0.020
gunite, good section	0.016	0.019	0.023
gunite, wavy section	0.018	0.022	0.025
on good excavated rock	0.017	0.020	
on irregular excavated rock	0.022	0.027	

Table 4.13 Values of the roughness coefficient n (Chow, 1959). (continued)

Type of Channel and Description	Minimum	Normal	Maximum
Concrete bottom float finish with sides of:			
dressed stone in mortar	0.015	0.017	0.020
random stone in mortar	0.017	0.020	0.024
cement rubble masonry, plastered	0.016	0.020	0.024
cement rubble masonry	0.020	0.025	0.030
dry rubble or riprap	0.020	0.030	0.035
Gravel bottom with sides of:			
formed concrete	0.017	0.020	0.025
random stone mortar	0.020	0.023	0.026
dry rubble or riprap	0.023	0.033	0.036
Brick			
glazed	0.011	0.013	0.015
in cement mortar	0.012	0.015	0.018
Masonry			
cemented rubble	0.017	0.025	0.030
dry rubble	0.023	0.032	0.035
Dressed ashlar	0.013	0.015	0.017
Asphalt			
smooth	0.013	0.013	
rough	0.016	0.016	
Vegetal lining	0.030		0.500

Table 4.14 Input block #4 with streambed data. Lines $14 + N_n$ through $32 + N_n$ are repeated N_{la} times.

line number	line description	data type	unit
1 - 2	comment lines		
3	number of points in profile N_n	integer	
4	comment line		
5 - $5 + N_n - 1$	station and elevation	real	m
$5 + N_n$	comment line		
$6 + N_n$	elevation of bed rock	real	m
$7 + N_n$	comment line		
$8 + N_n$	porosity of streambed	real	
$9 + N_n$	comment line		
$10 + N_n$	hiding factors	real	
$11 + N_n$ & $12 + N_n$	comment lines		
$13 + N_n$	number of soil layers N_{la}	integer	
$14 + N_n$	comment line		
$15 + N_n$	depth below bed surface	real	m
$16 + N_n$	comment line		
$17 + N_n - 29 + N_n$	bed composition	real	%
$30 + N_n$ & $31 + N_n$	comment lines		
$32 + N_n$	cohesive bed parameters	real	Pa, Pa, m/s·Pa
$14 + N_n + 19 \times N_{la}$	comment line		
$15 + N_n + 19 \times N_{la}$	Manning n	real	s/m ^{1/3}

Table 4.15 Input block #3 and #5 with streambank data.

line number	line description	data type	unit
1 - 2	comment lines		
3	number of points in profile N_n	integer	
4	comment line		
5 - $5 + N_n - 1$	station and elevation	real	m
$5 + N_n$	comment line		
$6 + N_n$	bank material properties	real	Pa, °, °, N/m ³
$7 + N_n$	comment line		
$8 + N_n - 20 + N_n$	bank material composition	real	%
$21 + N_n$	comment line		
$22 + N_n$	critical shear stress	real	Pa
$23 + N_n$	comment line		
$24 + N_n$	bank moisture parameters	real	m, -, °
$25 + N_n$	comment line		
$26 + N_n$	Manning n	real	s/m ^{1/3}

Lines $6 + N_n$, $8 + N_n$, and $10 + N_n$ contain bedrock elevation (m), streambed porosity, and hiding factors for silt, sand, and gravel in the surface layer, respectively. The channel cannot incise below bedrock elevation.

Line $13 + N_n$ contains the number of soil layers comprising the bed. The next lines contain information, for each layer, on depth below the bed surface (m), composition (%), and erodibility of cohesive material. This block is repeated N_{la} times. The user has to enter the fractional content of each of the 13 size classes as percentages. The parameters of a cohesive soil layer are entered as: (1) critical shear stress to deposit sediment particles (τ_d) in Pa, (2) critical shear stress to entrain sediment particles (τ_e) in Pa, and (3) erodibility coefficient in m/s·Pa.

Line $15 + N_n + 19 \times N_{la}$ contains the Manning n of the streambed.

Streambank Data Block (Blocks 3 and 5)

Blocks 3 and 5 containing streambank data consist of $26 + N_n$ lines of input (see Table 4.15), where N_n is the number of points in the bank profile. Line 3 contains the number of points in the bank profile (see Figure 1.8). Lines 5 through $4 + N_n$ contain the station and elevation values (m) of these points.

Line $6 + N_n$ contains effective cohesion (Pa), effective angle of internal friction (°), the angle indicating the increase in shear strength for an increase in matric suction (°), and the bulk weight of the bank material (N/m³). Lines $8 + N_n$ through $20 + N_n$ contain the fractional content of each of the 13 size

Table 4.16 Input block #2 and #6 with floodplain data.

line number	line description	data type	unit
1 - 2	comment lines		
3	number of points in profile N_n	integer	
4	comment line		
5 - $5 + N_n - 1$	station and elevation	real	m
$5 + N_n$	comment line		
$6 + N_n$	Manning n	real	s/m ^{1/3}

classes as percentages. Line $22 + N_n$ contains the critical shear stress to entrain bank material particles (Pa). Line $24 + N_n$ contains groundwater table (m), hydraulic gradient (m/m), and angle of seepage force (°). Line $26 + N_n$ contains Manning n of the streambank.

Floodplain Data Block (Blocks 2 and 6)

Blocks 2 and 6 containing floodplain data consist of $6 + N_n$ lines of input (see Table 4.16), where N_n is the number of points in the floodplain profile. Line 3 contains the number of points in the floodplain profile (see Figure 1.8). Lines 5 through $4 + N_n$ contain the station and elevation values (m) of these points. Line $6 + N_n$ contains the Manning n of the floodplain.

Hydraulic Structure Data

The four types of hydraulic structures (culvert, bridge crossing, drop structure, and generic structure) have common parameters and structure specific parameters. The common parameters comprise the first part of each structure's input file, followed by the structure specific data.

Table 4.17 lists the common data: a name field on line 5 of the input file, river kilometer (km) on line 7, Manning n on line 9, length of the structure (m) on line 11, the upstream and downstream inverts (m) on line 13, and the upstream and downstream elevations of the structure above the streambed (m) on line 15.

Culvert

The flow computation at culverts is based on the U.S. Federal Highway Administration's (1985) nomographs. CONCEPTS can simulate the flow at box and pipe culverts. Presently, we have not implemented other culvert shapes. All input parameters for pipe and box culverts are the same, except for their geometry.

Table 4.17 Input parameters common to the different types of structures.

line number	line description	data type	unit
1 - 4	comment lines		
5	name of structure	string	
6	comment line		
7	river kilometer	real	km
8	comment line		
9	Manning n	real	s/m ^{1/3}
10	comment line		
11	length	real	m
12	comment line		
13	inverts	real	m
14	comment line		
15	elevations above streambed	real	m

Table 4.18 Input data for culverts.

line number	line description	data type	unit
16 - 17	comment lines		
18	chart and scale numbers	integer	
19	comment line		
20	entrance loss coefficient	real	
21	comment line		
22	number of barrels	integer	
23 - 24	comment lines		
25	dimensions	real	m

Table 4.18 lists the input data required for culverts. Line 18 contains the USFHWA (1985) chart and scale numbers representing the shape of the culvert (see Table 4.19). Line 20 contains the entrance loss coefficient used when the culvert flow is controlled by the outlet (see Table 4.20). Line 22 contains the number of culvert barrels in the road crossing. Line 25 contains the dimensions of the culvert barrel: diameter (m) for a pipe culvert, and span (m) and rise (m) for a box culvert.

Bridge Crossing

CONCEPTS assumes that the shape of the bridge crossing is trapezoidal with a horizontal bed. Table 4.21 lists the input data required for bridge crossings. Line 18 contains the bottom width (m) and side slope of the cross section. Line 20 contains the total pier width (m), pier shape coefficient (Table 4.22), and pier loss coefficient.

Table 4.19 USFHWA (1985) chart and scale numbers for pipe and box culverts.

Chart Number	Scale Number	Description
1		Concrete Pipe Culvert
	1	square-edged entrance with headwall
	2	groove end entrance with headwall
	3	groove end entrance, pipe projecting from fill
2		Corrugated Metal Pipe Culvert
	1	headwall
	2	mitered to conform slope
	3	pipe projecting from fill
3		Concrete Pipe Culvert, beveled ring entrance
	1	small bevel
	2	large bevel
8		Box Culvert with Flared Wingwalls
	1	wingwalls flared 30 to 75 degrees
	2	wingwalls flared 90 to 15 degrees
	3	wingwalls flared 0 degrees (sides extended straight)
9		Box Culvert with Flared Wingwalls and Inlet Top Edge Bevel
	1	wingwall flared 45 degrees, inlet top edge bevel = $0.43D$
	2	wingwall flared 18 to 33.7 degrees, inlet top edge bevel = $0.083D$
10		Box Culvert, 90-degree Headwall, Chamfered or Beveled Inlet Edges
	1	inlet edges chamfered 3/4-inch
	2	inlet edges beveled 1/2-in/ft at 45 degrees
	3	inlet edges beveled 1-in/ft at 33.7 degrees
11		Box Culvert, Skewed Headwall, Chamfered or Beveled Inlet Edges
	1	headwall skewed 45 degrees, inlet edges chamfered 3/4-in
	2	headwall skewed 30 degrees, inlet edges chamfered 3/4-in
	3	headwall skewed 15 degrees, inlet edges chamfered 3/4-in
	4	headwall skewed 15 to 45 degrees, inlet edges beveled
12		Box Culvert, Non-Offset Flared Wingwalls, 3/4-inch Chamfer at Top of Inlet
	1	wingwalls flared 45 degrees, inlet not skewed
	2	wingwalls flared 18.4 degrees, inlet not skewed
	3	wingwalls flared 18.4 degrees, inlet skewed 30 degrees
13		Box Culvert, Offset Flared Wingwalls, Beveled Edge at Top of Inlet
	1	wingwalls flared 45 degrees, inlet top edge bevel = $0.042D$
	2	wingwalls flared 33.7 degrees, inlet top edge bevel = $0.083D$
	3	wingwalls flared 18.4 degrees, inlet top edge bevel = $0.083D$

Drop Structure

CONCEPTS assumes that the cross section of the drop structure is trapezoidal with a horizontal bottom. Table 4.23 lists the input data required for drop structures. Line 18 contains the bottom width (m) and side slope of the drop structure. Line 20 contains the entrance loss coefficient.

Table 4.20 Entrance loss coefficients for pipe and box culverts.

Type of Structure and Design of Entrance	Loss Coefficient
Concrete Pipe Projecting from Fill (no headwall)	
socket end of pipe (grooved end)	0.2
square cut end of pipe	0.5
Concrete Pipe with Headwall or Headwall and Wingwalls	
socket end of pipe	0.2
square cut end of pipe	0.5
rounded entrance	0.2
Concrete Pipe	
mitered to conform to fill slope	0.7
end section conformed to fill slope	0.5
beveled edges, 33.7 and 45 degree bevels	0.2
side slope tapered inlet	0.2
Corrugated Metal Pipe or Pipe-Arch	
projected from fill (no headwall)	0.9
headwall or headwall and wingwalls square edge	0.5
mitered to conform to fill slope	0.7
end section conformed to fill slope	0.5
beveled edges, 33.7 and 45 degree bevels	0.2
side slope tapered inlet	0.2
Concrete Box, Headwall Parallel to Embankment (no wingwalls)	
square-edged on three sides	0.5
three edges rounded to radius of 1/12 barrel dimension	0.2
Concrete Box, Wingwalls at 30 to 75 degrees to Barrel	
square-edge on crown	0.4
top corner rounded to radius of 1/12 barrel dimension	0.2
Concrete Box, Wingwalls at 10 to 25 degrees to barrel	
square-edge on crown	0.5
Concrete Box, Wingwalls parallel (extension of sides)	
square-edge on crown	0.7
side or slope tapered inlet	0.2

Table 4.21 Input data for bridge crossings.

line number	line description	data type	unit
16 - 17	comment lines		
18	bridge crossing geometry	real	m, -
19	comment line		
20	pier parameters	real	m, -, -

Table 4.22 Yarnell's pier shape coefficient for various pier shapes.

Pier Shape	Yarnell C_p Coefficient
semi-circular nose and tail	0.90
lens-shaped nose and tail	0.90
twin-cylinder piers with connecting diaphragm	0.95
twin-cylinder piers without diaphragm	1.05
90-degree triangular nose and tail	1.05
square nose and tail	1.25

Table 4.23 Input data for drop structures.

line number	description	data type	unit
16 - 17	comment lines		
18	drop structure geometry	real	m, m/m
19	comment line		
20	entrance loss coefficient	real	

Table 4.24 Input data for generic structures.

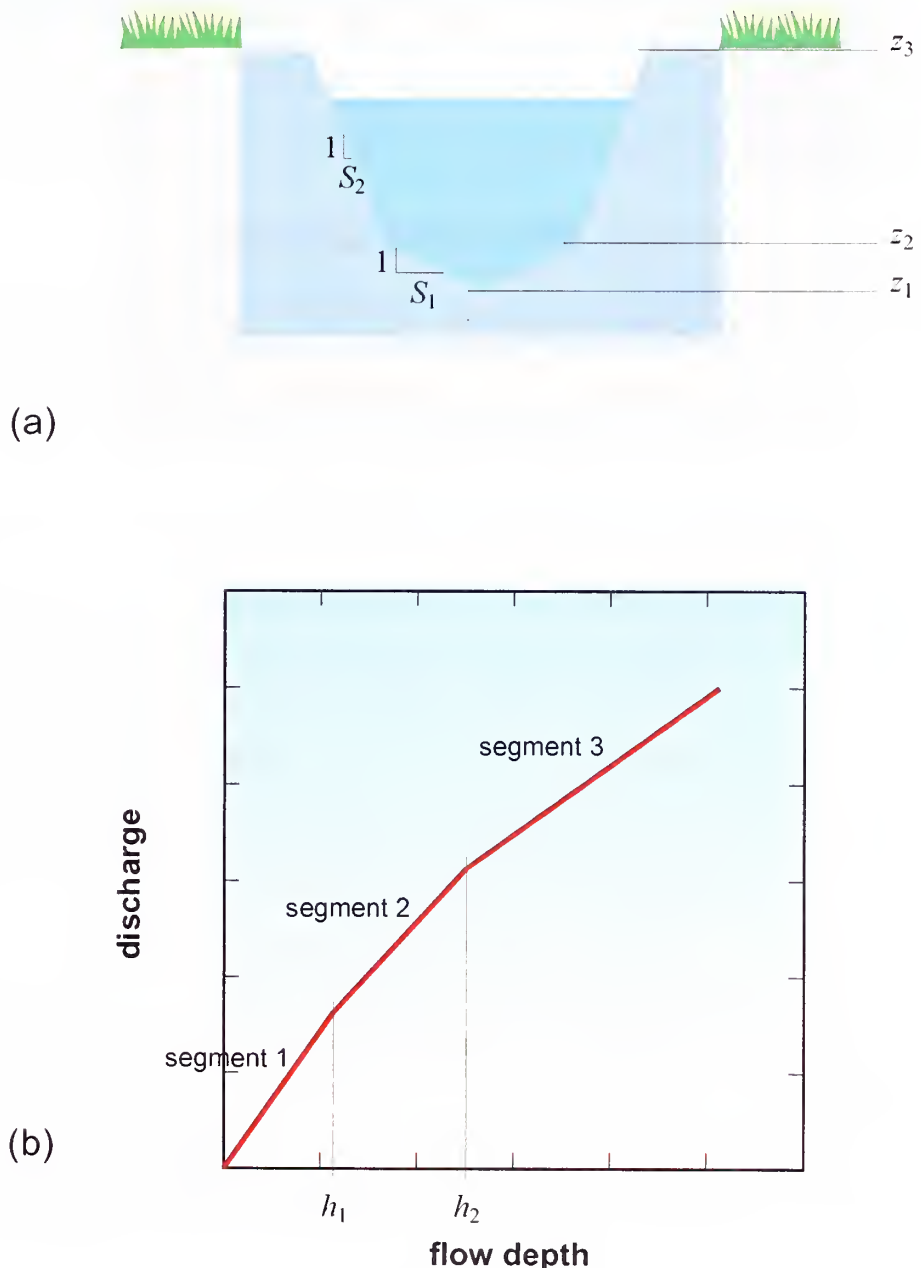
line number	line description	data type	unit
16 - 17	comment lines		
18	number of wall segments N_{se}	integer	
19	comment line		
20 - 20 + N_{se} - 1	segment elevation and slope	real	m, m/m
20 + N_{se}	top elevation	real	m
21 + N_{se} - 22 + N_{se}	comment lines		
23 + N_{se}	number of rating curve segments N_{rs}	integer	
24 + N_{se}	comment line		
25 + N_{se} - 25 + N_{se} + N_{rs} - 1	rating curve parameters	real	m, -, -

Generic Structure

A generic structure is any structure for which a rating curve is available. The main input data are the shape of the structure and the rating curve. CONCEPTS assumes that the cross section of the walls of the structure consist of linear elements characterized by an elevation and slope (see Figure 4.1a). The rating curve may comprise up to 4 segments (Figure 4.1b). Each segment is a power function.

Table 4.24 lists the input data required for generic structures. Line 18 contains the number of segments, N_{se} , comprising the walls of the structure. Lines 20 through 19 + N_{se} contain the bottom elevation (m) and slope of each segment (Figure 4.1a). Line 20 + N_{se} contains the elevation of the top of the structure (m).

Figure 4.1 Shape of a generic structure (a) and rating curve (b). S_i is side slope and z_i is starting elevation of wall segment i . h_i is breakpoint depth in the rating curve.



Line 23 + N_{se} contains the number of segments comprising the rating curve, N_{rs} . Lines 25 + N_{se} through 24 + $N_{se} + N_{rs}$ contain the starting depth (m) (see Figure 4.1b) and coefficient and exponent of the power function for each segment.

Table 4.25 Layout of each record in the upstream boundary conditions file.

	date field column 1	runoff status column 2	flow discharge column 3	sediment load columns 4-16
width	19	3	10	10
data type	string	integer	real	real
unit			m ³ /s	kg/s
example	06/07/1999 14:00:00	1	10.45	1.45E+01

Dynamic Upstream Boundary Conditions

CONCEPTS simulates unsteady flow. The user has to specify breakpoint flow and sediment discharge data at the upstream boundary of the modeling reach. Each record of the discharge input file consists of up to 16 fields (Table 4.25):

- 1 a 19-character date field,
- 2 a 3-character runoff status field,
- 3 a 10-character flow discharge field, and
- 4 13 10-character sediment load fields.

The first three columns are mandatory. If the user sets the flag indicating the upstream boundary condition option regarding sediment load to one (line 14 of the run control file), columns 4 through 16 contain the sediment load entering the stream corridor for each size fraction (kg/s).

The date is formatted as “mm/dd/yyyy hh:mm:ss,” for example “06/07/1999 14:00:00”. The storm status informs CONCEPTS on the beginning and end of runoff events. It takes the following values:

- a value of 1, beginning of runoff event;
- a value of 2, end of runoff event; and
- a value of 0, indicates data between beginning and end of a runoff event or data between runoff events.

The flow discharge is represented by a real number with two significant digits after the decimal point. The sediment loads are represented by real numbers in exponential form with two significant digits after the decimal point.

OUTPUT DATA

This chapter presents the output data structure of CONCEPTS and a way to process these data. Depending on the output options selected by the user, CONCEPTS creates three types of output files: (1) output at a certain location and for a certain runoff event, (2) time-series output at a certain location, and (3) output for a certain runoff event along a section of the modeling reach.

Output Data File Specification

CONCEPTS can generate three types of output files, see section on “Run Control Data” in Chapter 4. There are three output categories:

- 1 output at a certain location and for a certain runoff event,
- 2 time-series output at a certain location, and
- 3 output for a certain runoff event along a section of the modeling reach.

The names of the output files follow the following convention: run identifier + ‘ ’ + number + ‘.TXT’. For example, if the run identifier is SIMULATION, then the output file names are ‘SIMULATION 050.TXT’, ‘SIMULATION 051.TXT’, etc. (see also Chapter 4, page 69). The layout of the output file differs for each output category.

Output at a Certain Location and for a Certain Runoff Event

If the user requests output at a certain location and for a certain runoff event, CONCEPTS generates an output file for each requested cross section. Table 4.6 lists the parameters that the user can request as output. The output file comprises initial data (header) and data for each runoff event.

Initial Data

The initial data consist of a header and data that depend on the requested output parameters. The header comprises the name of the cross section, its river kilometer, type of data, and dates of the runoff events for which output is requested. For example:

example header

```
Output file for cross section "First cross section" at river kilometer
0.676

Output type = 17536
Output dates are: 12/27/1982 16:00:00
                  05/18/1983 16:45:00
                  09/20/1983 08:30:00
                  11/19/1983 19:30:00
```

CONCEPTS also produces initial data for the following parameters (cf. Table 4.6):

- cross-sectional geometry (data type 1024),

**example initial
geometry of cross
section**

INITIAL CROSS SECTION GEOMETRY

STATION (M)	ELEVATION (M)
0.000	76.950
1.000	75.950
101.400	75.950
102.590	74.460
107.470	73.910
119.230	73.150
123.800	73.150
130.910	73.050
135.810	72.970
138.220	72.570
144.160	72.170
144.960	71.900
146.360	71.840
151.330	71.650
152.300	71.810
153.430	72.600
156.290	75.830
158.700	75.860
258.700	75.860
259.700	76.860

- in-bank top and bottom widths of cross section (data type 2048),

**example initial in-
bank channel
widths**

INITIAL CHANNEL WIDTHS

BOTTOM (M)	FLOODPLAIN (M)
33.070	54.890

- height of left and right banks of cross section (data type 4096),

example initial bank heights

INITIAL BANK HEIGHTS

LEFT (M)	RIGHT (M)
2.800	4.020

- characteristic sediment particle sizes of surface layer of streambed (data type 16384), and

example initial characteristic sediment sizes

INITIAL BED MATERIAL CHARACTERISTICS

D16 (MM)	D50 (MM)	D84 (MM)	D90 (MM)	DMEAN (MM)
0.227	3.317	16.740	20.889	3.245

- composition of surface layer of streambed (data type 32768).

example initial sediment composition

INITIAL SIZE FRACTION DISTRIBUTION

DIAMETER (MM)	FRACTION (-)
0.004	0.000
0.016	0.000
0.040	0.000
0.127	1.479
0.458	32.143
1.297	8.354
2.594	4.877
4.362	6.653
7.336	10.075
12.338	12.073
20.749	14.220
32.000	8.112
43.713	2.014

Runoff Event Related Data

CONCEPTS writes the output data to a file following the sequence shown in Table 4.6, but grouping:

- peak discharge, peak flow depth, peak stage, and peak friction slope;
- sediment yield and cumulative sediment yield; and
- change in bed elevation, cumulative change in bed elevation, lateral erosion, and cumulative lateral erosion.

The first line in the output file for each runoff event is the date of the storm event:

example storm date output line

OUTPUT FOR THE STORM EVENT STARTED ON 12/25/1982 11:58: 0

This line is followed by eight groups of output:

Output Data

1 peak hydraulic variables (data types 1, 2, 4, and 8),

example output of
peak discharge
and peak flow
depth

TIME TO PEAK	DISCHARGE (CMS)	TIME TO PEAK	DEPTH (M)
12/25/1982 11:58: 0	10.460	12/25/1982 11:58: 0	2.451

2 sediment yield (data types 16 and 32),

example output of sediment yield

STORM EVENT GENERATED SEDIMENT YIELD				CUMULATIVE SEDIMENT YIELD			
SILT YLD (TONS)	SAND YLD (TONS)	GRAVEL YLD (TONS)	TOTAL YLD (TONS)	SILT YLD (TONS)	SAND YLD (TONS)	GRAVEL YLD (TONS)	TOTAL YLD (TONS)
4.93	71.24	6.52	82.69	1400.69	1419.18	144.25	2964.12

3 cross-sectional changes (data types 64, 128, 256, and 512),

example output of
cross-sectional
changes

CROSS-SECTIONAL CHANGES			
BED CHNG (M)	CUM BED (M)	LAT CHNG (M)	CUM LAT (M)
-0.016	-0.208	0.384	5.495

4 cross-section geometry (data type 1024),

example output of
cross section
geometry

CROSS SECTION GEOMETRY	
STATION	ELEVATION (M)
0.000	76.950
1.000	75.950
101.400	75.950
102.590	74.460
107.470	73.908
119.230	73.109
123.800	73.109
130.910	72.992
135.810	72.897
138.220	72.422
144.160	71.961
144.960	71.690
146.360	71.632
151.330	71.442
152.300	71.602
157.795	71.602
157.795	73.111
160.520	75.860
258.700	75.860
259.700	76.860

5 in-bank top and bottom width of cross section (data type 2048),

example output of
in-bank channel
widths

CHANNEL WIDTHS	
BOTTOM (M)	FLOODPLAIN (M)
38.565	59.120

6 height of left and right banks of cross section (data type 4096),

example output of bank heights

BANK HEIGHTS

LEFT (M)	RIGHT (M)
2.841	4.258

7 characteristic sediment particle sizes of surface layer of streambed (data type 16384), and

example output of characteristic sediment sizes

BED MATERIAL CHARACTERISTICS

D16 (MM)	D50 (MM)	D84 (MM)	D90 (MM)	DMEAN (MM)
0.236	4.566	17.784	22.164	3.607

8 composition of surface layer of streambed (data type 32768).

example output of composition of surface layer

SIZE FRACTION DISTRIBUTION

DIAMETER (MM)	FRACTION (-)
0.004	0.000
0.016	0.000
0.040	0.000
0.127	2.126
0.458	18.194
1.297	2.553
2.594	0.647
4.362	9.574
7.336	14.498
12.338	17.373
20.749	20.463
32.000	11.673
43.713	2.898

Time-Series Output at a Certain Location

If the user requests time-series output, CONCEPTS generates an output file for each requested cross section. Table 4.8 lists the parameters the user can request as output. The output file comprises initial data (header) followed by $n + 1$ columns of data, where n is the number of outputted variables.

Initial Data

The initial data comprise the name of the cross section, river kilometer, type of output data, and the start and end dates of each time series.

example header

Output time-series file for cross section "First cross section" at river kilometer 0.248

Output type = 595973

Output periods are: from 10/01/1981 00:00:00 to 12/31/1991 24:00:00

CONCEPTS then prints the header for the multi-column output, the first column of which is time followed by the name of the outputted variable and its unit. Following is a list of all possible columns in the header:

- time,

TIME

- discharge (data type 1),

DISCHARGE
(CMS)

- flow velocity (data type 2),

VELOCITY
(M/S)

- flow depth (data type 4),

DEPTH
(M)

- stage (data type 8),

STAGE
(M)

- flow area (data type 16),

AREA
(M²)

- flow top width (data type 32),

TOP WIDTH
(M)

- wetted perimeter (data type 64),

PERIMETER
(M)

- hydraulic radius (data type 128),

RADIUS
(M)

- conveyance (data type 256),

CONVEYANCE
(CMS)

- friction slope (data type 512),

F.SLOPE
(-)

- energy head (data type 1024),

HEAD
(M)

- Froude number (data type 2048),

FROUDE
(-)

- bed shear stress (data type 4096),

BED SHEAR
(Pa)

- sediment discharge (silt/sand/gravel/total) (data type 8192),

SILT DIS SAND DIS GRAVEL DIS TOTAL DIS
(CMS) (CMS) (CMS) (CMS)

- cumulative sediment yield (data type 16384),

SILT YLD SAND YLD GRAVEL YLD TOTAL YLD
(TONS) (TONS) (TONS) (TONS)

- cumulative change in bed elevation (data type 32768),

CUM BED
(M)

- thalweg elevation (data type 65536),

THALWEG
(M)

- cumulative lateral erosion (data type 131072),

CUM LAT
(M)

- factor of safety of left and right banks (data type 524288),

SAFETY L SAFETY R
(-) (-)

- apparent cohesion of left and right banks (data type 1048576),

AP COH L AP COH R
(Pa) (Pa)

- pore-water force of left and right banks per unit width (data type 2097152),

PORE L PORE R
(N/M) (N/M)

- matric suction force of left and right banks per unit width (data type 4194304),

MATRIC L MATRIC R
(N/M) (N/M)

- weight of failure block of left and right banks per unit width (data type 8388608),

W BLK L W BLK R
(N/M) (N/M)

- weight of water on the bank of left and right banks per unit width (data type 16777216),

W WATER L W WATER R
(N/M) (N/M)

- horizontal component of the confining force of left and right banks per unit width (data type 33554432),

HYD PR L HYD PR R
(N/M) (N/M)

- groundwater elevation of left and right banks (data type 67108864), and

PHREA L	PHREA R
(M)	(M)

- elevation of bank top of left and right banks (data type 134217728).

BANKTOP L	BANKTOP R
(M)	(M)

Continuous Data

After every completed time step CONCEPTS checks if time falls between the start and end time of all requested time series. When the model time is within the boundaries of a time series, CONCEPTS prints the requested parameters to the corresponding output file.

Output for a Certain Runoff Event along a Section of the Modeling Reach

If the user requests output for a certain runoff event along a section of the modeling reach, referred to as a *profile*, CONCEPTS generates an output file for each requested profile. Table 4.10 lists the parameters that the user can request as output. The output file comprises initial data (header) and data for each runoff event. CONCEPTS writes the output data following a multi-column layout. The first three lines are header information and the first column is river kilometer.

Initial Data

The initial data consist of a header and data that depends on the requested output parameters. The header comprises the name of the cross section, its river kilometer, type of data, and dates of the runoff events for which output is requested. For example:

example header

```
Output profile file for cross section "First cross section" at river
kilometer 0.676
to cross section "Last cross section" at river kilometer 2.906

Output type = 135
Output dates are: 12/27/1982 16:00:00
                  05/18/1983 16:45:00
                  09/20/1983 08:30:00
                  11/19/1983 19:30:00
```

CONCEPTS also produces initial data for the following parameters if requested:

- thalweg elevation (data type 4),

**example initial
thalweg elevation
profile**

RIVER KM (KM)	THALWEG (M)
0.248	73.270
0.499	72.110
0.819	71.080
1.002	70.620
1.348	69.640
1.593	69.160
1.831	68.420
2.148	68.120
2.421	67.330
2.606	67.100
2.726	66.950
2.906	66.800

- in-bank top width of cross section (data type 16),

**example initial in-
bank channel top
width profile**

RIVER KM (KM)	TOP WIDTH (M)
0.248	88.660
0.499	78.970
0.819	27.740
1.002	29.080
1.348	30.780
1.593	76.320
1.831	41.790
2.148	40.110
2.421	27.500
2.606	27.700
2.726	51.940
2.906	34.840

- height of left and right bank of cross section (data type 32), and

**example initial
bank-height profile**

RIVER KM (KM)	BANK HEIGHT	
	LEFT (M)	RIGHT (M)
0.248	2.450	3.420
0.499	2.350	2.500
0.819	3.840	4.510
1.002	1.560	3.990
1.348	4.720	2.860
1.593	4.510	3.320
1.831	5.190	1.550
2.148	3.660	2.560
2.421	4.750	3.900
2.606	5.230	3.260
2.726	3.870	1.150
2.906	3.110	3.170

Output Data

- characteristic sediment particle sizes of surface layer of streambed (data type 128).

example profile of initial characteristic sediment sizes

RIVER KM (KM)	D16 (MM)	D50 (MM)	D84 (MM)	D90 (MM)	DMean (MM)
0.248	0.227	3.317	16.740	20.889	3.245
0.499	0.227	3.317	16.740	20.889	3.245
0.819	0.227	3.317	16.740	20.889	3.245
1.002	0.194	0.981	13.179	17.268	2.200
1.348	0.194	0.981	13.179	17.268	2.200
1.593	0.194	0.981	13.179	17.268	2.200
1.831	0.194	0.981	13.179	17.268	2.200
2.148	0.194	0.981	13.179	17.268	2.200
2.421	0.189	0.617	8.795	12.087	1.676
2.606	0.189	0.617	8.795	12.087	1.676
2.726	0.189	0.617	8.795	12.087	1.676
2.906	0.189	0.617	8.795	12.087	1.676

Runoff Event Related Data

For each requested runoff event CONCEPTS writes the storm date and requested profiles to their output files. The first line in the output file for each runoff event is the date of the storm event:

example storm date output line

OUTPUT FOR THE STORM EVENT STARTED ON 12/25/1982 11:58: 0

The layout further consists of a header followed by multiple columns of which the first column is river kilometer. Following is a list of possible columns in the header:

- river kilometer,

RIVER KM
(KM)

- peak discharge (data type 1),

DISCHARGE
(CMS)

- peak stage (data type 2),

STAGE
(M)

- thalweg elevation (data type 4),

THALWEG
(M)

- change in bed elevation (data type 8)

BED CHNG
(M)

- in-bank top width of cross section (data type 16),

TOP WIDTH
(M)

- height of left and right bank of cross section (data type 32),

BANK HEIGHT	
LEFT	RIGHT
(M)	(M)

- storm event generated sediment yield (data type 64), and

STORM EVENT GENERATED SEDIMENT YIELD			
SILT YLD	SAND YLD	GRAVEL YLD	TOTAL YLD
(TONS)	(TONS)	(TONS)	(TONS)

- characteristic sediment particle sizes of surface layer of streambed (data type 128).

BED MATERIAL CHARACTERISTIC DIAMETERS				
D16	D50	D84	D90	DMEAN
(MM)	(MM)	(MM)	(MM)	(MM)

Processing of Output Data Files

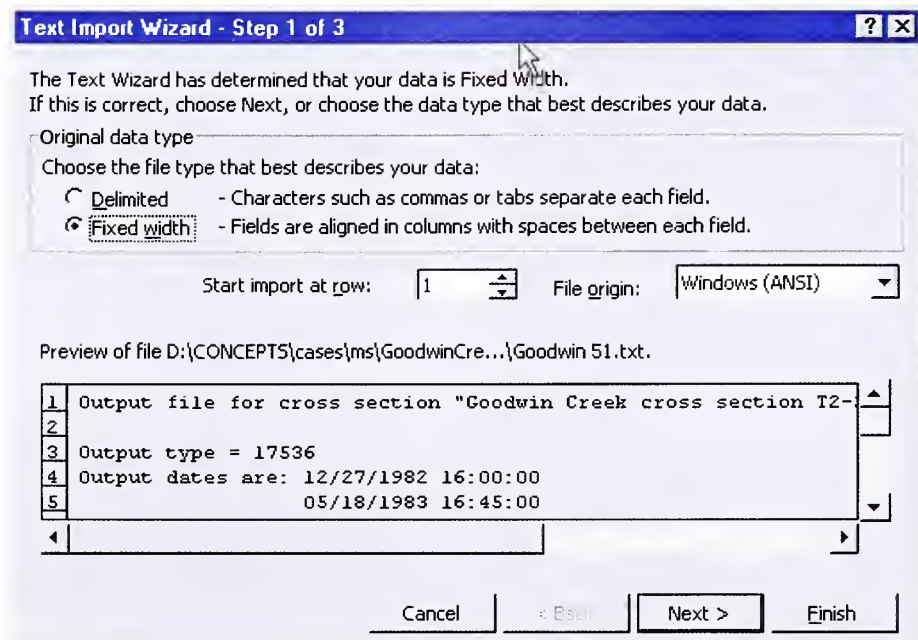
CONCEPTS does not produce graphical output, such as plots of hydrographs. However, the data columns in the output files have a fixed width of 10 characters, hence it is easy to import them as *text* files into ‘spreadsheet’ applications such as Microsoft® Excel or Corel® Quattro® Pro. Below we will show how you can produce graphs from the data in the three types of output files using Microsoft® Excel 2000.

Output at a Certain Location and for a Certain Runoff Event

You can produce charts of cross-sectional geometry, sediment particle size distribution, sediment yield, etc. using the outputted data at a certain location and for a certain runoff event. This section outlines the steps you need to take to import the data into Microsoft® Excel. You should refer to the Microsoft® Excel manuals or online help for additional support.

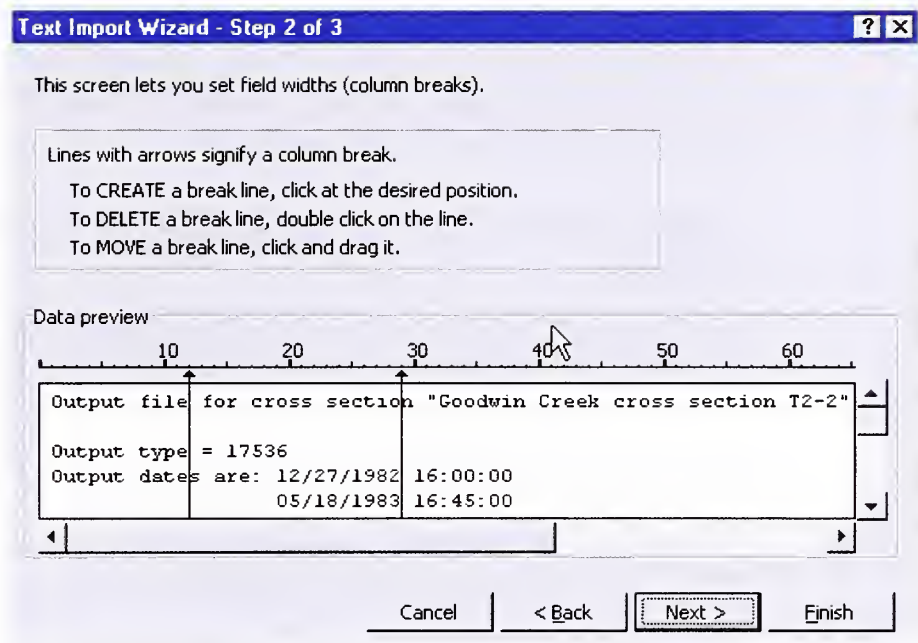
- 1 Start Microsoft® Excel.
- 2 Select “File>Open” and then “All Files” in the “Files of type:” select box.
- 3 Navigate to the folder that contains the output file. Select this file and open it. This will bring up the “Text Import Wizard – Step 1 of 3” window.

Figure 5.1 “Text Import Wizard – Step 1 of 3” window.



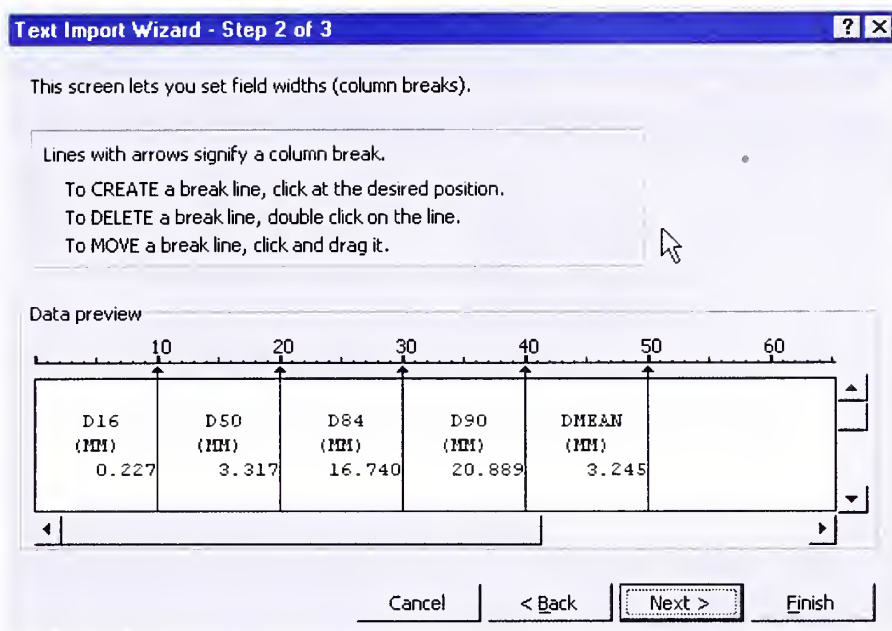
4 Select “Fixed width” as the “Original data type” and click on the “Next >” button. This will bring up the “Text Import Wizard – Step 2 of 3” window.

Figure 5.2 “Text Import Wizard – Step 2 of 3” window.



5 Scroll down to get a proper view of the data you will import. Create break lines at 10, 20, 30, 40, etc. depending on the output data type.

Figure 5.3 “Text Import Wizard – Step 2 of 3” window with break lines added.



- 6 Click on the “Finish” button. You have imported the output data in Microsoft® Excel (see Figure 5.4).

Now you can plot the data using the graphing capabilities of Microsoft® Excel. Figures 5.6 and 5.7 show examples of temporal changes in cross-section geometry and bed-material composition.

Time-Series Output at a Certain Location

You can produce graphs showing the progression of discharge, stage, thalweg elevation, factor of safety, etc. (see Table 4.8) using the outputted time-series data at a certain location. This section outlines the steps you have to take to import the data into Microsoft® Excel.

To import the time-series output text files you need to take the steps presented in the previous section “Output at a Certain Location and for a Certain Runoff Event”. However in step 5, you need to place the first break line at position 20 because the time column has a width of 20 characters. The next break lines need to be placed at positions 30, 40, 50, etc. (see Figure 5.5).

Figure 5.8 shows the imported output file in Microsoft® Excel. Figure 5.9 shows an XY plot of factor of safety of the right streambank against time.

Output for a Certain Runoff Event along a Section of the Modeling Reach

You can produce graphs showing the thalweg profile, distribution of d_{50} along the channel, etc. (see Table 4.10) at various points of time using the profile

Output Data

Figure 5.4 View of Microsoft® Excel spreadsheet after importing output data file.

The screenshot shows a Microsoft Excel spreadsheet titled "Goodwin 51.txt". The data is organized into several sections:

- Section 1:** Contains header information such as "Output file for cross section", "Goodwin Creek cross section T2-2" at river mile 676.0 meters, and dates/times (e.g., 2/27/82, 16:00:00).
- Section 2:** A table with columns for "Output type" (e.g., pe = 17536) and "Output data" (e.g., dates/times).
- Section 3:** A table with columns for "STATION" and "ELEVATION (M)".
- Section 4:** A table with columns for "STATION" and "ELEVATION (M)".
- Section 5:** A table with columns for "STATION" and "ELEVATION (M)".
- Section 6:** A table with columns for "STATION" and "ELEVATION (M)".
- Section 7:** A table with columns for "STATION" and "ELEVATION (M)".
- Section 8:** A table with columns for "STATION" and "ELEVATION (M)".
- Section 9:** A table with columns for "STATION" and "ELEVATION (M)".
- Section 10:** A table with columns for "STATION" and "ELEVATION (M)".
- Section 11:** A table with columns for "STATION" and "ELEVATION (M)".
- Section 12:** A table with columns for "STATION" and "ELEVATION (M)".
- Section 13:** A table with columns for "STATION" and "ELEVATION (M)".
- Section 14:** A table with columns for "STATION" and "ELEVATION (M)".
- Section 15:** A table with columns for "STATION" and "ELEVATION (M)".
- Section 16:** A table with columns for "STATION" and "ELEVATION (M)".
- Section 17:** A table with columns for "STATION" and "ELEVATION (M)".
- Section 18:** A table with columns for "STATION" and "ELEVATION (M)".
- Section 19:** A table with columns for "STATION" and "ELEVATION (M)".
- Section 20:** A table with columns for "STATION" and "ELEVATION (M)".
- Section 21:** A table with columns for "STATION" and "ELEVATION (M)".
- Section 22:** A table with columns for "STATION" and "ELEVATION (M)".
- Section 23:** A table with columns for "STATION" and "ELEVATION (M)".
- Section 24:** A table with columns for "STATION" and "ELEVATION (M)".
- Section 25:** A table with columns for "STATION" and "ELEVATION (M)".
- Section 26:** A table with columns for "STATION" and "ELEVATION (M)".
- Section 27:** A table with columns for "STATION" and "ELEVATION (M)".
- Section 28:** A table with columns for "STATION" and "ELEVATION (M)".
- Section 29:** A table with columns for "STATION" and "ELEVATION (M)".
- Section 30:** A table with columns for "STATION" and "ELEVATION (M)".
- Section 31:** A table with columns for "STATION" and "ELEVATION (M)".
- Section 32:** A table with columns for "STATION" and "ELEVATION (M)".
- Section 33:** A table with columns for "STATION" and "ELEVATION (M)".
- Section 34:** A table with columns for "STATION" and "ELEVATION (M)".

Figure 5.5 “Text Import Wizard – Step 2 of 3” window with break lines added.

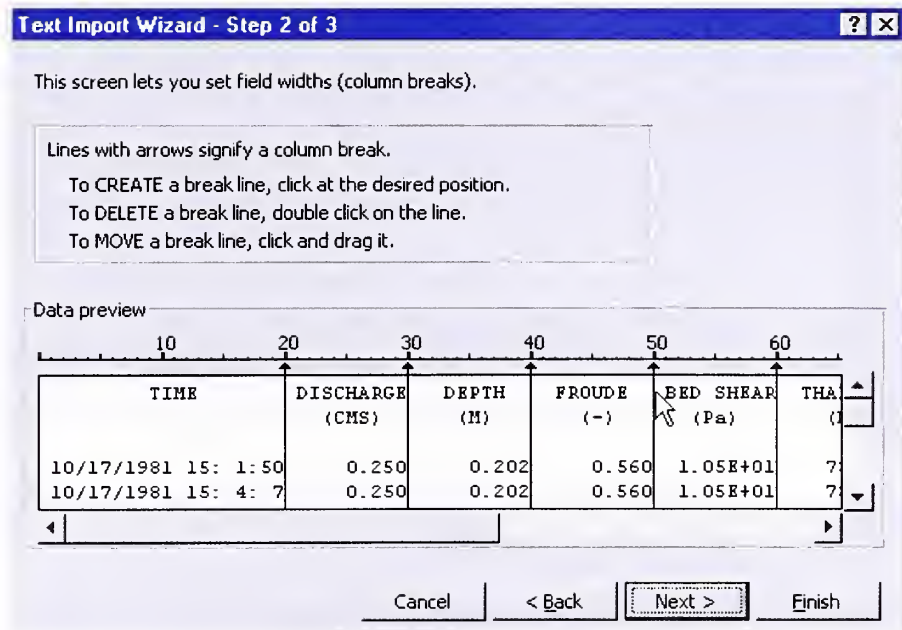


Figure 5.6 Example plot of temporal changes in cross-section geometry.

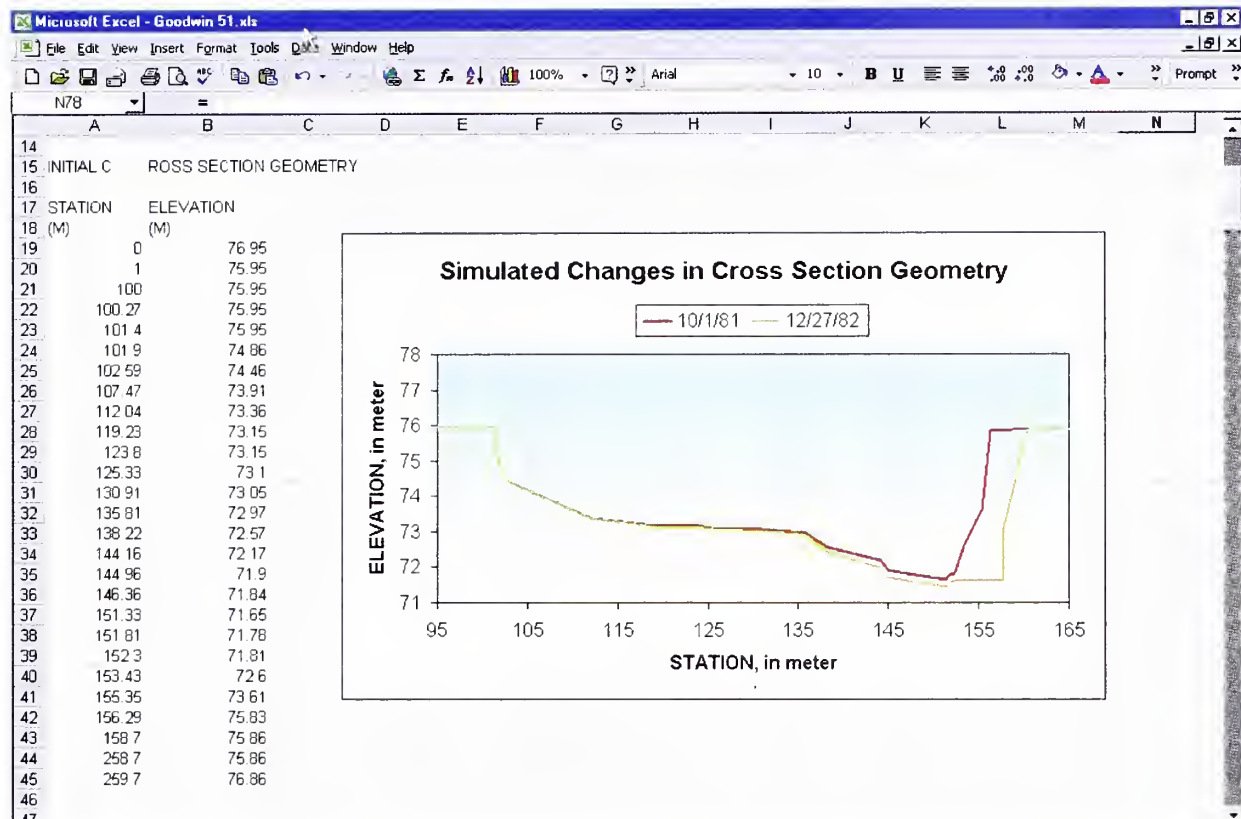
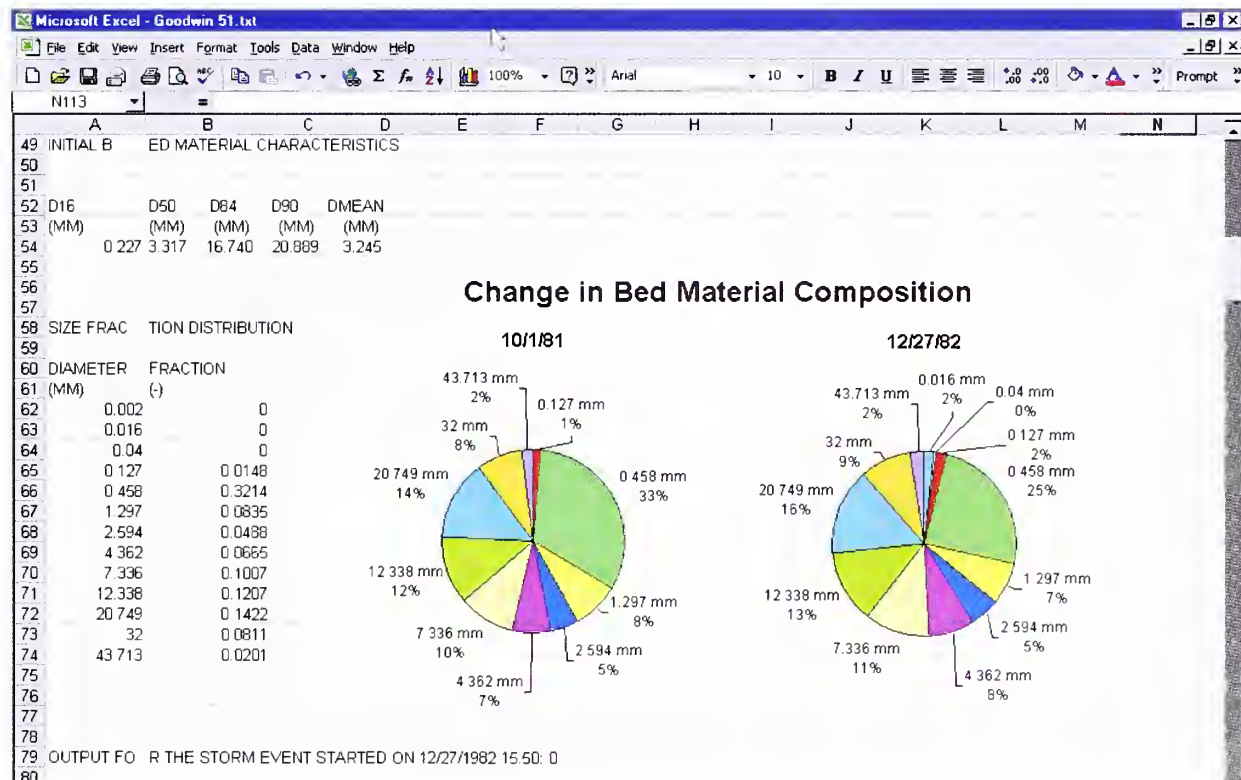


Figure 5.7 Example plot of temporal changes in bed-material composition.



Output Data

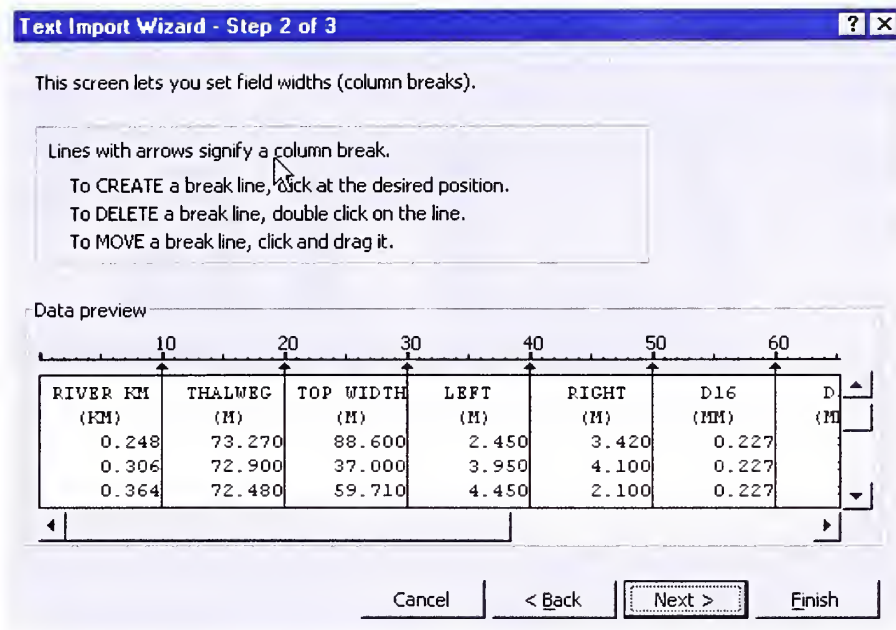
Figure 5.8 View of Microsoft® Excel spreadsheet after importing time-series output data file.

Output time-series								
	A	B	C	D	E	F	G	H
1	Output type =	5	95973					
2	Output periods are from	10/0	1/1/81 00:00:00	to 1	2/31/1991	24:00:00		
3								
4								
5								
6								
7	TIME	DISCHARGE	DEPTH	FROUDE	BED SHEAR	THALWEG	SAFETY L	SAFETY R
8		(CMS)	(M)	(-)	(Pa)	(M)	(-)	(-)
9								
10	10/17/81 15:01	0.250	0.202	0.560	10.500	73.270	9999 000	1.379
11	10/17/81 15:04	0.250	0.202	0.560	10.500	73.270	9999 000	1.378
12	10/17/81 15:06	0.250	0.202	0.560	10.500	73.270	9999 000	1.376
13	10/17/81 15:10	0.250	0.202	0.560	10.500	73.270	9999 000	1.375
14	10/17/81 15:14	0.250	0.202	0.560	10.500	73.270	9999 000	1.372
15	10/17/81 15:20	0.250	0.202	0.560	10.500	73.269	9999 000	1.370
16	10/17/81 15:27	0.250	0.202	0.560	10.500	73.269	9999 000	1.366
17	10/17/81 15:36	0.250	0.202	0.558	10.400	73.269	9999 000	1.362
18	10/17/81 15:44	0.250	0.202	0.559	10.500	73.269	9999 000	1.358
19	10/17/81 15:53	0.250	0.202	0.559	10.500	73.268	9999 000	1.354
20	10/17/81 16:01	0.250	0.202	0.559	10.500	73.268	9999 000	1.350
21	10/17/81 16:10	0.250	0.202	0.557	10.400	73.268	9999 000	1.346
22	10/17/81 16:19	0.250	0.202	0.559	10.500	73.268	9999 000	1.342
23	10/17/81 16:27	0.250	0.202	0.559	10.400	73.267	9999 000	1.338
24	10/17/81 16:36	0.250	0.202	0.557	10.400	73.267	9999 000	1.334
25	10/17/81 16:45	0.250	0.202	0.558	10.400	73.267	9999 000	1.330
26	10/17/81 16:53	0.250	0.202	0.558	10.400	73.267	9999 000	1.326
27	10/17/81 17:02	0.250	0.202	0.557	10.400	73.267	9999 000	1.322
28	10/17/81 17:11	0.250	0.202	0.558	10.400	73.266	9999 000	1.319
29	10/17/81 17:19	0.250	0.202	0.558	10.400	73.266	9999 000	1.315
30	10/17/81 17:28	0.250	0.202	0.556	10.300	73.266	9999 000	1.311
31	10/17/81 17:36	0.250	0.202	0.558	10.400	73.266	9999 000	1.307
32	10/17/81 17:45	0.250	0.202	0.557	10.400	73.266	9999 000	1.304

Figure 5.9 Example plot of the progression of factor of safety of the right streambank.



Figure 5.10 "Text Import Wizard – Step 2 of 3" window with break lines added.



output. This section outlines the steps you have to take to import the data into Microsoft® Excel.

To import the profile output text files you need to take the steps presented in the prior section “Output at a Certain Location and for a Certain Runoff Event”. In step 5, you need to place break lines at every 10th position, that is 10, 20, 30, 40, 50, etc. (see Figure 5.10).

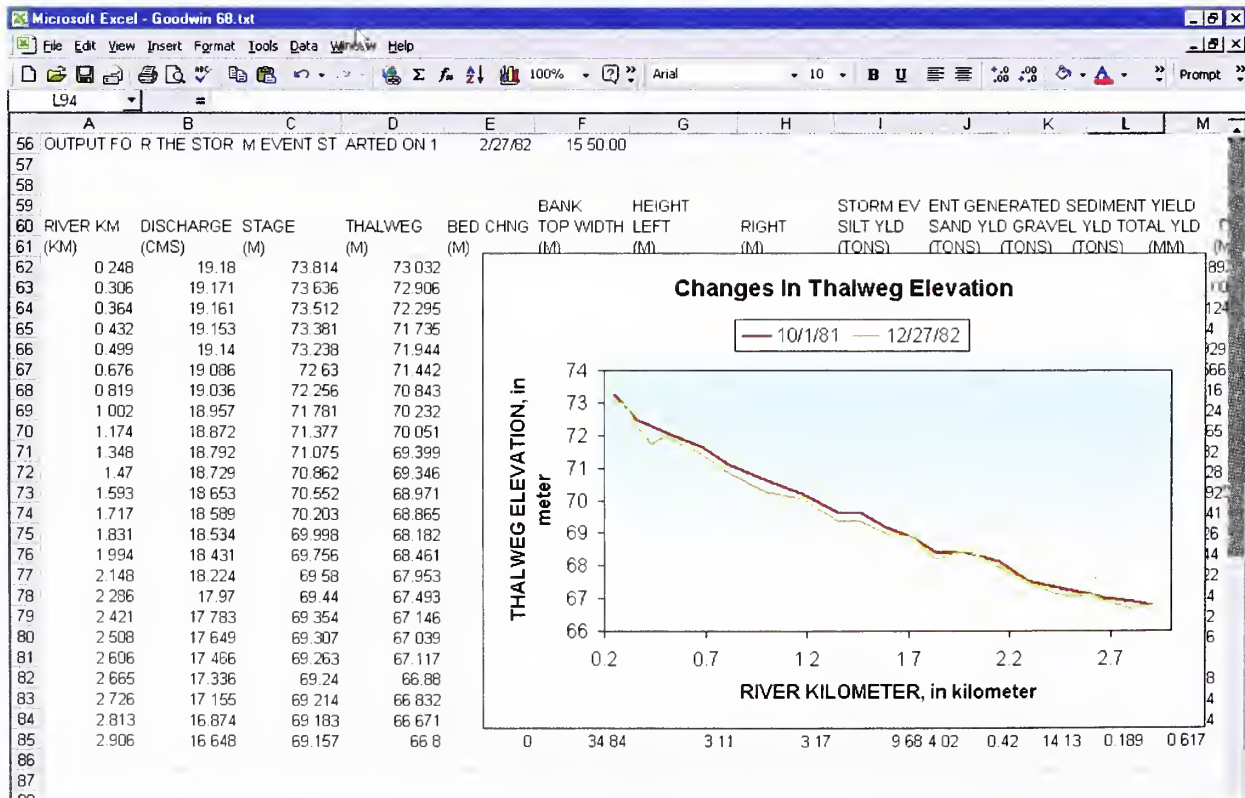
Figure 5.11 shows the imported output file in Microsoft® Excel. Figure 5.12 shows an example plot of temporal changes in thalweg profile.

Output Data

Figure 5.11 View of Microsoft® Excel spreadsheet after importing profile output data file.

A	B	C	D	E	F	G	H	I	J	K	L	M
1	Output pr	file file	from cros	s section	"Goodwin C	reek cross	section T	7A" at riv	er mile	248.1 meters.		
2	to cross	section "G	oodwin Cre	ek cross s	ection C4-	8" at riv	r mile 29	05.5 meter	s			
3												
4	Output ty	pe = 255										
5	Output da	tes are 1	2/27/82	16.00.00								
6		1	2/27/83	20.00.00								
7		1	2/5/84	17.00.00								
8		1	2/15/85	15.45.00								
9		1	2/23/86	7.00.00								
10		1	2/31/1987	16.00.00								
11		1	2/31/1988	11.00.00								
12		1	2/30/1989	22.30.00								
13		1	2/30/1990	14.30.00								
14		0	9/9/91	13.15.00								
15												
16												
17												
18												
19												
20	INITIAL D	ATA AT 10/	17/1981 15	00.00								
21												
22												
23												
24	RIVER KM	THALWEG	BANK	HEIGHT	BED	MATERIAL	CHARACTERI	STIC DIAME	TERS			
25	(KM)	(M)	TOP WIDTH	LEFT	RIGHT	D16	D50	D64	D90	DMEAN		
26	0.248	73.27	88.6	2.45	3.42	0.227	3.317	16.74	20.889	3.245		
27	0.306	72.9	37	3.95	4.1	0.227	3.317	16.74	20.889	3.245		
28	0.364	72.48	59.71	4.45	2.1	0.227	3.317	16.74	20.889	3.245		
29	0.432	72.3	70	4.45	4	0.227	3.317	16.74	20.889	3.245		
30	0.499	72.11	78.97	2.35	2.5	0.227	3.317	16.74	20.889	3.245		
31	0.676	71.65	54.89	1.49	4.02	0.227	3.317	16.74	20.889	3.245		
32	0.819	71.08	27.74	3.84	4.51	0.227	3.317	16.74	20.889	3.245		

Figure 5.12 Example plot of temporal changes in thalweg profile.



Part 3

SAMPLE APPLICATIONS

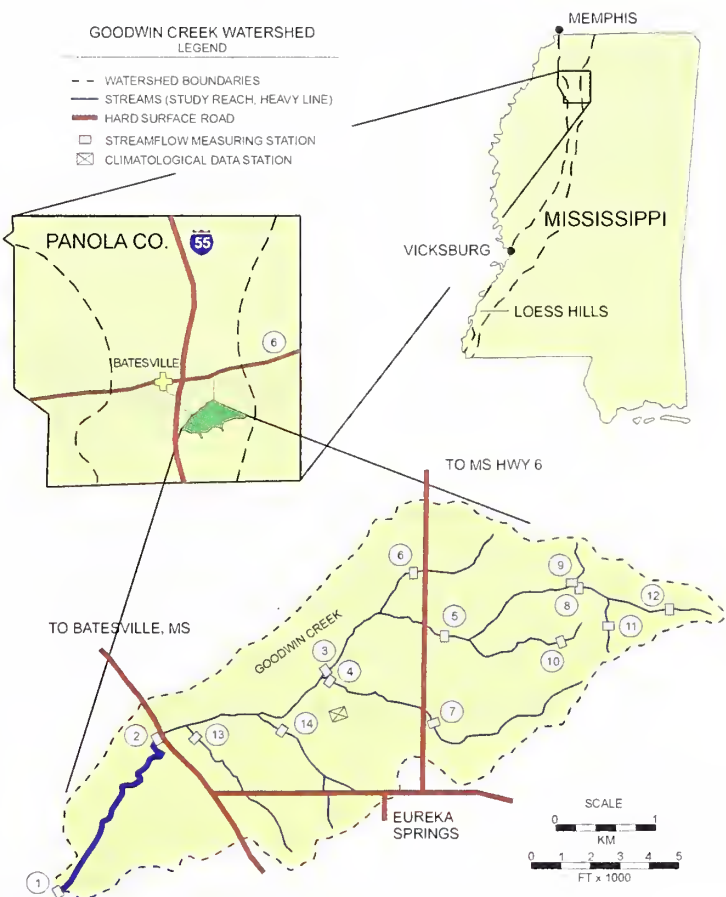
GOODWIN CREEK, MISSISSIPPI

This chapter presents an application of CONCEPTS to the lower 3.5 km of Goodwin Creek, Mississippi. You will find the physical characteristics of the channel, the input data necessary to perform the simulation, and results showing the effects of streambank erosion on the channel's morphology.

Study Area

Goodwin Creek is located in north-central Mississippi; its watershed is situated on the eastern side of the Bluff or Loess Hills physiographic subprovince (see Figure 6.1). In the upper reaches of the watershed, streamflow only occurs immediately after precipitation. In the lower reaches, a slight baseflow usually persists for most of the year. Storm flows carry heavy loads of coarse sediment (sand and gravel) derived from upland tributaries and gullies and from valley alluvium. The stream channels are greatly enlarged in places, are highly variable in form and are deeply incised. Terrain elevation ranges from 71 to 128 m above mean sea level, with an average channel slope of 0.004.

The Goodwin Creek watershed is highly instrumented to provide data needed to investigate the impact of landscape attributes and watershed processes on sediment yield, to test concepts developed in the study of these processes, and to validate models developed in the research (Alonso, 1997). The US Department of Agriculture-Agricultural Research Service-National Sedimentation Laboratory (NSL) operates the watershed. The watershed is divided into fourteen nested subcatchments with a flow measuring flume constructed at each of the drainage outlets. Twenty nine standard recording rain gages are uniformly located within and just outside the watershed. The average annual rainfall during 1982-1992 from all storms was 1440 mm and the mean annual runoff measured at the watershed outlet was $14 \times 10^6 \text{ m}^3$. Measuring flumes are designed to operate in the supercritical regime to prevent

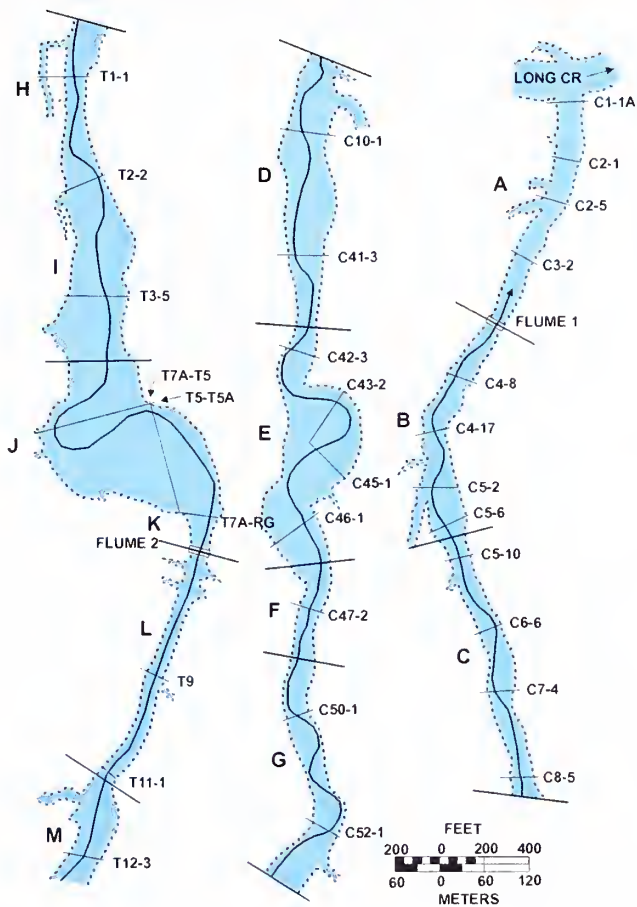
Figure 6.1 Map of the Goodwin Creek Watershed.

deposition of sediment in the flumes. Instrumentation at each gaging site includes an electronic data acquisition and radio telemetry system that collects, stores and transmits the data to a central computer at the NSL for processing and archival. Measurements collected at each site and transmitted through the telemetry system include water stage, accounting of automatically pumped sediment samples, air and water temperature, precipitation, and climatological parameters. Sampling of total sediment loads is carried out during storm events at selected stations using Helleys-Smith bedload samplers and DH-48 depth-integrating suspended sediment samplers. NSL has made available a comprehensive documentation of the Goodwin Creek Experimental Watershed and the database compiled for the period 1982-1993 for downloading from the NSL computer system at:

http://www.sedlab.olemiss.edu/cwp_unit/gcwd_ftp.html

The US Army Corps of Engineers prepared a detailed 2-ft contour interval topographic survey of all the main channel and primary tributaries of Goodwin Creek in 1977. In 1982 NSL resurveyed 30 of the 1977 cross sections in the lower 3.86 km of Goodwin Creek (see Figure 6.2; and Murphey and Grissinger, 1986). NSL has repeated these cross section surveys 26 times, and

Figure 6.2 Plan map of the 3.86 km study length of Goodwin Creek showing cross sections and flume locations.

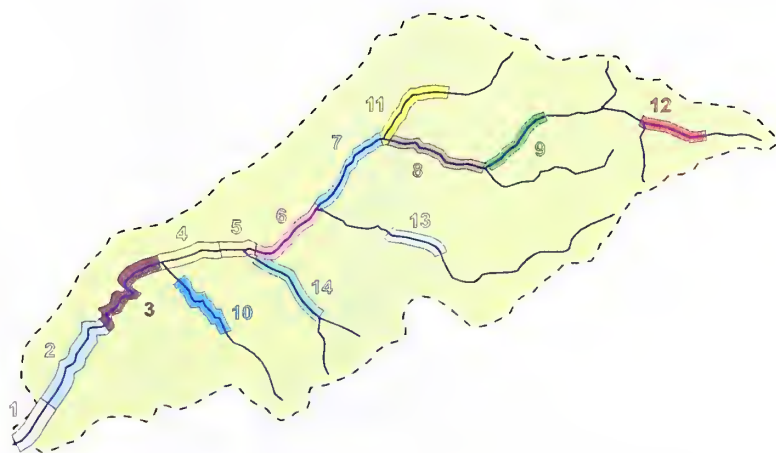


used them to document changes in channel geometry and to verify the sediment delivery budget of the channel system.

The bed material was sampled in 1994 (Kuhnle, 1996). The main channels were divided into a series of reaches with a mean length of 1,000 m. Figure 6.3 shows the median size of the bed material of 14 sampled reaches. Median sizes ranged from 0.5 to 7.4 mm. They are generally fine in the upstream portions of the watershed, coarsen toward the central part of the watershed, and become finer again towards the outlet of the watershed.

In the uplands three lithologic units overlie the Citronelle deposits of sand and gravel: (a) an early-Holocene sequence of channel lag, organic bog, and gray silt overlain by a massive silt deposit, (b) a mid-Holocene deposit of well-bedded relatively coarse-textured channel fill, and (c) a late-Holocene deposit of fine to coarse meander-belt alluvium (Murphey and Grissinger, 1986). Superimposed over these three deposits are massive amounts of finely-layered silt and fine sand that were washed from the hills following European settlement. Simon and Darby (1997) determined the following geotechnical characteristics of the bank material:

Figure 6.3 The 14 reaches along Goodwin Creek for which bed-material samples were collected. Bed material median sizes for the reaches are: 1) 1.0 mm, 2) 1.4 mm, 3) 4.4 mm, 4) 6.9 mm, 5) 3.5 mm, 6) 6.7 mm, 7) 3.9 mm, 8) 1.1 mm, 9) 1.4 mm, 10) 7.3 mm, 11) 1.4 mm, 12) 0.5 mm, 13) 2.4 mm, and 14) 7.4 mm.



- Early-Holocene unit: $c_a \approx 5$ kPa and $\phi' \approx 35^\circ$.
- Late-Holocene unit: $c_a \approx 35$ kPa and $\phi' \approx 28^\circ$.

Application

We have applied CONCEPTS to the lower 3.5 km of Goodwin Creek between flumes 1 and 2 (Figure 6.2) for water years 1982 through 1991. We have used the data presented in the previous section. The enclosed CDROM contains the input files to perform the simulation.

The modeling reach extends from cross section T7A-T5 to cross section C4-8 with a length of 2.7 km (Figure 6.2), and contains 22 surveyed cross sections. However, in this configuration numerical problems occurred near the inlet (upstream boundary, cross section T7A-T5) when discharge at the inlet increased rapidly causing the flow depth at the next cross section to drop significantly. We solved this problem by reducing the space steps near the inlet; that is, inserting a cross section halfway between cross sections T7A-T5 and T5-T5A and a cross section halfway between cross sections T5-T5A and T3-5. The geometries of the inserted cross sections assure a smooth transition from the surveyed cross section upstream to that downstream of the inserted cross sections. The simulation does not take into account the effects of flume 1 on channel hydraulics and morphology. We fixed the thalweg elevation at the downstream boundary of the modeling reach. We imposed the discharges measured at flume 2 at the upstream boundary of the modeling reach.

We have simulated the response of the modeling reach to the following two scenarios:

- 1 Channel can only adjust vertically. We only turned on the sediment transport submodel of CONCEPTS, which includes variations in streambed elevation.

2 Channel can adjust both vertically and horizontally. CONCEPTS simulates both streambed and streambank mechanics.

Figure 6.4 shows the *Run Control Data File*, Figure 6.5 shows an example of a *Cross Section Data File*, and Figure 6.6 shows part of the *Discharge Data File*.

Figure 6.4 Run control data file used in the simulation of the lower 3.5 km of Goodwin Creek, Mississippi.

```
!
! Main Input File
!
! case name
Goodwin
! project title
Goodwin Creek channel evolution simulation between 1982 and 1991
!----- Run Control Data -----
! upstream flow discharge file
GHydrography.txt
! flow-related data
0.25 0.00 0
! Sediment discharge at upstream end of the channel
0 0.00 0.00 0.00 0.975 0.975 0.99 0.99 1.00 1.00 1.00 1.00 1.00
! Silt Fraction and downstream bed control
0.30 1.0
! bank failure analysis
0 4
! type of flow resistance formulation
1
! water temperature
10.0
! sediment and streambank mechanics options
1 1 1
!----- Simulation Times -----
! start end time step
10/17/1981 15:00:00 09/31/1991 23:59:00 100
!----- Makeup of Modeling Reach -----
! number of links
1
! linktypes for the above number of links
1
!----- Link 1 -----
! REACH: number of cross sections and their data filenames
24
GCxsect01.txt
GCxsect01a.txt
GCxsect02.txt
GCxsect02a.txt
GCxsect03.txt
GCxsect04.txt
GCxsect05.txt
GCxsect06.txt
GCxsect07.txt
```

Figure 6.4 Run control data file used in the simulation of the lower 3.5 km of Goodwin Creek, Mississippi. (continued)

```

GCxsect08.txt
GCxsect09.txt
GCxsect10.txt
GCxsect11.txt
GCxsect12.txt
GCxsect13.txt
GCxsect14.txt
GCxsect15.txt
GCxsect16.txt
GCxsect17.txt
GCxsect18.txt
GCxsect19.txt
GCxsect20.txt
GCxsect21.txt
GCxsect22.txt

! ----- Output -----
! single point and time
1
17536
1 12
5
12/27/1983 20:00:00
12/15/1985 15:45:00
12/31/1987 16:00:00
12/30/1989 22:30:00
09/09/1991 13:15:00
! single point, continuously in time
7
595973
1 1
1
10/01/1981 00:00:00 12/31/1991 24:00:00
595973
1 5
1
10/01/1981 00:00:00 12/31/1991 24:00:00
1 9
1
10/01/1981 00:00:00 12/31/1991 24:00:00
595973
1 13
1
10/01/1981 00:00:00 12/31/1991 24:00:00
1 17
1
10/01/1981 00:00:00 12/31/1991 24:00:00
595973
1 21
1
10/01/1981 00:00:00 12/31/1991 24:00:00

```

Figure 6.4 Run control data file used in the simulation of the lower 3.5 km of Goodwin Creek, Mississippi. (continued)

```

595973
1 24
1
10/01/1981 00:00:00 12/31/1991 24:00:00
! profile at specific time points
1
255
1 1 1 24
5
12/27/1983 20:00:00
12/15/1985 15:45:00
12/31/1987 16:00:00
12/30/1989 22:30:00
09/09/1991 13:15:00

```

Figure 6.5 A sample cross section data file used in the simulation of the lower 3.5 km of Goodwin Creek, Mississippi.

```

!
! Input file of cross section 14.
!
! Name of xsection and rivermile in (km)
Goodwin Creek cross section C10-1
2.1477
! friction factor
0.06
! discharge fraction due to tributary inflow
0.00
!----- Left FloodPlain -----
! number of nodes
6
! station and elevation for above number of coordinates in (m)
0.00    74.21
1.00    73.21
98.63   73.21
100.00   73.21
100.27   73.21
102.07   73.21
! Manning's n of left floodplain
0.10
!----- Left Bank -----
! number of nodes
2
! station and elevation for above number of coordinates in (m)
102.07   73.21
106.77   69.55
! bank material
9830.0 17.1 15.0 21000.0
! bank sediment composition
30.700

```

Figure 6.5 A sample cross section data file used in the simulation of the lower 3.5 km of Goodwin Creek, Mississippi. (continued)

```

37.300
19.300
1.600
4.400
1.400
1.200
2.500
1.600
0.000
0.000
0.000
0.000
0.000
! critical shear stress for erosion
4.0
! groundwatertable, hydraulic gradient, and angle of seepage force
70.55 1.00 0.00
! Manning's n
0.06
!----- Channel Bed -----
! number of nodes
7
! station and elevation for above number of coordinates in (m)
106.77 69.55
109.20 69.16
120.76 69.15
124.26 69.09
125.18 68.73
130.17 68.49
135.11 68.12
! Elevation of bedrock (m)
0.00
! porosity
0.4
! hiding factors
0.00 0.95 0.70
! Surface layer and Substratum data
! number of sediment layers composing the bed
1
! Layer 1, layer depth below bed surface
0.00
! bed composition
0.000
0.000
0.000
2.684
40.237
9.675
4.464
5.939
8.881

```

Figure 6.5 A sample cross section data file used in the simulation of the lower 3.5 km of Goodwin Creek, Mississippi. (continued)

```

10.656
11.541
5.043
0.880
! critical shear stresses for erosion of and deposition on cohesive
beds
! and erodibility coefficient
    0.10      4.00  5.00E-06
! Manning's n
0.04
----- Right Bank -----
! number of nodes
6
! station and elevation for above number of coordinates in (m)
135.11      68.12
135.42      68.45
136.36      68.85
138.25      69.31
139.10      70.13
142.18      70.77
! bank material
9830.0  17.1  15.0  21000.0
! bank sediment composition
30.700
37.300
19.300
1.600
4.400
1.400
1.200
2.500
1.600
0.000
0.000
0.000
0.000
! critical shear stress for erosion
4.0
! groundwatertable, hydraulic gradient, and angle of seepage force
69.12  1.00  0.00
! Manning's n
0.06
----- Right FloodPlain -----
! number of nodes
10
! station and elevation for above number of coordinates in (m)
142.18      70.77
146.11      70.77
147.88      70.77
152.12      72.08

```

Figure 6.5 A sample cross section data file used in the simulation of the lower 3.5 km of Goodwin Creek, Mississippi. (continued)

153.58	73.24
154.37	73.55
154.98	73.64
156.08	73.64
256.08	73.64
257.08	74.64
! Manning's n of right floodplain	
0.10	

Figure 6.6 Part of the discharge data file used in the simulation of the lower 3.5 km of Goodwin Creek, Mississippi.

11/30/1981 17:40:00	0	0.11
11/30/1981 18:10:00	1	0.20
11/30/1981 18:30:00	0	0.28
11/30/1981 18:40:00	0	0.34
11/30/1981 19:00:00	0	0.48
11/30/1981 19:08:00	0	0.63
11/30/1981 19:16:00	0	0.95
11/30/1981 19:20:00	0	1.17
11/30/1981 19:24:00	0	1.54
11/30/1981 19:26:00	0	1.78
11/30/1981 19:28:00	0	2.03
11/30/1981 19:32:00	0	2.20
11/30/1981 19:40:00	0	2.63
11/30/1981 19:52:00	0	3.18
11/30/1981 20:00:00	0	3.59
11/30/1981 20:10:00	0	3.62
11/30/1981 20:20:00	0	3.67
11/30/1981 20:30:00	0	3.67
11/30/1981 20:36:00	0	3.62
11/30/1981 20:48:00	0	3.54
11/30/1981 21:00:00	0	3.50
11/30/1981 21:11:00	0	3.30
11/30/1981 21:20:00	0	3.14
11/30/1981 21:22:00	0	3.11
11/30/1981 21:34:00	0	2.85
11/30/1981 21:44:00	0	2.64
11/30/1981 21:56:00	0	2.41
11/30/1981 22:00:00	0	2.34
11/30/1981 22:07:00	0	2.20
11/30/1981 22:20:00	0	1.96
11/30/1981 22:30:00	0	1.79
11/30/1981 22:42:00	0	1.59
11/30/1981 22:54:00	0	1.41
11/30/1981 23:00:00	0	1.33
11/30/1981 23:04:00	0	1.29
11/30/1981 23:16:00	0	1.16
11/30/1981 23:26:00	0	1.07
11/30/1981 23:30:00	0	1.03

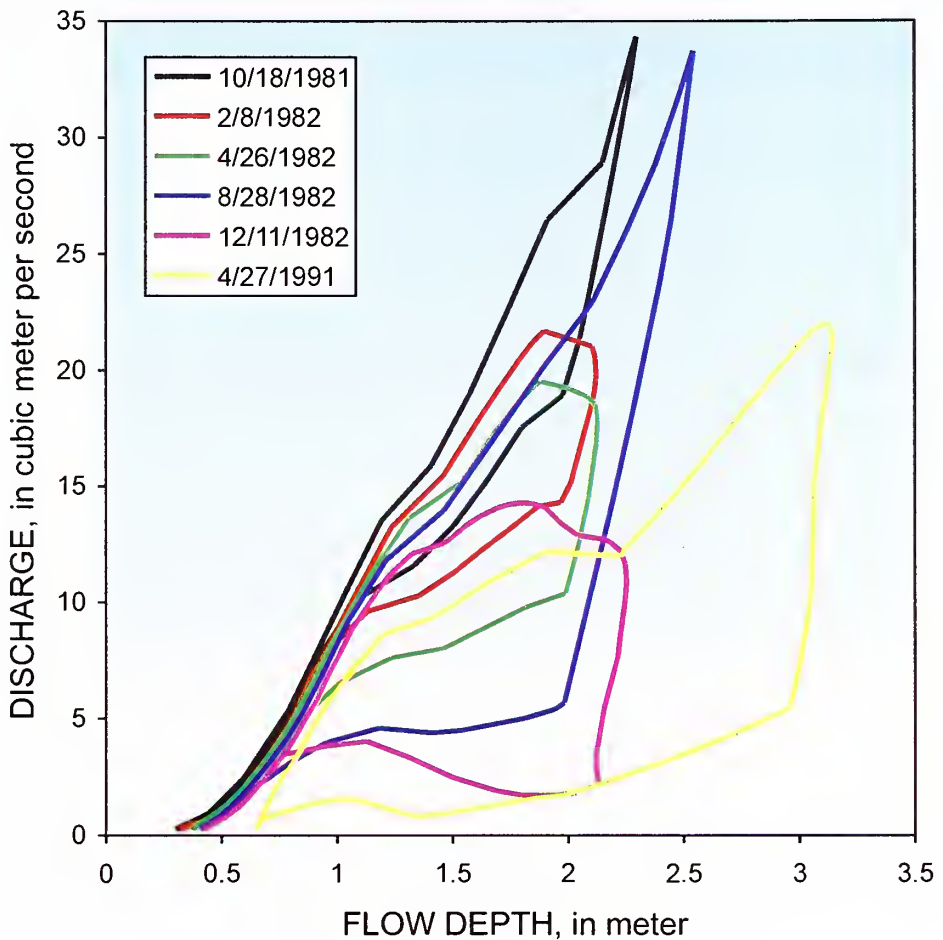
Figure 6.6 Part of the discharge data file used in the simulation of the lower 3.5 km of Goodwin Creek, Mississippi. (continued)

11/30/1981	23:38:00	0	0.96
11/30/1981	23:48:00	0	0.86
12/01/1981	00:00:00	0	0.75
12/01/1981	00:01:00	0	0.73
12/01/1981	00:12:00	0	0.69
12/01/1981	00:20:00	0	0.66
12/01/1981	00:22:00	0	0.66
12/01/1981	00:29:00	0	0.62
12/01/1981	00:36:00	0	0.59
12/01/1981	00:52:00	0	0.53
12/01/1981	01:02:00	0	0.49
12/01/1981	01:10:00	0	0.47
12/01/1981	01:21:00	0	0.44
12/01/1981	01:34:00	0	0.42
12/01/1981	01:49:00	0	0.38
12/01/1981	02:16:00	2	0.33
12/01/1981	03:10:00	0	0.26
12/01/1981	03:30:00	0	0.24
12/01/1981	03:47:00	0	0.22
12/01/1981	05:08:00	0	0.16
12/01/1981	05:32:00	0	0.14
12/01/1981	06:58:00	0	0.11
01/02/1982	20:44:00	0	0.11
01/02/1982	20:45:00	0	0.13
01/02/1982	20:47:00	0	0.15
01/02/1982	20:49:00	1	0.18
01/02/1982	20:52:00	0	0.24
01/02/1982	20:54:00	0	0.34
01/02/1982	20:55:00	0	0.43
01/02/1982	20:56:00	0	0.56
01/02/1982	20:58:00	0	0.76
01/02/1982	21:00:00	0	1.05
01/02/1982	21:02:00	0	1.29
01/02/1982	21:03:00	0	1.39
01/02/1982	21:04:00	0	1.53

Hydraulics

Figure 6.7 shows changes in the shape of the rating curve at the outlet of the modeling reach during 1982 and at the end of the simulation period. We obtained these results for the second scenario; however, the predicted changes in rating-curve shape are similar for scenario one. Figure 6.7 shows that:

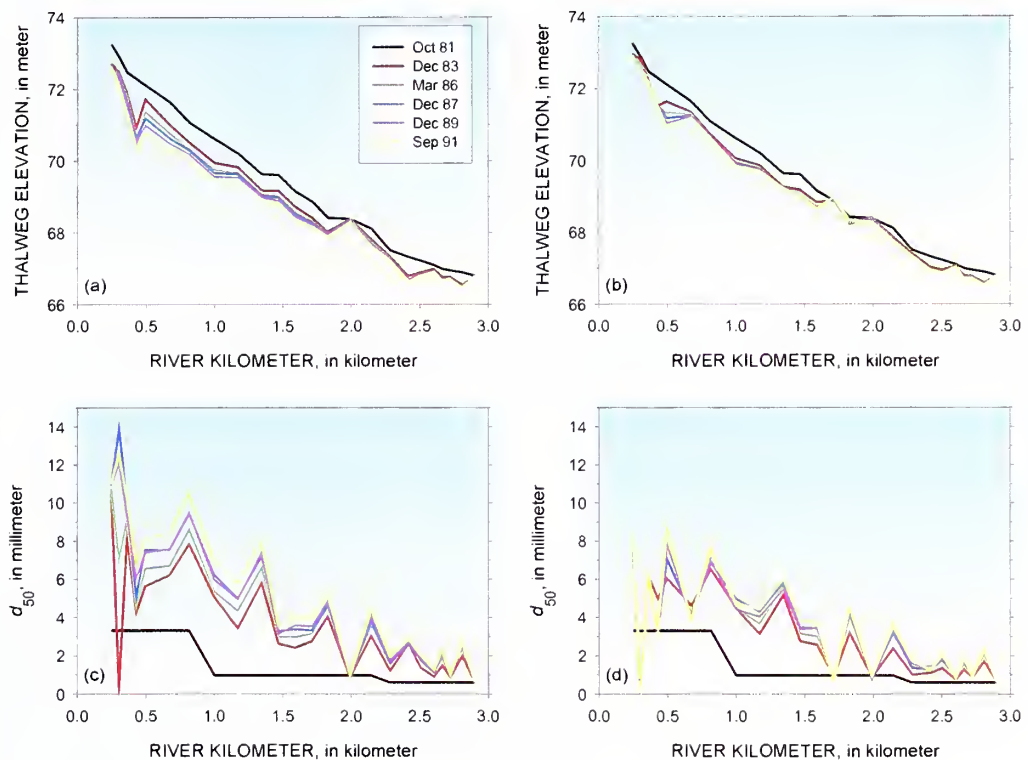
- flow depth at base flow increases;
- average slope of the rating curve, that is dQ/dh , decreases; and
- difference in flow depths for the same discharge on the rising and falling limb of the hydrograph increases.

Figure 6.7 Simulated storm rating-curves at the outlet of the modeling reach.

We can relate the above points to adjustments of channel geometry, which is discussed in the next section on “Morphology”. The changes in shape of the rating curve and the larger flow depth at base flow infer that channel slope has reduced over the simulation period. The types of flood waves propagating through the channel have changed from diffusion to dynamic waves.

The mean slope of the rating curve, dQ/dh , of the storm event occurring on October 18, 1981, is $16.0 \text{ m}^2/\text{s}$, whereas it is $5.5 \text{ m}^2/\text{s}$ for the storm event occurring on April 27, 1991. Assuming that changes in the derivative of conveyance with respect to flow depth, dK/dh , are negligible, the channel slope has reduced by a factor of 8.5. Figure 6.8 shows that channel slope has approximately reduced from 0.0012 to 0.0002 along the downstream most 0.5 km. This agrees well with the change in mean slope of the rating curve.

Figure 6.8 Simulated changes in profiles of: thalweg elevation ((a) scenario 1 and (b) scenario 2) and d_{50} ((c) scenario 1 and (d) scenario 2).



Morphology

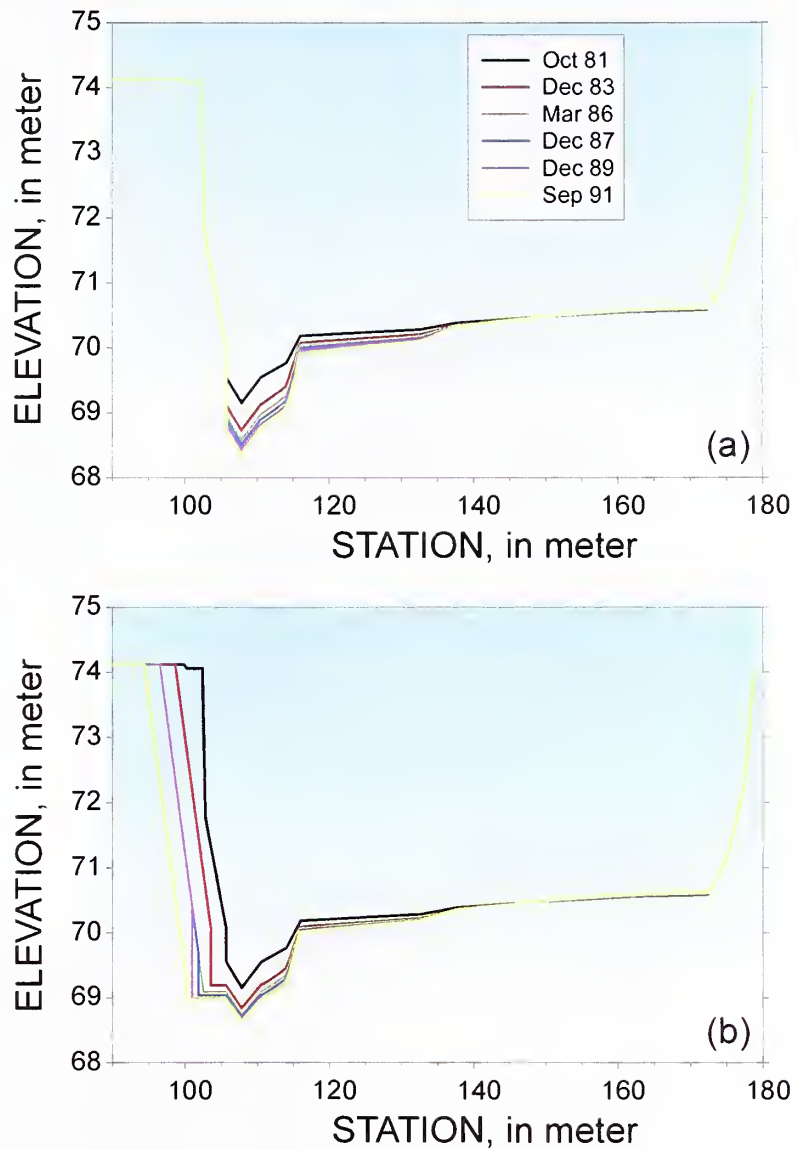
Figure 6.8 shows simulated profiles of thalweg elevation and d_{50} for the two scenarios. Changes in the thalweg profile occur mainly in the first two years of the simulation period. This agrees well with the changes in the shape of the rating curve, which mainly occur in the first year of the simulation period (see Figure 6.7). The modeling reach incises more in the case where it can adjust only vertically (scenario 1, Figure 6.8a) than in the case where it can adjust both vertically and horizontally (scenario 2, Figure 6.8b). At the end of the simulation period the modeling reach continues to adjust for scenario 1 (Figure 6.8a), whereas it has reached a quasi-dynamic equilibrium for scenario 2 (Figure 6.8b).

The composition of the bed surface is coarser for scenario 1 (Figure 6.8c) than for scenario 2 (Figure 6.8d), because:

- 1 Incision is larger for scenario 1 than scenario 2. Hence, more ‘finer’ particles are removed from the bed in scenario 1.
- 2 Bank failures occurring in scenario 2 add fine material to the sediment transport.

Figure 6.9 shows simulated changes in geometry of cross section C45-1. The cross section is incising. There is some minor deposition on the bar near the

Figure 6.9 Simulated changes in geometry of cross section C45-1: (a) scenario 1 and (b) scenario 2.



right bank. In scenario 2, three left-bank failures occur, mainly because the flow removes bank material from the bank toe.

GOODWIN CREEK BENDWAY, MISSISSIPPI

This chapter presents the application of CONCEPTS to a bendway in Goodwin Creek, Mississippi. You will find the physical characteristics of the bendway, the input data necessary to perform the simulation, and results showing the capability of CONCEPTS to accurately predict streambank erosion.

Study Area

Since February 1996 the US Department of Agriculture-Agricultural Research Service-National Sedimentation Laboratory (NSL) has conducted extensive research on streambank failure mechanics along a bendway of Goodwin Creek, northern Mississippi (Simon *et al.*, 1999). The following data are being collected:

- cross section geometry,
- water surface elevations,
- bank-material properties,
- bank-material shear-strength parameters,
- pore-water pressures in the bank,
- root mapping and tensile strength, and
- plant stem flow.

Two flow measuring flumes (flumes #3 and #4, see Figure 6.1) in upstream tributaries provide continuous discharge and fine sediment data. Figures 7.1 and 7.2 show a photo and a plan view of the bendway with locations of ten surveyed cross sections, respectively. The flow is from top to bottom.

Bank material consists of about 2 m of brown, clayey-silt of late Holocene age (LH unit) overlying 1.5 m of early Holocene gray, blocky silt of lower permeability (EH unit). These units are separated by a thin (0.1 to 0.2 m) layer

Figure 7.1 Photo of the Goodwin Creek Bendway study site. Flow is from right to left.



containing manganese nodules and characterized by very low permeability, which perches water. These materials overlie 1 m of sand and 1.5 m of packed sandy gravel.

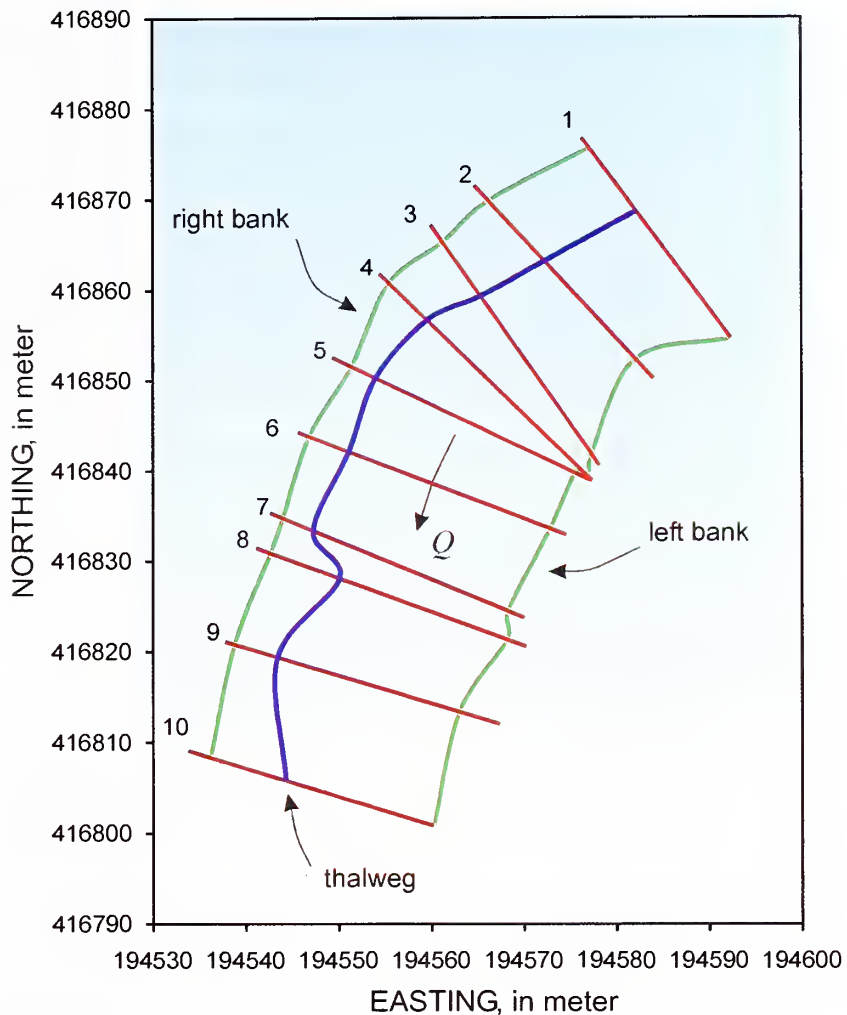
Apparent cohesion and effective angle of internal friction were measured *in situ* using an Iowa Borehole Shear Tester (Luttenegger and Hallberg, 1981). For the LH unit, results revealed an apparent cohesion varying between 0.0 and 8.4 kPa with an average friction angle of 28.1°. The underlying EH unit has apparent cohesion values varying between 0.0 and 37.9 kPa with an average friction angle of 28.5° for the period between June 1996 and July 1998 (Simon *et al.*, 1999). Simon *et al.* (1999) provide the following values for effective cohesion and angle ϕ^b :

- LH unit, $c' = 2.67$ kPa and $\phi^b = 10.4^\circ$; and
- EH unit, $c' = 13.0$ kPa and $\phi^b = 17.5^\circ$.

Four major failure episodes occurred at the research site between February and December 1996, resulting in up to 2 m of top-bank retreat. This rate is greater than the 30-year average of about 0.5 m/yr, and is attributed to persistent precipitation, manifest in 10 discharge peaks with a 1-year recurrence interval or greater (Simon and Darby, 1997). Planar and cantilever failures were relatively common along the steepest section of the 4.7 m high banks. Cantilevers were formed by:

- 1 preferential erosion of sands and silts by fluvial undercutting about 3.0 to 3.5 m below the top bank, and

Figure 7.2 Plan view of the Goodwin Creek Bendway field study site. The surveyed cross sections are shaded red.



2 by sapping and small pop-out failures in the region of contrasting permeabilities in the Holocene units about 1.6 to 2 m below the top bank.

Both processes resulted in oversteepening at the base of the EH unit and subsequent collapse during wet periods.

Application

We employed CONCEPTS to simulate the above failure processes between March 1, 1996 and March 31, 1997. The modeling reach contains 10 surveyed cross sections (see Figure 7.2) and one inserted cross section 20 m downstream of cross section 10. This cross section is a copy of cross section 10, and was inserted to prevent the downstream boundary condition from affecting the simulated results. Observed bed elevations did not vary much during this period, so we turned off the sediment transport and bed adjustment module to

fix the bed. We imposed the combined discharges measured at flumes 3 and 4 at the upstream boundary of the modeling reach.

Because CONCEPTS assumes that bank-material properties are homogeneous, we used the following average shear-strength parameters: $c' = 4.5$ kPa,

$\phi' = 28.3^\circ$, and $\phi^b = 13.5^\circ$. The phreatic surface was located 3.5 m below the top of the bank. CONCEPTS follows the *excess shear-stress* method of Osman and Thorne (1988), see the section on “Fluvial Erosion Process” in Chapter 3, to calculate the lateral erosion at the bank toe. Critical shear stresses varied along the right bank from 8 Pa at cross section 1 to 1.5 Pa at the apex of the bend (cross section 6) to 4 Pa at cross section 10. Because CONCEPTS is only applicable to straight channels, we have to vary the critical shear stresses to simulate channel widening due to bend migration.

Figure 7.3 shows the *Run Control Data File*, Figure 7.4 shows an example of a *Cross Section Data File*, and Figure 7.5 shows part of the *Discharge Data File*.

Figure 7.3 Run control data file used in the simulation of the Goodwin Creek Bendway field study site.

```
!
! Main Input File
!
! case name
GCB
! project title
Goodwin Creek Bendway 1 bank stability analysis
!----- Run Control Data -----
! upstream flow discharge file
GCBHydrography.txt
! flow-related data
0.10 0.0 0
! sediment discharge at upstream end of the channel
0 0.10 0.10 0.10 0.05 0.00 0.00 0.00 0.00 0.00 0.00 0.00 0.00
! silt fraction and downstream bed control
0.30 1.0
! bank failure analysis
7 10
! type of flow resistance formulation
1
! water temperature
10.0
! sediment and streambank mechanics options
0 1 1
!----- Simulation Times -----
! start end time step
03/03/1996 00:00:00 03/31/1997 24:00:00 100
!----- Makeup of Modeling Reach -----
! number of links
1
! linktypes for the above number of links
```

Figure 7.3 Run control data file used in the simulation of the Goodwin Creek Bendway field study site. (continued)

```

1
!----- Link 1 -----
! REACH: number of cross sections and their data filenames
11
CrossSection01.txt
CrossSection02.txt
CrossSection03.txt
CrossSection04.txt
CrossSection05.txt
CrossSection06.txt
CrossSection07.txt
CrossSection08.txt
CrossSection09.txt
CrossSection10.txt
CrossSection11.txt
!----- Output -----
! single point and time
6
17536
1 1
14
03/06/1996 00:00:00
03/25/1996 11:45:00
04/22/1996 22:30:00
06/12/1996 08:00:00
07/24/1996 23:15:00
09/21/1996 05:00:00
11/07/1996 12:45:00
11/30/1996 10:15:00
12/16/1996 18:00:00
12/26/1996 18:00:00
01/24/1997 00:30:00
02/04/1997 03:15:00
03/02/1997 04:00:00
03/18/1997 22:45:00
17536
1 3
14
03/06/1996 00:00:00
03/25/1996 11:45:00
04/22/1996 22:30:00
06/12/1996 08:00:00
07/24/1996 23:15:00
09/21/1996 05:00:00
11/07/1996 12:45:00
11/30/1996 10:15:00
12/16/1996 18:00:00
12/26/1996 18:00:00
01/24/1997 00:30:00
02/04/1997 03:15:00

```

Figure 7.3 Run control data file used in the simulation of the Goodwin Creek Bendway field study site. (continued)

```
03/02/1997 04:00:00
03/18/1997 22:45:00
17536
1    5
14
03/06/1996 00:00:00
03/25/1996 11:45:00
04/22/1996 22:30:00
06/12/1996 08:00:00
07/24/1996 23:15:00
09/21/1996 05:00:00
11/07/1996 12:45:00
11/30/1996 10:15:00
12/16/1996 18:00:00
12/26/1996 18:00:00
01/24/1997 00:30:00
02/04/1997 03:15:00
03/02/1997 04:00:00
03/18/1997 22:45:00
17536
1    6
14
03/06/1996 00:00:00
03/25/1996 11:45:00
04/22/1996 22:30:00
06/12/1996 08:00:00
07/24/1996 23:15:00
09/21/1996 05:00:00
11/07/1996 12:45:00
11/30/1996 10:15:00
12/16/1996 18:00:00
12/26/1996 18:00:00
01/24/1997 00:30:00
02/04/1997 03:15:00
03/02/1997 04:00:00
03/18/1997 22:45:00
17536
1    8
14
03/06/1996 00:00:00
03/25/1996 11:45:00
04/22/1996 22:30:00
06/12/1996 08:00:00
07/24/1996 23:15:00
09/21/1996 05:00:00
11/07/1996 12:45:00
11/30/1996 10:15:00
12/16/1996 18:00:00
12/26/1996 18:00:00
01/24/1997 00:30:00
```

Figure 7.3 Run control data file used in the simulation of the Goodwin Creek Bendway field study site. (continued)

```

02/04/1997 03:15:00
03/02/1997 04:00:00
03/18/1997 22:45:00
17536
1 10
14
03/06/1996 00:00:00
03/25/1996 11:45:00
04/22/1996 22:30:00
06/12/1996 08:00:00
07/24/1996 23:15:00
09/21/1996 05:00:00
11/07/1996 12:45:00
11/30/1996 10:15:00
12/16/1996 18:00:00
12/26/1996 18:00:00
01/24/1997 00:30:00
02/04/1997 03:15:00
03/02/1997 04:00:00
03/18/1997 22:45:00
! single point, continuously in time
6
602125
1 1
1
03/01/1996 00:00:00 03/31/1997 23:59:59
602125
1 3
1
03/01/1996 00:00:00 03/31/1997 23:59:59
602125
1 5
1
03/01/1996 00:00:00 03/31/1997 23:59:59
602125
1 6
1
03/01/1996 00:00:00 03/31/1997 23:59:59
602125
1 8
1
03/01/1996 00:00:00 03/31/1997 23:59:59
602125
1 10
1
03/01/1996 00:00:00 03/31/1997 23:59:59
! profile at specific time points
1
7
1 1 1 10

```

Figure 7.3 Run control data file used in the simulation of the Goodwin Creek Bendway field study site. (continued)

```
14
03/06/1996 00:00:00
03/25/1996 11:45:00
04/22/1996 22:30:00
06/12/1996 08:00:00
07/24/1996 23:15:00
09/21/1996 05:00:00
11/07/1996 12:45:00
11/30/1996 10:15:00
12/16/1996 18:00:00
12/26/1996 18:00:00
01/24/1997 00:30:00
02/04/1997 03:15:00
03/02/1997 04:00:00
03/18/1997 22:45:00
```

Figure 7.4 A sample cross section data file used in the simulation of the Goodwin Creek Bendway field study site.

```
!
! Input file of cross section 5.
!
! Name of xsection and rivermile in (km)
Cross Section 5 Goodwin Creek Bendway 1
    0.0337
! friction factor
0.06
! discharge fraction due to tributary inflow
0.00
!----- Left FloodPlain -----
! number of nodes
5
! station and elevation for above number of coordinates in (m)
-100.00    85.37
-100.00    84.37
    0.00    84.37
    0.54    84.36
    1.97    84.11
! Manning's n of left Floodplain
0.10
!----- Left Bank -----
! number of nodes
6
! station and elevation for above number of coordinates in (m)
    1.97    84.11
    3.39    83.17
    7.58    82.65
   11.10    81.83
   13.24    81.41
   13.77    81.17
```

Figure 7.4 A sample cross section data file used in the simulation of the Goodwin Creek Bendway field study site. (continued)

Figure 7.4 A sample cross section data file used in the simulation of the Goodwin Creek Bendway field study site. (continued)

Figure 7.4 A sample cross section data file used in the simulation of the Goodwin Creek Bendway field study site. (continued)

```
!----- Right FloodPlain -----
! number of nodes
5
! station and elevation for above number of coordinates in (m)
28.90    84.39
31.11    84.52
31.20    84.67
131.20   84.67
131.20   85.67
! Manning's n of right Floodplain
0.05
```

Figure 7.5 Part of the discharge data file used in the simulation of the Goodwin Creek Bendway field study site.

03/20/1996	11:59:00	0	0.13
03/20/1996	21:20:00	2	0.10
03/24/1996	23:39:00	1	0.10
03/24/1996	23:41:00	0	0.11
03/24/1996	23:44:00	0	0.13
03/24/1996	23:45:00	0	0.14
03/24/1996	23:46:00	0	0.19
03/24/1996	23:48:00	0	0.28
03/24/1996	23:51:00	0	0.56
03/24/1996	23:52:00	0	0.74
03/25/1996	00:00:00	0	2.15
03/25/1996	00:01:00	0	2.42
03/25/1996	00:05:00	0	3.33
03/25/1996	00:08:00	0	3.93
03/25/1996	00:10:00	0	4.52
03/25/1996	00:14:00	0	5.52
03/25/1996	00:16:00	0	6.09
03/25/1996	00:19:00	0	6.88
03/25/1996	00:20:00	0	7.39
03/25/1996	00:25:00	0	9.33
03/25/1996	00:27:00	0	10.27
03/25/1996	00:28:00	0	10.80
03/25/1996	00:30:00	0	11.83
03/25/1996	00:37:00	0	14.25
03/25/1996	00:38:00	0	14.60
03/25/1996	00:47:00	0	17.33
03/25/1996	00:49:00	0	17.93
03/25/1996	00:50:00	0	18.11
03/25/1996	00:59:00	0	20.11
03/25/1996	01:01:00	0	20.60
03/25/1996	01:02:00	0	20.80
03/25/1996	01:07:00	0	21.89
03/25/1996	01:11:00	0	22.77
03/25/1996	01:12:00	0	22.94
03/25/1996	01:14:00	0	23.26

Figure 7.5 Part of the discharge data file used in the simulation of the Goodwin Creek Bendway field study site. (continued)

03/25/1996 01:15:00	0	23.41
03/25/1996 01:19:00	0	23.92
03/25/1996 01:24:00	0	24.35
03/25/1996 01:25:00	0	24.46
03/25/1996 01:33:00	0	24.98
03/25/1996 01:35:00	0	25.02
03/25/1996 01:36:00	0	24.98
03/25/1996 01:42:00	0	24.99
03/25/1996 01:43:00	0	24.99
03/25/1996 01:47:00	0	24.90
03/25/1996 01:51:00	0	24.80
03/25/1996 01:55:00	0	24.53
03/25/1996 01:58:00	0	24.35
03/25/1996 02:01:00	0	24.21
03/25/1996 02:04:00	0	24.03
03/25/1996 02:09:00	0	23.75
03/25/1996 02:10:00	0	23.71
03/25/1996 02:13:00	0	23.42
03/25/1996 02:19:00	0	22.93
03/25/1996 02:21:00	0	22.76
03/25/1996 02:31:00	0	21.96
03/25/1996 02:43:00	0	20.94
03/25/1996 02:52:00	0	20.31
03/25/1996 02:57:00	0	20.04
03/25/1996 03:11:00	0	19.25
03/25/1996 03:21:00	0	18.64
03/25/1996 03:31:00	0	17.87
03/25/1996 03:33:00	0	17.70
03/25/1996 03:48:00	0	16.48
03/25/1996 04:18:00	0	13.75
03/25/1996 04:39:00	0	11.42
03/25/1996 04:41:00	0	11.20
03/25/1996 04:47:00	0	10.50
03/25/1996 04:51:00	0	10.06
03/25/1996 04:57:00	0	9.53
03/25/1996 05:02:00	0	8.97
03/25/1996 05:10:00	0	8.34
03/25/1996 05:15:00	0	7.92
03/25/1996 05:24:00	0	7.24
03/25/1996 05:28:00	0	6.94
03/25/1996 05:36:00	0	6.46
03/25/1996 05:46:00	0	5.87
03/25/1996 05:49:00	0	5.68
03/25/1996 05:56:00	0	5.32
03/25/1996 06:04:00	0	5.04
03/25/1996 06:11:00	0	4.81
03/25/1996 06:18:00	0	4.56
03/25/1996 06:30:00	0	4.19
03/25/1996 06:40:00	0	3.87
03/25/1996 06:45:00	0	3.73

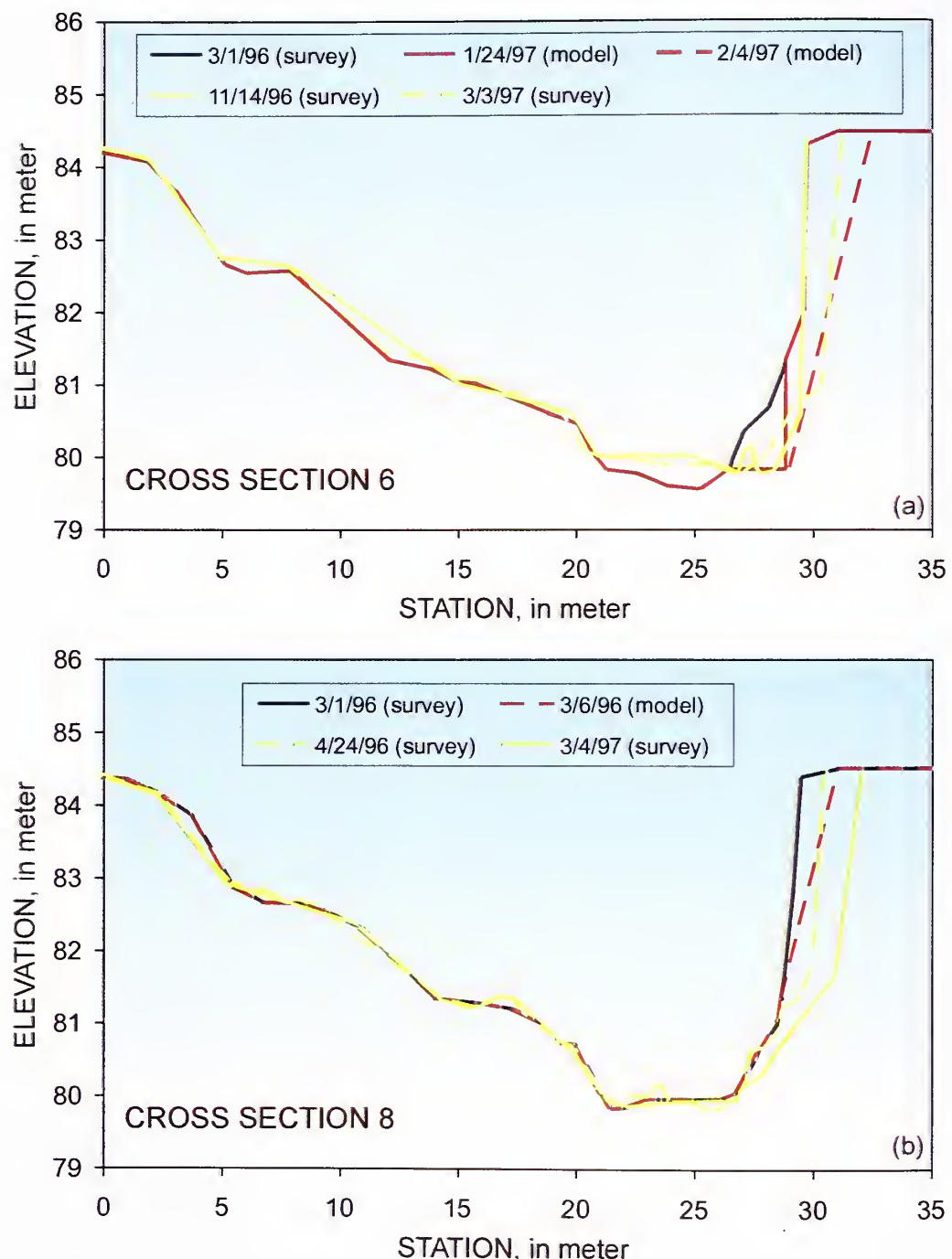
Figure 7.5 Part of the discharge data file used in the simulation of the Goodwin Creek Bendway field study site. (continued)

03/25/1996 06:56:00	0	3.49
03/25/1996 07:11:00	0	3.16
03/25/1996 07:13:00	0	3.12
03/25/1996 07:27:00	0	2.86
03/25/1996 07:42:00	0	2.58
03/25/1996 07:47:00	0	2.49
03/25/1996 07:57:00	0	2.47
03/25/1996 08:28:00	0	2.32
03/25/1996 08:50:00	0	2.26
03/25/1996 09:04:00	0	2.20
03/25/1996 09:34:00	0	2.08
03/25/1996 09:59:00	0	2.01
03/25/1996 10:48:00	0	1.87
03/25/1996 11:41:00	0	1.76
03/25/1996 12:17:00	0	1.68
03/25/1996 13:50:00	0	1.49
03/25/1996 15:34:00	0	1.29
03/25/1996 17:31:00	0	1.09
03/25/1996 19:56:00	0	0.87
03/25/1996 22:45:00	0	0.62
03/25/1996 23:29:00	0	0.56
03/26/1996 00:00:00	0	0.53
03/26/1996 00:01:00	0	0.53
03/26/1996 00:57:00	0	0.48
03/26/1996 01:05:00	0	0.48
03/26/1996 09:13:00	0	0.39
03/26/1996 09:18:00	0	0.39
03/27/1996 00:00:00	0	0.25
03/27/1996 00:01:00	0	0.23
03/27/1996 13:05:00	0	0.17
03/28/1996 00:00:00	0	0.12
03/28/1996 12:20:00	2	0.10
04/20/1996 09:20:00	1	0.10
04/20/1996 09:21:00	0	0.42

Figure 7.6 compares simulated and surveyed cross sections 6 and 8. The right bank of cross section 6 underwent two successive failures on December 1, 1996 and midwinter 1997 (Figure 7.6a). The retreat of the top bank was 0.6 m and 1 m, respectively. CONCEPTS simulated failure of the bank on February 4, 1997, with the top bank retreating 2.7 m (Figure 7.6a). CONCEPTS underpredicted the rate of basal scour. Also, the observed failure plane angle is greater than that computed. Cantilever failures will generally occur along steeper slip surfaces than planar failures. The cantilever failure is not yet implemented in CONCEPTS.

Figure 7.6b shows that the right bank of cross section 8 fails in late April, 1996 (retreat of the top bank is 1.0 m) and again on February 3, 1997 (retreat of top bank is 1.6 m). CONCEPTS simulated failure of the bank on March 6, 1997. The slip surface intersects the bank 3.1 m below the top bank. CONCEPTS

Figure 7.6 Comparison of observed and simulated bank failures at the Goodwin Creek Bendway field study site: (a) cross section 6 and (b) cross section 8.



was unable to predict the ‘February 1997’ failure because the flow did not remove all of the slumped material from the ‘March 1996’ failure. On March 31, 1997, $0.05 \text{ m}^3/\text{m}$ of the modeled, slumped material remained. In CONCEPTS the next simulated flow event after March 31, 1997 should be able to erode the remaining slumped material and continue to steepen the bank, which may then fail in the spring of 1997.

Figure 7.7 Predicted factor of safety for the right banks of cross sections 6 and 8.

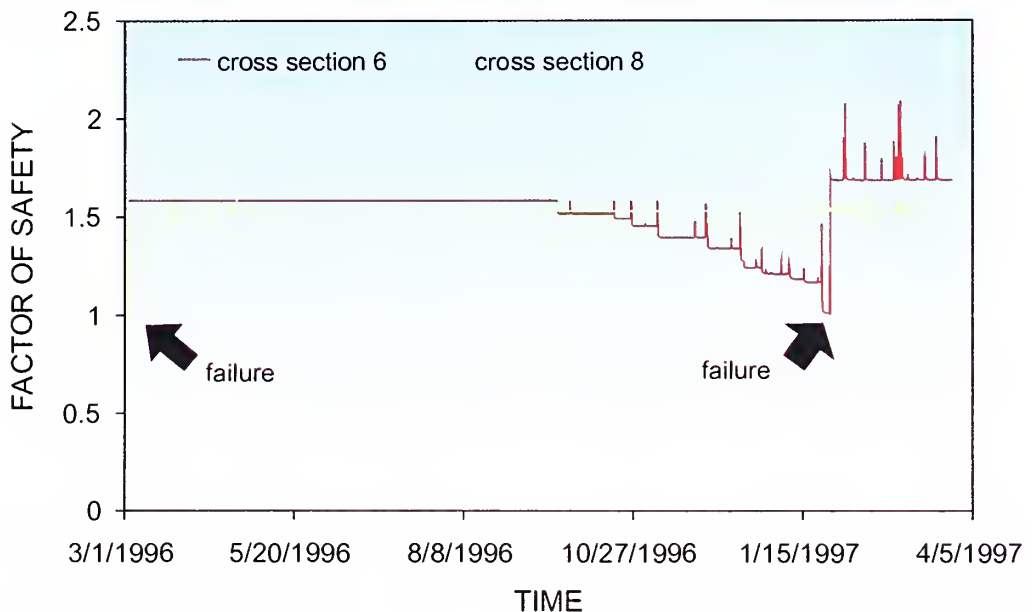


Figure 7.7 shows how the factor of safety of the right bank of cross section 6 reduces after each runoff event. Scour of bank material near the bank toe steepens the bank and reduces the factor of safety. The spikes in the factor of safety represent the increase in factor of safety due to rising flow stage and thus an increase in confining pressure.

Goodwin Creek Bendway, Mississippi

LITTLE SALT CREEK, NEBRASKA

This chapter presents the application of CONCEPTS to the middle reach of Little Salt Creek in eastern Nebraska. You will find (1) the physical characteristics of the channel, (2) the input data necessary to perform the simulation, and (3) results showing the capability of CONCEPTS to simulate the morphology of a channel made up of cohesive bed and bank material and the effects of grade control structures on channel stability.

Study Area

The Little Salt Creek is a tributary of Salt Creek and drains approximately 119 km² (see Figure 8.1). Bed and bank materials are cohesive. The average channel slope is about 0.0015. Saline wetlands in the Salt Creek basin have diminished from 16,000 acres to approximately 1,200 acres. They hold a diversity of wildlife and contain rare plant communities. A saline wetland north of raymond Road (Figure 8.2) is endangered by channel incision, which may lead to draining of the wetland. Channel incision may also lead to additional streambank failures and loss of wetland area (Figure 8.3).

Scientists of the US Department of Agriculture-Agricultural Research Service-National Sedimentation Laboratory (NSL) have collected data in cooperation with the US Geological Survey (USGS) on streambank shear-strength parameters and streambed erodibility. In addition, the USGS surveyed the study reach (Raymond Road to Bluff Road, see Figure 8.1), took bed and bank-material samples, and collected discharge data.

Figure 8.1 Map of Little Salt Creek, Lancaster County, Nebraska.

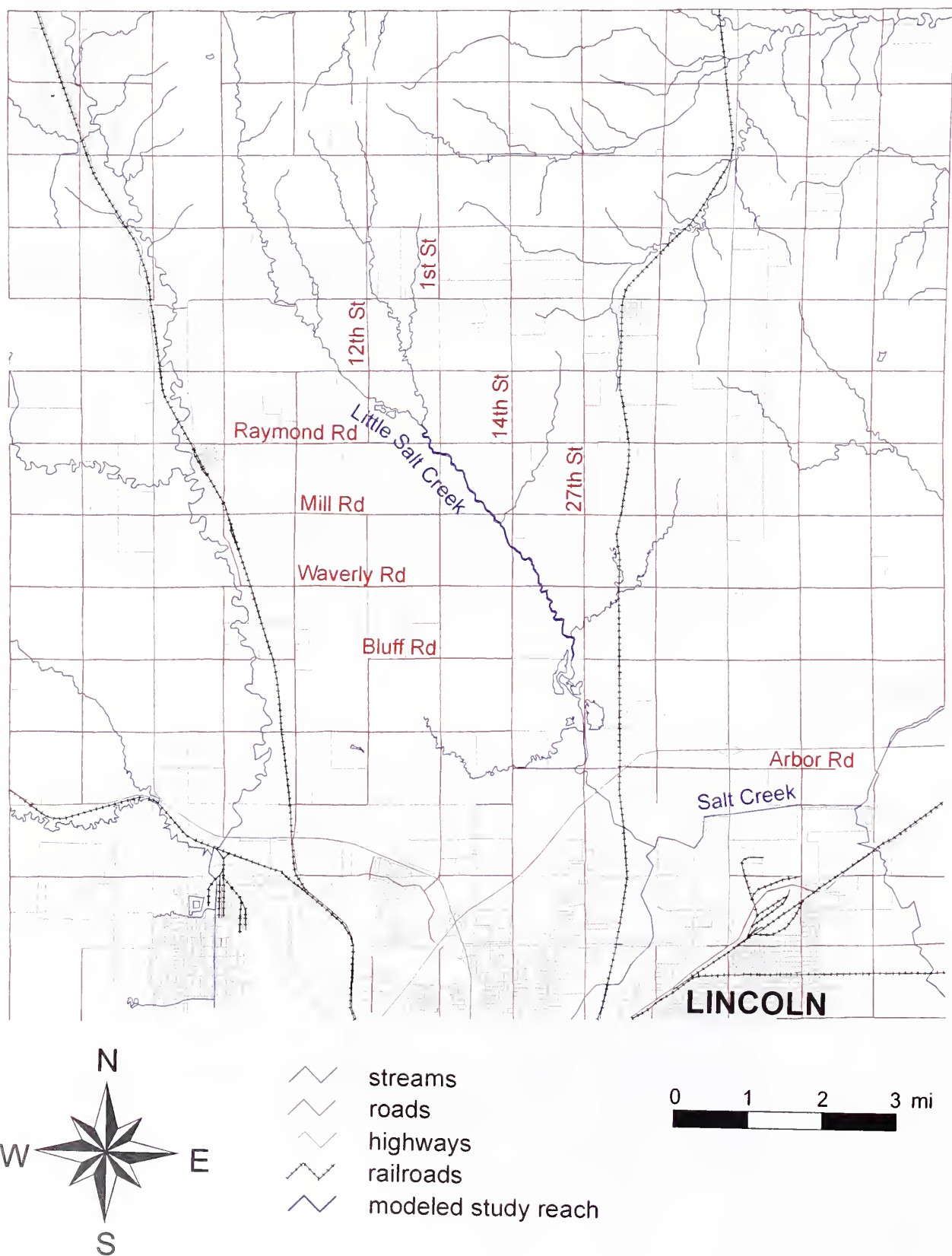


Figure 8.2 View of Little Salt Creek and wetlands upstream of Raymond Road.



Figure 8.3 Streambank failure along Little Salt Creek north of Raymond Road.



Channel Geometry

The USGS surveyed seven cross sections upstream of Raymond Road, six cross sections upstream of Mill Road, and seven cross sections near Bluff

Road. There are two reaches that could not be surveyed because they were inaccessible:

- 1** A reach extending from raymond Road to the first surveyed cross section upstream of Mill Road. The length of this reach is 1.7 km. Seven simulated cross sections were inserted along this reach with equidistant spacing. Their geometries gradually varied from that of the most downstream surveyed cross section at Raymond Road to that of the most upstream surveyed cross section at Mill Road.
- 2** A reach extending from Mill Road to the most upstream surveyed cross section near Bluff Road. The length of this reach is 3.6 km. Seventeen simulated cross sections were similarly inserted along this reach between Mill and Bluff Roads.

Hydrographs

A USGS gaging station is located at Arbor Road on Little Salt Creek. The USGS provided:

- daily discharges for water years 1969 through 1998,
- peak-flow data above a base discharge of $15.6 \text{ m}^3/\text{s}$ for the same time period, and
- half-hourly instantaneous discharges for water years 1991-1994 and 1996-1998.

Mean-daily discharges may not, however, be a good representative of actual flow because they cannot account for the peak discharge and the commonly rapid rise from base flow to peak flow. The largest shear stresses exerted by the flow on the streambed often occur near peak flow. It is important to properly calculate the bed shear stress to accurately predict the evolution of the streambed. The following procedure was used to convert daily discharges to unsteady flow hydrographs:

- 1** We selected a base-flow discharge of $0.12 \text{ m}^3/\text{s}$ after analysis of the daily discharge values.
- 2** Using the available peak-flow data, we determined a ratio between peak discharge and its corresponding daily discharge for each of the 90 peak discharges. The average of all ratios was 3.9.
- 3** We traced runoff events from the daily discharges. We set discharges smaller than the base-flow discharge equal to the base-flow discharge. We then multiplied the maximum daily discharge in a runoff event by 3.9 to obtain peak discharge. We replaced calculated peak discharge by that observed for known peak discharges. This resulted in breakpoint data for each runoff event. We assumed that each discharge value occurred at noon of that day. We added two breakpoints to the day of peak flow to preserve runoff volume.

CONCEPTS requires discharge hydrographs at the upstream boundary of the modeling reach. Using drainage-area analysis, we converted discharges at the gaging station to those at the upstream boundary near Raymond Road. Similarly, we can determine discharges at the downstream boundary near Bluff Road. Hence, we can calculate the coefficient C_Q in (4.1) as

$$C_Q = \frac{1}{L} \left(\left(\frac{DA_{\text{Bluff}}}{DA_{\text{Raymond}}} \right)^{\xi} - 1 \right) \quad (8.1)$$

where L is channel length between Raymond and Bluff Roads, DA is drainage area, and the exponent ξ varies between 0.7 and 1.0 (Leopold, 1994). Here,

$C_Q = 9.07 \times 10^{-5}$ using $DA_{\text{Raymond}} = 43.8 \text{ km}^2$, $DA_{\text{Bluff}} = 85.8 \text{ km}^2$, $\xi = 0.8$, and $L = 7.86 \text{ km}$.

Bed-Material Properties

We performed *in situ* field experiments using a submersible jet device (Hanson, 1990) to measure the erodibility coefficient and critical shear stress of the cohesive streambed material (cf. (2.7)). The apparatus consists of a submerged jet with a nozzle diameter of 13 mm, set at a height of 0.22 m above the initial soil surface. Monitoring of the depth of scour during a test yields the erodibility coefficient and critical shear stress. The USGS collected bed-material samples to determine particle-size distributions.

Critical shear stress is fairly constant along the modeling reach (Langendoen and Simon, 2000). The average critical shear stress is 7.7 Pa. The average erodibility (defined here as e/τ_c) is $0.28 \times 10^{-6} \text{ m/Pa}\cdot\text{s}$. The streambed material is a silt loam with a clay content of approximately 14%.

Bank-Material Properties

We performed a series of *in situ* field experiments using a borehole shear test (BST) device (Luttenegger and Hallberg, 1981) to determine the shear strength of the cohesive streambank material. The BST determines consolidated, drained apparent cohesion and effective angle of internal friction. Using the known elevation of the phreatic surface, we calculated average effective cohesion as 4.3 kPa and average angle of internal friction as 29° .

The USGS collected bank-material samples at the BST locations to determine bank-material composition and unit weight. The average bulk density is 1.58 g/cm^3 .

Application

We employed CONCEPTS to study the long-term stability of Little Salt Creek between Raymond and Bluff Roads using the 30-year discharge breakpoint data between 1969 and 1998. The modeling reach contains 20 surveyed cross sections and 26 simulated cross sections. We inserted two of the simulated cross sections between the third and fourth surveyed cross section near Bluff Road to represent a drop in the streambed.

Data on the critical shear stress to entrain bank-material particles was unavailable. We assumed it to equal that of bed-material particles, that is 7.7 Pa. We assumed the bulk unit weight of the bank material to be 17 kN/m³, which is a 10% increase over the average dry bulk unit weight to include water content of the bank material. The angle ϕ^b indicating the increase in shear strength for an increase in matric suction was assumed to be 17°. The groundwater table at each streambank was 1 m above the elevation of the bank toe.

Hereafter, we refer to the distance downstream of the upstream boundary of the modeling reach as *model kilometer*.

Figure 8.4 shows the *Run Control Data File*, Figure 8.5 shows an example of a *Cross Section Data File*, and Figure 8.6 shows part of the *Discharge Data File*.

Figure 8.4 Run control data file used in the simulation of the long term stability of Little Salt Creek, Nebraska.

```
!
! Main Input File
!
! case name
Salt
! project title
Little Salt Creek channel evolution simulation
!----- Run control data -----
! upstream flow discharge file
LSChydrography.txt
! flow-related data
 0.12  9.07E-5  0
! sediment discharge at upstream end of the channel
 0  0.10 0.10 0.10 0.05 0.00 0.00 0.00 0.00 0.00 0.00 0.00 0.00 0.00
! silt fraction
 0.30
! bank failure analysis
 0  3
! type of flow resistance formulation
1
! water temperature
10.0
!----- Simulation Times -----
!          start           end       time step
```

Figure 8.4 Run control data file used in the simulation of the long term stability of Little Salt Creek, Nebraska. (continued)

```

02/25/1969 00:00:00 09/30/1998 23:59:00      100
!----- Makeup of Modeling Reach -----
! number of links
1
! linktypes for the above number of links
1
!----- Link 1 -----
! REACH: number of cross sections and their data filenames
46
Ray-xs-1.txt
Ray-xs-2.txt
Ray-xs-3.txt
Ray-xs-4.txt
Ray-xs-5.txt
Ray-xs-6.txt
Ray-xs-7.txt
RM-xs-1.txt
RM-xs-2.txt
RM-xs-3.txt
RM-xs-4.txt
RM-xs-5.txt
RM-xs-6.txt
RM-xs-7.txt
Mil-xs-1.txt
Mil-xs-2.txt
Mil-xs-3.txt
Mil-xs-4.txt
Mil-xs-5.txt
Mil-xs-6.txt
MW-xs-1.txt
MW-xs-2.txt
MW-xs-3.txt
MW-xs-4.txt
MW-xs-5.txt
MW-xs-6.txt
MW-xs-7.txt
MW-xs-8.txt
MW-xs-9.txt
MW-xs-10.txt
MW-xs-11.txt
WB-xs-1.txt
Wav-xs-1.txt
WB-xs-2.txt
WB-xs-3.txt
WB-xs-4.txt
WB-xs-5.txt
Blu-xs-1.txt
Blu-xs-2.txt
Blu-xs-3.txt
Blu-xs-3B.txt

```

Figure 8.4 Run control data file used in the simulation of the long term stability of Little Salt Creek, Nebraska. (continued)

```
Blu-xs-3C.txt
Blu-xs-4.txt
Blu-xs-5.txt
Blu-xs-6.txt
Blu-xs-7.txt
!----- Output -----
! single point and time
3
17536
1 7
5
03/30/1976 06:00:00
11/10/1983 06:00:00
01/22/1989 06:00:00
12/22/1993 22:00:00
06/20/1998 17:00:00
17536
1 19
5
03/30/1976 06:00:00
11/10/1983 06:00:00
01/22/1989 06:00:00
12/22/1993 22:00:00
06/20/1998 17:00:00
17536
1 39
5
03/30/1976 06:00:00
11/10/1983 06:00:00
01/22/1989 06:00:00
12/22/1993 22:00:00
06/20/1998 17:00:00
! single point, continuously in time
19
602125
1 1
1
01/01/1969 00:00:00 09/30/1998 23:59:59
602125
1 7
1
01/01/1969 00:00:00 09/30/1998 23:59:59
602125
1 12
1
01/01/1969 00:00:00 09/30/1998 23:59:59
602125
1 17
1
01/01/1969 00:00:00 09/30/1998 23:59:59
```

Figure 8.4 Run control data file used in the simulation of the long term stability of Little Salt Creek, Nebraska. (continued)

```

602125
1 22
1
01/01/1969 00:00:00 09/30/1998 23:59:59
602125
1 28
1
01/01/1969 00:00:00 09/30/1998 23:59:59
602125
1 33
1
01/01/1969 00:00:00 09/30/1998 23:59:59
602125
1 39
1
01/01/1969 00:00:00 09/30/1998 23:59:59
602125
1 46
1
01/01/1969 00:00:00 09/30/1998 23:59:59
! profile at specific time points
1
7
1 1 1 46
5
03/30/1976 06:00:00
11/10/1983 06:00:00
01/22/1989 06:00:00
12/22/1993 22:00:00
06/20/1998 17:00:00

```

Figure 8.5 A sample cross section data file used in the simulation of the long-term stability of Little Salt Creek, Nebraska.

```

!
! Input file of cross section 19.
!
! Name of xsection and rivermile in (km)
Cross Section 5 U/S Mill Road
2.9263
! friction factor
0.06
! discharge fraction due to tributary inflow
0.00
!----- Left FloodPlain -----
! number of nodes
4
! station and elevation for above number of coordinates in (m)
-69.33 355.85
-69.33 354.85

```

Figure 8.5 A sample cross section data file used in the simulation of the long-term stability of Little Salt Creek, Nebraska. (continued)

Figure 8.5 A sample cross section data file used in the simulation of the long-term stability of Little Salt Creek, Nebraska. (continued)

Figure 8.5 A sample cross section data file used in the simulation of the long-term stability of Little Salt Creek, Nebraska. (continued)

```

0.000
0.000
0.000
! critical shear stress for erosion
7.7
! groundwatertable, hydraulic gradient, and angle of seepage force
(degrees)
352.38 1.00 0.00
! Manning's n
0.06
!----- Right FloodPlain -----
! number of nodes
4
! station and elevation for above number of coordinates in (m)
6.58 354.86
15.08 354.94
65.08 354.94
65.08 355.94
! Manning's n of right Floodplain
0.15

```

Figure 8.6 Part of the discharge data file used in the simulation of the long-term stability of Little Salt Creek, Nebraska.

02/28/1969	12:00:00	0	0.52
03/01/1969	12:00:00	2	0.29
03/01/1969	13:00:00	1	0.29
03/02/1969	12:00:00	0	0.32
03/03/1969	00:00:00	0	0.38
03/03/1969	04:35:00	0	1.75
03/03/1969	12:20:00	0	0.45
03/04/1969	12:00:00	0	0.30
03/05/1969	12:00:00	0	0.23
03/06/1969	12:00:00	0	0.20
03/07/1969	12:00:00	0	0.18
03/08/1969	12:00:00	0	0.16
03/09/1969	12:00:00	0	0.14
03/10/1969	12:00:00	0	0.13
03/11/1969	12:00:00	0	0.13
03/12/1969	12:00:00	2	0.12
03/13/1969	13:00:00	1	0.12
03/14/1969	12:00:00	0	0.15
03/15/1969	12:00:00	0	0.68
03/16/1969	12:00:00	0	2.33
03/17/1969	00:00:00	0	2.81
03/17/1969	04:35:00	0	6.00
03/17/1969	12:20:00	0	3.30
03/18/1969	12:00:00	0	1.61
03/19/1969	12:00:00	0	0.64
03/20/1969	12:00:00	0	0.49
03/21/1969	12:00:00	0	0.27

Figure 8.7 Simulated evolution of the thalweg profile, Little Salt Creek, for a 30-year period.

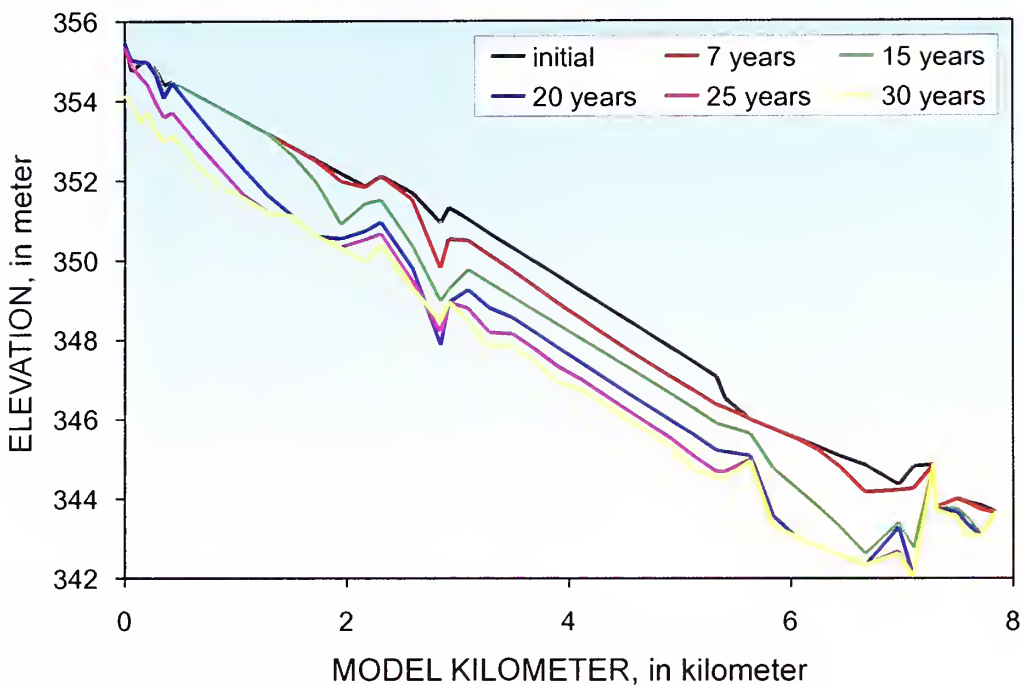


Figure 8.7 shows the predicted thalweg profiles of the modeling reach at various points of time. Figure 8.8 shows the simulated changes in cross-sectional geometry at cross sections upstream of Raymond Road, upstream of Mill Road, and near Bluff Road.

The erodibility of the streambed material governs the morphology of the modeling reach. *In situ* field experiments suggest that erodibility of the streambed material is similar along the modeling reach. As a result, channel incision increases along the modeling reach because of increasing discharge and, therefore, shear stress. Channel incision varies from about 4.3 m near the downstream end of the channel (model kilometer 7.1) to 1.5 m at the upstream end of the channel. The increase in bank height associated with incision leads to bank failures along the entire modeling reach. The average widening is 0.6 m upstream of Raymond Road, 1.5 m upstream of Mill road, 0.4 m upstream of North 14th Street and Waverly Road, and 1.2 m near Bluff Road.

Given the observed erodibility of the surface of the streambed and types of flows occurring between 1969 and 1998. Little Salt Creek will incise further. Figure 8.7 shows that incision progresses from the middle and downstream end of the modeling reach to its upstream end. Hence, controlling channel grade at selected locations may deter incision.

We performed a simulation in which we controlled the grade of all bridge crossings along the modeling reach. Figure 8.9 shows the resulting simulated evolution of the thalweg profile. With the addition of the simulated grade-control structures at the bridge crossings there is no incision upstream of

Figure 8.8 Computed changes in cross section geometry at selected cross sections along Little Salt Creek for a 30-year period: (a) cross section at model kilometer 0.29 upstream of Raymond, (b) cross section at model kilometer 2.93 upstream of Mill Road, and (c) cross section at model kilometer 6.98 near Bluff Road.

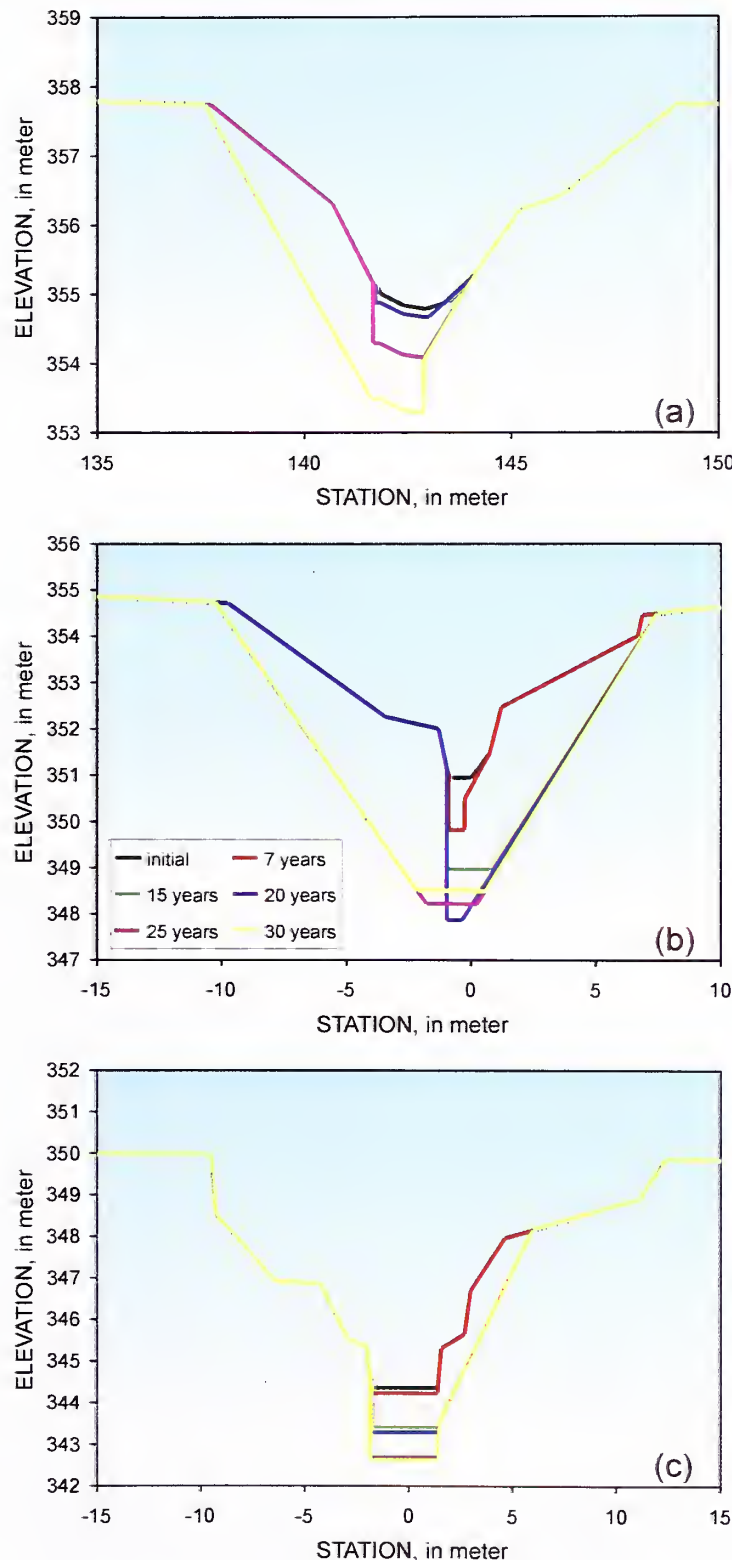
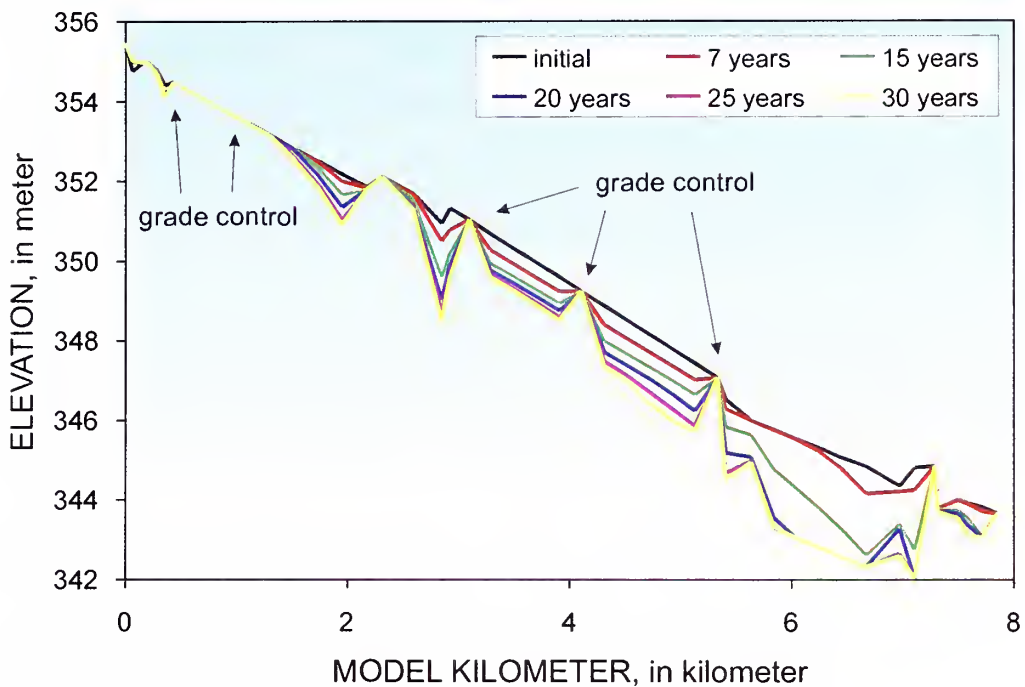


Figure 8.9 Simulated evolution of the thalweg profile, Little Salt Creek, for a 30-year period and the streambed controlled at each bridge crossing.



Raymond Road at the saline wetlands. The simulated structures reduce incision between North 1st Street and Bluff Road by approximately 60 percent. Figure 8.9 also shows that the second grade-control structure, bridge crossing at North 1st Street, may be omitted.

References

Abbott, M. B. (1966). *An Introduction to the Method of Characteristics*. Elsevier, New York, NY.

Abbott, M. B., and Basco, D. R. (1989). *Computational Fluid Dynamics: An Introduction for Engineers*. Longman Scientific & Technical, United Kingdom.

Alonso, C. V. (1997). "Field monitoring, remote sensing, and hydrologic evaluations in the Goodwin Creek Experimental Watershed." *Management of Landscapes Disturbed by Channel Incision: Stabilization, Rehabilitation, and Restoration*. S. S. Y. Wang, E. J. Langendoen, and F. D. Shields Jr., eds., 846–852.

Ariathurai, R., and Arulanandan, K. (1978). "Erosion rates of cohesive soils." *J. Hydr. Div.*, 104(HY2), 279–283.

Armanini, A., and Di Silvio, G. (1988). "A one-dimensional model for the transport of a sediment mixture in non-equilibrium conditions." *J. Hydr. Res.*, 26(3), 275–292.

Arulanandan, K., Gillogley, E., and Tully, R. (1980). "Development of a quantitative method to predict critical shear stress and rate of erosion of natural undisturbed cohesive soils." *Report GL-80-5*, U.S. Army Corps of Engineers, Waterways Experiment Station, Vicksburg, MS.

ASCE (1998). "River width adjustment. I: Processes and mechanisms." *J. Hydr. Engrg.*, 124(9), 881–902.

Basco, D. R. (1987). "Improved robustness of the NWS DAMBRK algorithm." *Hydraulic Engineering '87*, ASCE, New York, NY, 846–852.

Bennett, J. P. (1974). "Concepts of mathematical modeling of sediment yield." *Water Resour. Res.*, 10(3), 485–492.

Bishop, A. W. (1955). "The use of the slip circle in the stability analysis of slopes." *Geotechnique*, 5, 7–17.

Bishop, A. W., and Morgenstern, N. R. (1960). "Stability coefficients for earth slopes." *Geotechnique*, 19(3), 129–150.

Bodhaine, G. L. (1968). "Measurement of peak discharge at culverts by indirect methods." *Techniques of Water-Resources Investigations of the United States Geological Survey*, Book 3, Chapter A3, US Government Printing Office, Washington, DC.

Borah, D. K., Alonso, C. V., and Prasad, S. N. (1982). "Routing graded sediments in streams: Formulations." *J. Hydr. Div.*, 108(12), 1486–1503.

Brownlie, W. R. (1981). "Compilation of alluvial channel data: Laboratory and field." *Report No. KH-R-43B*, W. M. Keck laboratory of Hydraulics and Water Resources, California Institute of Technology, Pasadena, CA.

Celia, M. A., and Gray, W. G. (1992). *Numerical Methods for Differential Equations*. Prentice Hall, Englewood Cliffs, NJ.

Chow, V. T. (1959). *Open Channel Hydraulics*. McGraw-Hill, New York, NY.

Coon, W. F. (1998). "Estimation of roughness coefficients for natural stream channels with vegetated banks." *USGS Water-Supply Paper 2441*, U.S. Geological Survey, U.S. Department of the Interior.

Coppin, N. J., and Richards, I. G. (1990). *Use of Vegetation in Civil Engineering*. Butterworths, Boston, MA.

Cowan, W. L. (1956). "Estimating hydraulic roughness coefficients." *Agricultural Engrg.*, 37(7), 473–475.

Cui, Y., Parker, G., and Paola, C. (1996). "Numerical simulation of aggradation and downstream fining." *J. Hydr. Res.*, 34(2), 185–204.

Cunge, J. A., Holly Jr., F. M., and Verwey, A. (1980). *Practical Aspects of Computational River Hydraulics*. Pitman Publishing, Inc., Boston, MA.

Darby, S. E., and Thorne, C. R. (1996). "Development and testing of riverbank-stability analysis." *J. Hydr. Engrg.*, 122(8), 443–454.

Fellenius, W. (1936). "Calculation of the stability of earth dams." *Trans. 2nd Congress on Large Dams*, Washington, DC, 4, 445–462.

Foster, G. R., and Meyer, L. D. (1972). "A closed-form soil erosion equation for upland areas." *Sedimentation Symposium to Honor Professor Hans Albert Einstein*, H. W. Shen, ed., Colorado State University, Fort Collins, 12-1–12-19.

Fread, D. L. (1988). "The NWS DAMBRK Model: Theoretical background/User documentation." *Rep. No. HRL-256*, Hydrologic Research Laboratory, National Weather Service, Silver Spring, MD.

Fread, D. L. (1996). "Flow routing." *Handbook of Hydrology*, D. R. Maidment, editor in chief, McGraw Hill, Inc., New York, NY, Chapter 10, 10.1–10.36.

Fredlund, D. G. (1995). *User's Guide SLOPE/W*. GEO-SLOPE International, Ltd., Calgary, Canada.

Fredlund, D. G., and Krahn, J. (1977). "Comparison of slope stability methods of analysis." *Can. Geotech. J.*, 14, 429–439.

Fredlund, D. G., and Rahardjo, H. (1993). *Soil Mechanics for Unsaturated Soils*. John Wiley & Sons, Inc., New York, NY.

Garbrecht, J. (1990). "Analytical representation of cross-section hydraulic properties." *J. Hydrology*, 119, 43–56.

Garbrecht, J., Kuhnle, R. A., and Alonso, C. V. (1996). "A transport algorithm for variable sediment sizes: Fundamental concepts and equations." *Proceedings of the Sixth Federal Interagency Sedimentation Conference*, Las Vegas, Nevada, VI-8–VI-15.

Garcia, M., and Parker, G. (1991). "Entrainment of bed sediment into suspension." *J. Hydr. Engrg.*, 117(4), 414–435.

Gear, C. W. (1971). *Numerical Initial Value Problems in Ordinary Differential Equations*. Prentice-Hall, Englewood Cliffs, NJ.

Gray, D. H., and Leiser, A. T. (1982). *Biotechnical Slope Protection and Erosion Control*. Krieger Publishing Co., Inc., Malabar, FL.

Hagerty, D. J. (1990). "Piping/sapping erosion. I: Basic considerations." *J. Hydr. Engrg.*, 117(8), 991–1008.

Hanson, G. J. (1990). "Surface erodibility of earthen channels at high stresses. Part II – Developing an in-situ testing device." *Transactions of the ASAE*, 33(1), 132–137.

Henderson, F. M. (1966). *Open Channel Flow*. MacMillan Publishing Co., New York, NY.

Hirano, M. (1971). "River bed degradation with armoring." *Proceedings Japan Society of Civil Engineers*, 195, 55–65.

Hirsch, C. (1988). *Numerical Computation of Internal and External Flows*. John Wiley & Sons, New York, NY.

Huang, Y. H. (1983). *Stability Analysis of Earth Slopes*. Van Nostrand Reinhold Company, New York, NY.

Karim, F. (1995). "Bed configuration and hydraulic resistance in alluvial-channel flows." *J. Hydr. Engrg.*, 121(1), 15–25.

Kouwen, N., Unny, T. E., and Hill, H. M. (1969). "Flow retardance in vegetated channels." *J. Irrigation and Drainage Div.*, ASCE, 95(IR2), 329–342.

Krone, R. B. (1962). "Flume studies of the transport of sediment in estuarine shoaling processes." *Final Report*, Hydraulic Engineering Laboratory, University of California, Berkeley.

Kuhnle, R. A. (1996). "Variations in bed material size on Goodwin Creek." *Proceedings of the Sixth Federal Interagency Sedimentation Conference*, Las Vegas, Nevada, II-68–II-74.

Kuhnle, R. A., Garbrecht, J., and Alonso, C. V. (1996). "A transport algorithm for variable sediment sizes: Application to wide sediment size distributions." *Proceedings of the Sixth Federal Interagency Sedimentation Conference*, Las Vegas, Nevada, VI-1–VI-7.

Lambert, J. D. (1973). *Computational Methods in Ordinary Differential Equations*. John Wiley & Sons, New York, NY.

Langendoen, E. J., and Simon, A. (2000). "Stream channel evolution of Little Salt Creek and North Branch West Papillion Creek, eastern Nebraska." *Report*, US Department of Agriculture, Agricultural Research Service, National Sedimentation Laboratory, Oxford, MS.

Laursen, E. (1958). "The total sediment load of streams." *J. Hydr. Div.*, 84(HY1), 1530-1–1530-36.

Leopold, L. B. (1994). *A View of the River*. Harvard University Press, Cambridge, MA.

LeVeque, R. J., and Yee, H. C. (1990). "A study of numerical methods for hyperbolic conservation laws with stiff source terms." *J. Comp. Phys.*, 86, 187–210.

Lohnes, R. A., and Handy, R. L. (1968). "Slope angles in friable loess." *J. of Geology*, 76, 247–258.

López, F., and García, M. (1997). "Open-channel flow through simulated vegetation: Turbulence modeling and sediment transport." *Wetlands Research Program Tech. Rep. WRP-CP-10*, U.S. Army Corps of Engineers, Waterways Experiment Station, Vicksburg, MS.

Luttenegger, J. A., and Hallberg, B. R. (1981). "Borehole shear test in geotechnical investigations." *American Society of Testing Materials, Special Publication*, 740, 566–578.

Mehta, A. J., Parchure, T. M., Dixit, J. G., and Ariathurai, R. (1982). "Resuspension potential of deposited cohesive sediment beds." *Estuarine Comparisons*, V. S. Kennedy, ed., Academic Press, New York, NY, 591–609.

Mehta, A. J., Hayter, E. J., Parker, W. R., Krone, R. B., and Teeter, A. M. (1989). "Cohesive sediment transport. I: Process description." *J. Hydr. Engrg.*, 115(8), 1076–1093.

Meyer-Peter, E., and Mueller, R. (1948). "Formula for bed-load transport." *Proceedings of the International Association for Hydraulic Research*, 2nd Meeting, Stockholm.

Morgenstern, N. R., and Price, V. E. (1965). "The analysis of the stability of general slip surfaces." *Geotechnique*, 15, 79–83.

Murphrey, J. B., and Grissinger, E. H. (1986). "Channel adjustments in a Yazoo bluffline tributary." *Proc. 4th Federal Interagency Sedimentation Conference*, 5-123-5-132.

Osman, A. M., and Thorne, C. R. (1988). "Riverbank stability analysis. I: Theory." *J. Hydr. Engrg.*, 114(2), 134–150.

Parchure, T. M., and Mehta, A. J. (1985). "Erosion of soft cohesive sediment deposits." *J. Hydr. Engrg.*, 111(10), 1308–1326.

Phillips, B. C., and Sutherland, A. J. (1989). "Spatial lag effects in bed load sediment transport." *J. Hydr. Res.*, 27(1), 115–133.

Ponce, V. M., Li, R.-M., and Simons, D. B. (1978). "Applicability of kinematic and diffusion models." *J. Hydr. Div.*, 104(3), 353–360.

Preissmann, A. (1961). "Propagation des intumescences dans les canaux et rivieres." *Proceedings of the First Congress of the French Association for Computation*, Grenoble, France, 433–442.

Rahuel, J. L., Holly, F. M., Chollet, J. P., Belleudy, P. J., and Yang, G. (1989). "Modeling of riverbed evolution for bedload sediment mixtures." *J. Hydr. Engrg.*, 115(11), 1521–1542.

Roache, P. J. (1977). *Computational Fluid Dynamics*. Hermosa Publ. Co., Albuquerque, NM.

Sands, L. B., and Kapitzke, I. R. (1998). "Monitoring and modelling streambank subsurface water conditions in North Queensland, Australia." *Water Resources Engineering 98*, S. R. Abt, J. Young-Pezeshk, and C. C. Watson, eds., ASCE, Reston, VA, 1882–1887.

Simon, A., and Collison, A. (2001). "Scientific basis for streambank stabilization using riparian vegetation." *Proc. 7th Federal Interagency Sedimentation Conference*, Reno, NV, on CDROM.

Simon, A., Curini, A., Darby, S. E., and Langendoen, E. J. (1999). "Streambank mechanics and the role of bank and near-bank processes in incised channels." *Incised River Channels*, S. E. Darby and A. Simon, eds., John Wiley & Sons, New York, NY, 123–152.

Simon, A., and Darby, S. E. (1997). "Bank erosion processes in two incised meander bends: Goodwin Creek, Mississippi." *Management of Landscapes Disturbed by Channel Incision*, S. S. Y. Wang, E. J. Langendoen, and F. D. Shields Jr., eds., 256–261.

Simon, A., Wolfe, W. J., and Molinas, A. (1991). "Mass-wasting algorithms in an alluvial channel model." *Proc. 5th Federal Interagency Sedimentation Conference*, Las Vegas, NV, 8-22–8-29.

Taylor, D. W. (1948). *Fundamentals of Soil Mechanics*. John Wiley & Sons, New York, NY.

Terzaghi, K. (1943). *Theoretical Soil Mechanics*. John Wiley & Sons, New York, NY.

Terzaghi, K., and Peck, R. B. (1967). *Soil Mechanics and Engineering Practice*. John Wiley & Sons, New York, NY.

Thorne, C. R. (1990). "Effects of vegetation on riverbank erosion and stability." *Vegetation and Erosion*, J. B. Thorne, ed., Chapter 10, John Wiley & Sons, Chichester, United Kingdom, 125–144.

U.S. Federal Highway Administration (USFHWA) (1979). "Design charts for open-channel flow." *Hydraulic Design Series*, 3, U.S. Department of Transportation, Washington, DC.

U.S. Federal Highway Administration (USFHWA) (1985). "Hydraulic design of highway culverts." *Hydraulic Design Series*, 5, U.S. Department of Transportation, Washington, DC.

U.S. Interagency Committee on Water Resources, Subcommittee on Sedimentation (USICWR) (1963). "Measurement and analysis of sediment loads in streams." *Report No. 14*.

U.S. Soil Conservation Service (USSCS) (1975). "Hydraulics." *Engineering Field Manual*, 5, U.S. Department of Agriculture, Washington, DC.

van Niekerk, A., Vogel, K., Slingerland, R. L., and Bridge, J. S. (1992). "Routing of heterogeneous sediments over movable bed: Model development." *J. Hydr. Engrg.*, 118(2), 246–262.

Vanoni, V. A. (1975). "Sedimentation engineering." Prepared by the ASCE Task Committee for the Preparation of the Manual on Sedimentation of the Sedimentation Committee of the Hydraulics Division, ASCE, *Manual and Reports on Engineering Practices*, 54.

Wu, S., and Rajaratnam, N. (1996). "Submerged flow regimes of rectangular sharp-crested weirs." *J. Hydr. Engrg.*, 122(7), 412–414.

Wu, S., and Rajaratnam, N. (1998). "Impinging jet and surface flow regimes at drop." *J. Hydr. Res.*, 36(1), 69–74.

Yanenko, N. N. (1971). *The Method of Fractional Steps*. Springer Verlag, New York, NY.

Yang, C. T. (1973). "Incipient motion and sediment transport." *J. Hydr. Div.*, 99(HY10), 1679–1704.

Yarnell, D. L. (1934a). "Pile trestles as channel obstructions." *Tech. Bull.*, 429, US Department of Agriculture, Washington, DC.

Yarnell, D. L. (1934b). "Bridge piers as channel obstructions." *Tech. Bull.*, 442, US Department of Agriculture, Washington, DC.

